FINITE ELEMENT MODELING OF STRESS URINARY INCONTINENCE MECHANICS

THOMAS A. SPIRKA

Bachelor of Science in Chemical Science

Xavier University

December, 1995

Master of Science in Chemical Engineering

Cleveland State University

May, 2005

Submitted in partial fulfillment of requirement for the degree

DOCTOR OF ENGINEERING IN APPLIED BIOMEDICAL ENGINEERING

at the

CLEVELAND STATE UNIVERSITY

DECEMBER, 2010

This dissertation has been approved

for the Department of CHEMICAL AND BIOMEDICAL ENGINEERING

and the College of Graduate Studies by

Dissertation Chairperson, Margot S. Damaser Ph.D.

Department & Date

George P. Chatzimavroudis Ph.D.

Department & Date

Rama S. Gorla Ph.D.

Department & Date

Jeff Dean Ph.D.

Department & Date

Ahmet Erdemir Ph.D.

Department & Date

Matthew Barber M.D.

Department & Date

ACKNOWLEDGEMENTS

I would like to thank Dr. Margot S. Damaser for providing me with the opportunity to conduct the research presented in this dissertation. In addition, I would also like to thank her for all of the advice, encouragement and support offered during the process of completing this research. I would also like to thank Dr. George P. Chatzimavroudis, Dr. Rama S. Gorla, Dr. Jeff Dean, Dr. Ahmet Erdemir and Dr Matthew Barber for serving on the dissertation committee and reviewing the manuscript of this thesis. Their advice and suggestions were greatly appreciated and extremely helpful in completing this dissertation. Many thanks also go to Dr. Linda Brubaker and Dr. Kimberly Kenton of the Loyal University of Chicago, Stritch School of Medicine for their helpful suggestions and providing the urodynamic data that made this project possible. Lastly, I would also like to thank my family and friends for their continuous support and encouragement without which this research would not have been possible.

FINITE ELEMENT MODELING OF STRESS URINARY INCONTINENCE MECHANICS

THOMAS SPIRKA

ABSTRACT

Stress urinary incontinence is characterized by the involuntary transurethral loss of urine caused by an increase in abdominal pressure in the absence of a bladder contraction that raises the vesical pressure to a level that exceeds urethral pressure. Adult women are most commonly affected by SUI which is believed to be caused in part by injuries to the pelvic floor sustained during childbirth. In spite of the large number of women affected by SUI, little is known about the mechanics associated with the maintenance of continence in women. In theory the mechanics underlying the mechanics of female continence can be investigated through the use of complex dynamic finite element models of the lower urinary tract and pelvic floor. However, several modeling challenges must be overcome to construct such a model. The work in this dissertation focused on overcoming the challenges associated with modeling the bladder and the urethra in the context of stress urinary incontinence and incorporating clinically obtained urodynamic data into these models. In the first part of the dissertation, the effect of varying the material properties of the bladder and the urethra on the vesical pressure predicted by the model was studied. The results indicated that the material properties of the bladder and urethra had minimal effect on the vescial pressure predicted by the model indicating that vesical pressure could not be utilized as the lone validation criteria in subsequent models. The second portion of the study focused on identifying a method that could be used to model the fluid structure interactions that occur as the urine contained

within the bladder is forced into and through the urethral lumen and determining which parameters may affect the flow of urine through the urethra. The split operator form of the arbitrary lagrangian eulerian method was identified as a method that could be utilized to model these interactions. In addition, the results of the modeling effort suggest that the stiffness of the urethra, the pressure applied to the urethra and the boundary conditions constraining the urethra all have an impact on the flow of urine through the urethra during modeled stress events.

TABLE OF CONTENTS

ACKNOWLEDGEMENTS		iv
ABSTRACT		v
CHAPTER I	INTRODUCTION	1
CHAPTER II	OBJECTIVES AND SPECIFIC AIMS	3
	2.1 Objective 1	3
	2.2 Objective 2	4
CHAPTER III	BACKGROUND AND LITERATURE REVIEW	6
	3.1 Bladder Anatomy	6
	3.2 Urethra Anatomy	8
	3.3 Anatomy of Support Structures	11
	3.4 Continence Theories	15
	3.4.1 Pressure Transmission Theory	16
	3.4.2 Integral Theory	16
	3.4.3 Hammock Theory	22
	3.5 Bladder Models	25
	3.6 Urethra Models	27
	3.7 Models of Stress Urinary Incontinence	29
	3.8 Summary	32
CHAPTER IV	FINITE ELEMENT METHODS	34
	4.1 Introduction	34
	4.2 Finite Element Method	35
	4.3 Dynamic Finite Element Method	37
	4.4 Implicit vs. Explicit Approaches to Solving Dynamic Finite Element Problems	38
	4.5 Finite Element Modeling of Fluid Structure Interactions	41
	4.5.1 Lagrangian Formulation	41
	4.5.2 Eulerian Formulation	42
	4.5.3 Arbitrary Lagrangian Eulerian Formulation	44
	4.5.4 Operator Split Method	46
	4.6 Material Properties	50

CHAPTER V	MODELING THE BLADDER AND URETHRA DURING A CONTINENT COUGH	53
	5.1 Methods	53
	5.1.1 Urodynamics	53
	5.1.2 Modeling	56
	5.1.3 Simulations	59
	5.2 Results	63
	5.3 Discussion	73
	5.4 Conclusions	77
CHAPTER VI	MODELING THE BLADDER AND URETHRA IN THE CONTEXT OF STRESS URINARY INCONTINENCE: EFFECT OF GRID DENSITY, MASS SCALING AND TIME SCALING	79
	6.1 Methods	79
	6.2 Model Characterization	86
	6.2.1 Grid Dependence	86
	6.2.2 Effect of Mass and Time Scaling	88
	6.3 Results	89
	6.3.1 Grid Dependence	89
	6.3.2 Effect of Mass and Time Scaling	91
	6.4 Discussion	100
	6.5 Conclusions and Future Work	103
CHAPTER VII	MODELING THE BLADDER AND URETHRA IN THE CONTEXT OF STRESS URINARY INCONTINENCE: EFFECT OF URETHRAL STIFFNESS, APPLIED URETHRAL PRESSURE AND URETHRAL SUPPORT	104
	7.1 Methods	104
	7.1.1 Modeling	104
	7.1.2 Simulations	105
	7.2 Results	113
	7.3 Discussion	123
	7.4 Conclusions	126
CHAPTER VIII	OVERALL CONCLUSIONS AND FUTURE WORK	127
BIBLIOGRAPHY		130

APPENDICES 139

A Abridged LS Dyna Keyword File: First Objective Non-Linear Model 139

B Abridged LS Dyna Keyword File: First Objective Non-Linear Model 143

C Abridged LS Dyna Keyword File: Second Objective Non Leaking Model 146

D Abridged LS Dyna Keyword File: Second Objective Leaking Model 159

E Copyright Permission Documentation 172

LIST OF TABLES

Table I	Published linear material properties of the structures of the lower urinary tract and pelvic floor	50
Table II	Published linear and non-linear material properties for the structures of the lower urinary tract and pelvic floor	52
Table III	Mesh Density	58
Table IV	Simulation Details	61
Table V	Material properties used in non-linear and linear models	61
Table VI	Model details for 5 additonal subjects	62
Table VII	Effect of non-linear and linear material properties on the difference between predicted Pves and measured Pves	64
Table VIII	Effect of varying non-linear material property parameters on predicted Pves	65
Table IX	Effect of varying linear material property parameters on predicted Pves	66
Table X	Maximum and minimum pressure differences between predicted and measure Pves	68
Table XI	Comparison of predicted Pves to measured Pves for subject 1	69
Table XII	Comparison of predicted Pves to Measured Pves for Subject 2	70
Table XIII	Comparison of predicted Pves to Measured Pves for Subject 3	71
Table XIV	Comparison of predicted Pves to Measured Pves for Subject 4	72
Table XV	Comparison of predicted Pves to Measured Pves for Subject 5	73
Table XVI	Element distribution if grid dependence simulations	87

Table XVII	Simulations to determine effects of mass and time scaling	88
Table XVIII	Effects of varying mesh density on urine penetration depth	89
Table XIX	Effect of mass and time scaling on urine penetration depth	92
Table XX	Simulations utilized in sensitivity analysis	105
Table XXI	Summary of Sensitivity Analysis Results	116

LIST OF FIGURES

Figure 1	Anatomy of the female pelvic floor and lower urinary tract of a woman in the supine position	11
Figure 2	Anatomy of the female lower urinary tract and pelvic floor detailing support structures	15
Figure 3	Integral Theory of Continence	22
Figure 4	Schematic of penalty coupling method	49
Figure 5	Example of a urethral pressure profile	55
Figure 6	Example of urodynamic pressure measurements acquired during a 1.8 second cough	55
Figure 7	FEM model based on urodynamic data	56
Figure 8	Pressure loads	60
Figure 9	Abdominal pressure loads curves for cough events modeled in additional subjects	63
Figure 10	Displacements at peak abdominal pressure	67
Figure 11	Model of subject 1 in undeformed and deformed configurations	69
Figure 12	Model of subject 2 in undeformed and deformed configurations	70
Figure 13	Model of subject 3 in undeformed and deformed configurations	71
Figure 14	Model of subject 4 in undeformed and deformed configurations	72
Figure 15	Model of subject 5 in undeformed and deformed configurations	73
Figure 16	Shell FEM model based on urodynamic data	80
Figure 17	Lagrangian mesh embedded in the Eulerian mesh	81

Figure 18	Material Property Definitions	82
Figure 19	Constraints assigned to bladder base	83
Figure 20	Abdominal pressure loads corresponding to a cough	84
Figure 21	Urethral pressure profile corrected to baseline for a cough	85
Figure 22	Urethral pressure loads corresponding to a cough	86
Figure 23	Illustration of element clustering	87
Figure 24	Effect of grid density on urine penetration depth	90
Figure 25	Effect of mass and time scaling on urine penetration depth	92
Figure 26	Effect of mass and time scaling on stress distributions	94
Figure 27	Kinetic and Internal Energy vs Time for Simulation F	96
Figure 28	Kinetic and Internal Energy vs Time for Simulation G	96
Figure 29	Kinetic and Internal Energy vs Time for Simulation H	97
Figure 30	Kinetic and Internal Energy vs Time for Simulation I	97
Figure 31	Kinetic and Internal Energy vs Time for Simulation J	98
Figure 32	Error associated with dynamic effects in Simulations F through I	98
Figure 33	Error associated with dynamic effects in Simulations F, G and H	99
Figure 34	Pressure loads associated with modeled cough	107
Figure 35	Relationship between measured vesical pressure and applied urethral pressure loads during a cough	108
Figure 36	Abdominal pressure load corresponding to a four second valsalva maneuver	109
Figure 37	Urethral pressure profile corrected to baseline for a valsalva maneuver	111

Figure 38	Urodynamic pressure loads associated with a valsalva maneuver	111
Figure 39	Relationship between measured vesical pressure and applied urethral pressure loads during a valsalva manuever	112
Figure 40	Depth of urine penetration at peak Pabd in simulations K, L and M	116
Figure 41	Depth of urine penetration at second Pabd peak in simulations K, L and M	117
Figure 42	Depth of urine penetration at peak Pabd in simulations K, N and O	117
Figure 43	Depth of urine penetration at second Pabd peak in simulations K, N and O	118
Figure 44	Depth of urine penetration at peak Pabd in simulations K, P and Q	118
Figure 45	Depth of urine penetration at second Pabd peak in simulations K, P and Q	119
Figure 46	Depth of urine penetration at peak Pabd in simulations K, R and S	119
Figure 47	Depth of urine penetration at second Pabd peak in simulations K, R and S	120
Figure 48	Depth of urine penetration at peak Pabd (Valsalva) in simulations T and U	120
Figure 49	Depth of urine penetration at time = 3.0 seconds in a valsalva maneuver simulations T and U	121
Figure 50	Depth of urine penetration at peak Pabd in simulations K, V and W	121
Figure 51	Depth of urine penetration at second Pabd peak in simulations K, V and W	122
Figure 52	Effect of varying urethral constraints on funneling	123

CHAPTER I

INTRODUCTION

In 2001, it was reported in a study by Wilson et al that the direct cost of urinary incontinence in the United States was $16.3 billion (in 1995 dollars). This study further reported that three quarters of this total was spent in diagnosing and treating urinary incontinence in women.[1] Stress urinary incontinence (SUI) is a condition that affects mainly women and is characterized by the involuntary leakage of urine caused by an increase in abdominal pressure in the absence of a bladder contraction that occurs in conjunction with a cough, laugh, sneeze or a strain that raises the vesical or bladder pressure to a level that exceeds the urethral closure pressure. The root cause of SUI still remains unknown, however, it is believed to be caused in part by injuries to the nerves and musculature of the pelvic floor that are sustained during vaginal child birth. While

not a life threatening condition, SUI can have a devastating impact on the quality of life of the women that suffer from this condition.[2]

In spite of the large number of women affected by SUI, little is known about the mechanics associated with the maintenance of continence in females. To date, the knowledge of the mechanics of female continence is limited to three conflicting theories: the pressure transmission theory proposed by G. Enhorning which stresses the importance of effective transmission of abdominal pressure to the urethra in the maintenance of continence, the hammock theory proposed by J.O.L. Delancy which stresses the importance of the levator ani muscle in the maintenance of continence and the integral theory proposed by P.E.P. Petros which stresses the importance of the pubourethral ligaments in the maintenance of continence.[3-12] The mechanics behind these theories has never been biomechanically validated. In theory, the mechanics underlying the above theories can be investigated through the use of a complex dynamic finite element model of the lower urinary tract and pelvic floor. However, there are several modeling challenges that must be overcome before it is possible to begin construction of such a model. Therefore, the main goal of this study was to take the first steps towards building such a model by attempting to overcome the challenges associated with constructing a dynamic finite element model of the bladder and the urethra.

CHAPTER II

OBJECTIVES AND SPECIFIC AIMS

2.1 Objective 1

Construct a dynamic finite element model of the bladder and the urethra during a cough incorporating urodynamic data from a continent patient wherever possible to set model dimensions, loads, and validation criteria.

The focus of this objective was to model the mechanics of the bladder and urethra during a cough in a continent woman. In these models it was assumed that the urethra remains completely closed throughout the event and that the entire volume of urine remains within the bladder during the entire event. This work focused on determining how clinically obtained urodynamic data could be incorporated into the model and gaining insight into how the modeled bladder and urethra would be deformed by applied abdominal pressure loads. In addition, this work also focused on determining the effects of material properties on the vesical pressure and displacements predicted by the model.

This was done by comparing the predicted vesical pressure and displacements when non-linear material properties were incorporated versus the predicted values of these parameters obtained when linear material properties were incorporated. In order to further study the effect of the material properties on these parameters stiffer and more compliant material properties were also incorporated into the model.

To further characterize the subject specific performance of the model, an additional five models were created each incorporating urodynamic data from a different patient. The goal of this portion of the work was to determine if the modeling technique developed in the initial model would be able to produce similar results when urodynamic data obtained from different individuals were used to construct the model.

2.2 Objective 2

Construct a dynamic finite element model of the bladder and urethra that is capable of modeling the fluid structure interactions observed during a rise in abdominal pressure. The model constructed to achieve this objective must be able to model both continent and stress incontinent events.

The main goal of the second objective was to expand on the work completed in the first objective and create a model in which the modeled urine was no longer constrained to the bladder but free to flow under appropriate circumstances into and through the urethra. It was the intention of this objective to create models and identify techniques that could be used as a starting point with which to create more complex models of the lower urinary tract and pelvic floor to further study the mechanics of stress urinary incontinence. The models created in this objective would once again incorporate

clinical urodynamic data where ever possible in the construction of the model. Although it was not the intention of this objective to fully define and detail the mechanics of stress urinary incontinence, it was envisioned that this portion of the work could provide general insights into the mechanics by which continence is maintained by evaluating the effects of applied urethral pressure, urethral stiffness and urethral support on the mechanics predicted by the model specifically the fluid mechanics of the urine during a rise in abdominal pressure.

CHAPTER III

BACKGROUND AND LITERATURE REVIEW

3.1 Bladder Anatomy

The bladder is a hollow muscular organ which sits in the pelvis supported by the musculature of the pelvic floor and in females is indirectly supported by the ligaments supporting the uterus. Together the bladder and the urethra comprise what is known as the lower urinary tract (LUT) with both organs playing key roles in the storage and voiding of urine from the body (Figure 1). The walls of the bladder are composed of three separate layers, the serosal layer, the muscular layer and the submucosal layer. The serosal layer forms the outermost layer of the bladder and serves as a barrier between the muscular layer and the abdominal cavity while the submucosal layer constitutes the innermost layer and functions as a barrier to prevent the penetration of urine into the muscular layer. [13,14]

The muscular layer, also known as the detrusor muscle, is composed of three layers of smooth muscle fibers. The most important portion of these layers in regards to

bladder function are the obliquely oriented smooth muscle fibers which are located along the sides of the bladder in the external layers of the detrusor muscle. It is the contraction of these intersecting muscle fibers that cause urine to be expelled from the bladder and voided from the body.[13,14]

The bladder structure can be further divided into three regions, the dome, the trigone, and the bladder neck. The upper portion of the bladder is referred to as the dome. The dome region can be described as a balloonlike structure that is composed of the layers previously mentioned. The two main functions of this structure are to expand to accommodate and store the inflow of urine from the ureters and to contract via the detrusor muscle to void urine from the bladder during the micturition process. The base of the bladder is shaped like an upside down tetrahedron and comprises the region of the bladder known as the trigone. It is in this region where the ureters that transport urine from the kidneys to the bladder connect to the bladder. The primary function of the trigone region is to prevent the reflux of urine back into the ureters and the kidneys. This function is performed by the muscular layer of the trigone which contracts to flatten the meatus of the ureter after each passing peristaltic wave to prevent the reflux. [13,14]

The bladder neck lies at the most distal region of the bladder where the urethra attaches to the bladder which is also referred to as the urethrovesical junction. It has been theorized that this region may play a role in the maintenance of continence as in some females, muscle fibers associated with the detrusor muscle extend to form a 'U' shaped loop around the urethrovesical junction. It is theorized that these muscles can aid in the maintenance of continence by constricting the lumen of the proximal urethra and bladder neck. [4-8] However, this does not appear to be the case in all women as it has also been

reported, that in 25% of nulliparous women (women who have never had children) the bladder neck remains constantly open without any episodes of incontinence. [15]

3.2 Urethra Anatomy

The urethra can be described as a tube comprised primarily of three layers of smooth muscle fibers that run from the internal urethral meatus which is located in the region of the urethro-vesical junction to the external urethral meatus. The three smooth muscle layers that make up the urethra are the inner longitudinal layer, the outer circular layer and the outer longitudinal layer. All three smooth muscle layers are thought to play a role in maintaining the shape of the urethra. In addition, the longitudinal layers are believed to contract during voiding process, causing the urethra to become shorter and wider which reduces the resistance to flow associated with the inner urethral wall during micturition. The circular smooth muscle layer is believed to play a role in maintaining continence by collapsing the lumen of the urethra through its contraction.[4-8,15,16]

Located within the smooth muscle layers of the urethra are the submucosal and the mucosal layers. The mucosal layer is comprised primarily of stratified squamous epithelial cells while the submucosal layer is comprised of loose connective tissue, elastic fibers and smooth muscle cells. It is believed that the main function of these structures is to form a barrier to prevent the penetration of urine into the underlying smooth muscle layers during micturition. Even though smooth muscle cells are located within the mucosal layer it is not believed that this layer performs any role in the maintenance of continence.[15]

The vascular plexus which is primarily composed of arteriovenous anastomoses is located concurrent to the submucosal layer. It is thought that this structure may play a role in the maintenance of continence by helping to generate a water tight seal of the urethra. This seal is thought to be achieved by arterial blood flowing into the plexus which causes the plexus to expand toward the urethral lumen due to the fact that it is surrounded by what has been described as the rigid muscular sheath of the smooth muscle layers of the urethra. Some authors believe that as much as one third of the urethral pressure measured during urodynamics occurs as a result of the dilation of the vascular plexus.[17-20]

Exterior to the smooth muscle tube of the urethra is a striated muscle known as the external urethral sphincter, the anatomy of this muscular structure remains the subject of much debate. Delancey and Ashton-Miller locate this structure by dividing the urethra into percentiles with the 0^{th} percentile corresponding to the internal urethral meatus located proximally at the bladder neck and the 100^{th} percentile corresponding to the external urethral meatus located distally at the skin. According to their published descriptions, the urethral sphincter is located between the 15^{th} and 64^{th} percentile.[4-8] The urethral sphincter has been described by various authors as a striated muscle composed of Type I muscle fibers that are oriented tangent to the tube of smooth muscle that constitutes the urethra. [4-8,15,21-25] There is disagreement as to the exact shape of the sphincter as some authors propose that the sphincter completely encircles the urethra while others describe the urethral sphincter as being omega (Ω) shaped. [15,21-25] It is believed by some though not all that contraction of this muscle is critical to the maintenance of continence. [4-11,15,21-25] Those who describe the urethra as being circular

shaped propose that the closure of the urethral lumen is achieved by constriction, while those ascribing to the omega shape description argue that closure is achieved by compression of the urethra against the anterior wall of the vagina .[15,21-25]

In addition to the smooth muscle fibers of the detrusor muscle surrounding the proximal urethra and the striated muscle fibers of the urethral sphincter the urethra is also surrounded by the striated muscle fibers of the compressor urethrae and the urethrovaginal sphincter. Both structures are located between the 54th and 76th percentile of the urethra and run continuously with the urethral sphincter in this region. The muscle fibers of the compressor urethrae loop over the urethra and insert into the connective tissue of the perineal membrane on either side of the urethra. The fibers of the urethrovaginal sphincter surround both the vagina and the urethra. Due to the orientation of the muscle fibers of these two structures they are believed to affect closure of the urethra by compressing it against the anterior wall of the vagina rather than by constricting the urethra. [4-8,15] It should be noted however that this description of the anatomy and function of these structures is not universally accepted. [9,16,24,26]

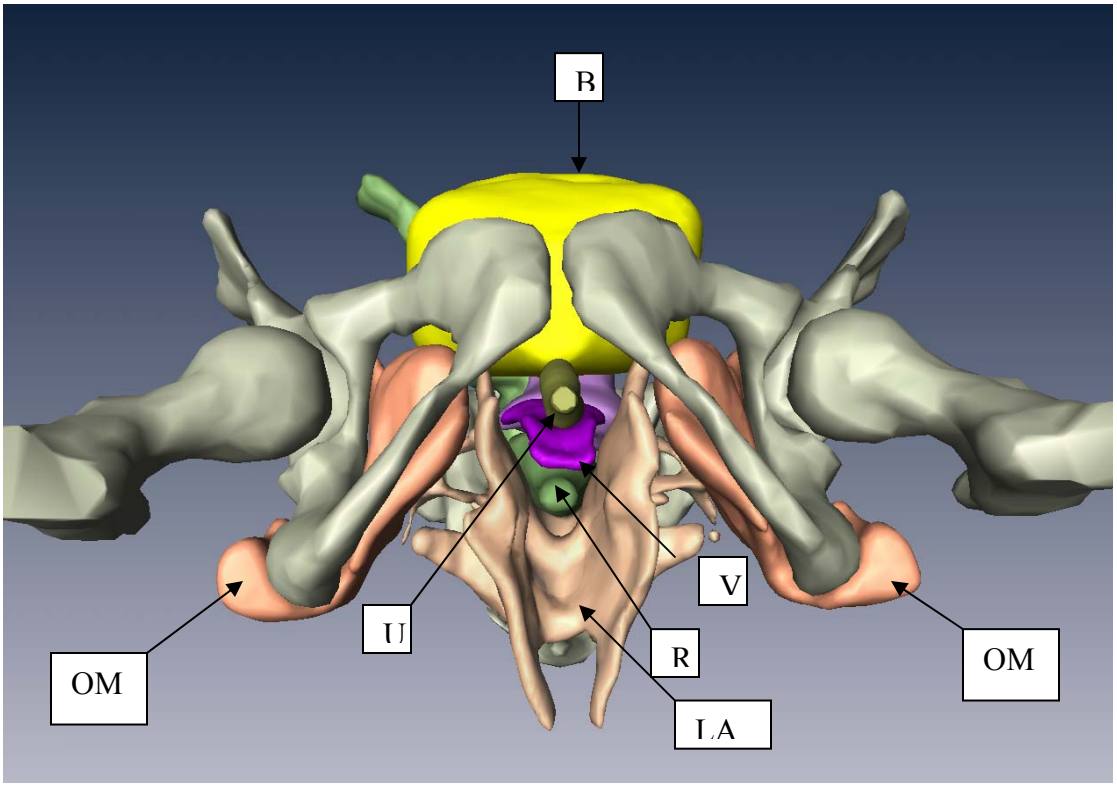

Figure 1: Anatomy of the female pelvic floor and lower urinary tract shown of a woman in the supine position B = Bladder, U = Urethra, V = Vagina, R = Rectum, LA = Levator Ani Muscles, OM = Obtuator Muscles

3.3 Anatomy of Support Structures

It is impossible to discuss the support structures of the bladder and the urethra without discussing the support structures of the vagina as the urethra lies directly on top of and is connected to the anterior wall of the vagina by a dense layer of connective tissue. As a result, the support for both the urethra and vagina are inextricably linked with both structures being supported either directly or indirectly by the endopelvic fascia, the arcus tendineus fasciae pelvis and the levator ani muscles (Figure 2). [4-11,15,21-25]

The endopelvic fascia, has been described as a dense fibrous connective tissue layer that surrounds the vagina. It is the endopelvic fascia surrounding the anterior wall

of the vagina that fuses the distal two-thirds of the urethra to the anterior wall of the vagina . The vagina is supported by the endopelvic fascia through its lateral connections to the arcus tendineus fascia pelvis on either side of the vagina. [4-8,27]

The arcus tendineus fascia pelvis acts as a cablelike support structure that is connected ventrally to the pubic bone and laterally to the ischial spines. Together with the endopelvic fascia this structure supports the vagina in much the same way the cables support the deck of a suspension bridge. The shape of the arcus tendineus fascia pelvis resembles that of a fan, in that near its insertion at the pubic bone, the arcus tendineus fascia pelvis has a well defined tendon like structure that spreads out to become a "broad aponeurotic structure" near its connections to the ischial spines. Along the sheet-like portion of its structure the arcus tendineus fascia pelvis merges with the endopelvic fascia and the levator ani muscle.[4-8,27]

The levator ani muscle is comprised of three individual muscles, the iliococcygeal muscle, the pubovisceral muscle and the puborectal muscle. The iliococcygeal muscle has a sheet like geometry that forms a shelf spanning the gap from one side of the pelvis to the other. The pubovisceral muscle arises on either side the pubic bone at one end and is attached to the walls of the perineal body (puboperineus), the vagina (pubovaginalis), and the intersphincteric groove of the anal canal (puboanalis) at its opposite terminal ends. Lastly the puborectal muscle forms a sling-like structure that is located around and behind the rectum. The fascia covering these muscles and the muscles themselves are considered to form what is known as the pelvic diaphragm which can be described as a sling-like structure that encircles and attaches to the perineum and the pelvic floor organs while being secured to the pubic bone and ischial spines. The opening in this sling like

structure located near the pubic bone through which the vagina, urethra and rectum pass is referred to as the urogenital hiatus.[4-8,28-31]

Under normal conditions, the urogenital hiatus is maintained in its closed orientation, meaning that the levator ani muscle can be considered to be under going constant contraction. In its closed orientation, the contraction of the levator ani muscle creates tension in its sling- like structure which in turn compresses the rectum, vagina, and urethra against the pubic bone. The continuous contraction of the levator ani muscle has been described as being similar to the continuous contractions seen in postural muscles. It is also believed that the levator ani muscle can be voluntarily contracted to increase the compressive force acting on the rectum, vagina, and urethra above the levels observed during its usual continuous activity.[4-8,28-30]

In closing the urogenital hiatus, an intact levator ani muscle will also function as a shelf on which the pelvic and abdominal organs will rest, thereby minimizing the tension occurring in their associated connective tissues and ligaments. [4-8,28-30] It has been theorized that if the levator ani muscle does not function properly or is injured, then this support will be compromised and the fascia and ligaments that support these organs will be placed under increased tensile loads that potentially can cause their supporting structures to fail. In such cases, a combination of abdominal pressure and gravity will force the organs in a caudal direction which can cause these organs to prolapse.[4-8]

In addition to the structures discussed above, some authors also contend that the pubourethral ligaments are also critical to the support of the urethra [9-11]. However this is not without controversy as other studies have stated that these ligaments do not exist and

what were thought to be ligaments are actually fine strands of smooth muscle tissue that are incapable of providing the support that some authors attribute to them.[21,32,33]

Three sagitally symmetric sets of pubourethral ligaments have been identified, the proximal pubourethral ligaments (PPL), the distal pubourethral ligaments (DPL) and the intermediate pubourethral ligaments (IPL). The shape of the PPLs has been described as triangular with the apex side being attached to the symphysis pubis and the base side being attached to the dorsal wall of the proximal urethra on one end and the anterior surface of the bladder neck at the other end. Structurally, the PPLs are described as being fibrous and resistant to stretching and have been shown to be composed primarily of collagen and elastin as well as bundles of smooth muscle fibers that were located near the attachments to the bladder neck and the proximal urethra.[32]

The DPLs are attached on one end to the lower border of the symphysis pubis and on the other end to the distal urethra near the external urethral meatus. These ligaments are composed mainly of elastin and smooth muscle fibers.[32]

The IPLs were reported as being attached to the symphysis pubis and the mid anterior wall of the urethra. The IPLs are reported to consist mainly of loose cellular adipose tissue and venules which are believed to have little if any support function .[32] It is interesting to note that based on the above descriptions it appears that the PPLs are the only pair of ligaments that could provide any structural support.

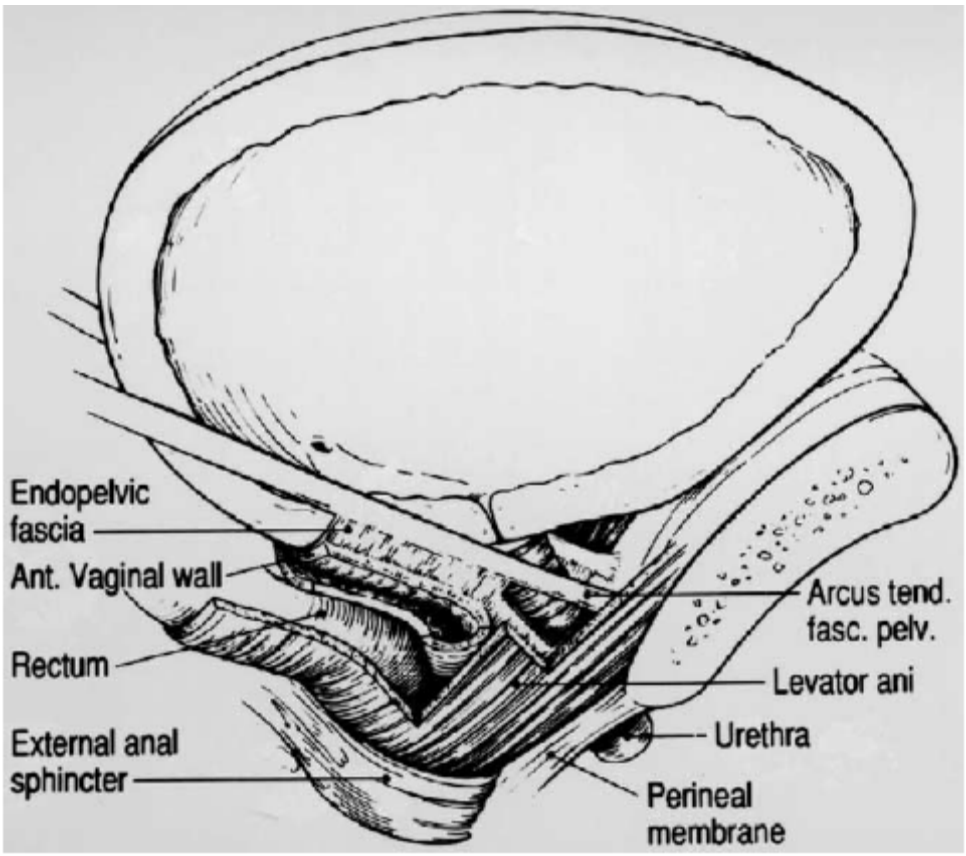

Figure 2: Anatomy of the female lower urinary tract and pelvic floor detailing support structures (Reprinted from Gastroenterology Volume No. 126 Authors: JOL Delancey and JA Ashton-Miller Title: Pathophysiology of Adult Urinary Incontinence S23-S32 2004 with kind permission from Elsevier)

3.4 Continence Theories

To date there are three main theories that have been used to conceptualize how females maintain continence during an increase in abdominal pressure, the pressure transmission theory as proposed by Enhorning, the integral theory as proposed by Petros and Ulmsten and the hammock theory as proposed by Delancey and Ashton-Miller. The three theories however contradict one another as there is little agreement between them as to which structures play a role in the maintenance of continence and the role that these structures play. The following sections present an overview of the three theories focusing

on which structures each consider important and how each theory proposes that these structures function in order to maintain continence.

3.4.1 The Pressure Transmission Theory

The pressure transmission theory as proposed by G. Enhorning focuses on the location of the proximal urethra in relation to the abdominal cavity. This theory is based on the idea that in healthy women the bulk of the proximal urethra lies within the abdominal cavity and is therefore exposed to rises in abdominal pressure. Enhorning theorized that passive transmission of abdominal pressure to the urethra during such events as coughs, sneezes or strains fully compresses the urethra which allows for continence to be maintained during these types of events. This theory further proposed that in stress incontinent women, the bulk of the urethra has descended outside of the abdominal cavity resulting in inefficient transmission of abdominal pressure and therefore incomplete compression of the urethra which causes leakages of urine to occur during stress events. This theory gave rise to the idea that in order to treat stress incontinence, the proximal urethra should be repositioned in such a manner that the bulk of the proximal urethra once again lies within the abdominal cavity so that it will once again be subjected to the full transmission of abdominal pressures which would allow complete compression of the urethra thereby restoring continence.[3,34,35]

3.4.2 The Integral Theory

Petros and Ulmsten have proposed in the Integral Theory that the following structures play a role in maintaining continence in females.[9-11]

1) Vagina
2) Pubourethral Ligaments (Anterior and Intermediate)
3) Pubococcygeous Muscle
4) Levator Plate
5) Uterosacral Ligaments
6) Cardinal Ligaments
7) Pubic Bone
8) Longitudinal Muscle of the Anus
9) Connecting Muscle of the Longitudinal Muscle of the Anus
10) External Anal Sphincter
11) Periurethral Striated Muscle
12) Bladder
13) Urethra

In their description of the functional anatomy of the lower urinary tract and pelvic floor, the vagina is divided into three distinct segments, the anterior segment, and the horizontal segment also known as the superlevator vagina and the zone of critical elasticity. The anterior segment of the vagina comprises the distal two-thirds of the vagina and is referred to as the "hammock" portion of the vagina. In this region, the vagina is tightly connected to the distal portion of the urethra by a layer of dense connective tissue which causes the vagina to support the urethra in much the same way a body is supported in a hammock. The anterior segment of the vagina is supported by the anterior and intermediate pubourethral ligaments which are anchored into the pubic bone. It is the insertion point of these ligaments along with the insertion point of the anterior pubococcygeous muscle on the ventral wall of the vagina that mark the proximal border of the anterior segment and the distal border of the horizontal segment. From this border region, the horizontal segment of the vagina makes a 130º turn dorsally. The terminus of this segment is the insertion point of the uteral sacral and the cardinal ligaments which

provide support for this segment along with the levator plate which also supports the horizontal portion of the vagina.[9-11]

The region where the superlevator vagina makes the 130º turn is termed the zone of critical elasticity, the Integral Theory proposes that this zone allows the vagina to act like a hinge and be pulled in two different directions at the same time. It is this feature of the vagina that the authors believe allow for continence to be maintained by the mechanisms described in this theory.[9-11]

The first mechanism of continence as proposed by the Integral Theory involves the contraction of the pubococcygeous muscle which exerts a tensile force on the anterior segment or hammock portion of the vagina pulling the vagina tight against the urethra. This tightening of the vaginal hammock serves to close the urethra while at the same time closing the gap between the cresta urethalis and the periurethral striated muscle (urethral sphincter) which immobilizes the insertion points of the periurethral sphincter muscle allowing for the isometric contraction of this muscle. In this theory it is stated that the force generated by the contraction of periurethral sphincter is not sufficient to close the urethra and that this contraction only serves to allow the sphincter to seal the urethral lumen to make it water tight. Urethral closure in the Integral Theory is affected by the contraction of the pubococcygeous muscle with the periurethral sphincter (urethral sphincter) performing a secondary function (sealing the urethral lumen). This theory holds that if the vagina is lax, the pubococcygeous muscle contraction will not sufficiently tension the vagina enough to cause the compression of the urethra. In addition the laxity of the vagina will cause, the insertion points of the periurethral

sphincter to be insufficiently immobilized which will prevent the isometric contraction of the sphincter required to seal the vagina from occurring effectively.[9-11]

While the first mechanism of continence affects the closure of the distal urethra, the second mechanism of continence simultaneously affects the closure of the bladder neck. The second mechanism of the integral theory states that the contraction of the anterior pubococcygeous muscle described in the first mechanism effectively immobilizes the portion of the urethra that is connected to the anterior portion of the vagina. During this contraction, the pubourethral ligaments function as a "passive anchoring point which allows them to act as a fulcrum against which the pubococcygeous muscle contracts. At the same time that the pubococcygeous muscle is pulling the ventral wall of the vagina forward and immobilizing the anterior urethra, the levator plate portion of the levator ani muscle contracts causing the horizontal or superlevator segment of the vagina to be stretched dorsally using the pubourethral ligaments as an anchor. The contraction of the levator plate muscle in the opposite direction of the pubococcygeous muscle contraction effectively causes the lateral portion of the pubococcygeous muscle to become semi-rigid due to the opposing forces acting on it. It is at this point of the mechanism that the longitudinal muscle of the anus which is connected to the pubococcygeous muscle by the connecting muscle contracts causing the pubococcygeous muscle to be pulled downwards against the anchoring pubourethral ligament. This causes the vagina to bend like a hinge in the zone of critical elasticity. This bending of the vagina causes the proximal urethra and bladder base to be tugged in a downwards direction which effectively kinks the urethra at the region where it is the least rigid. In order for this mechanism to function properly, the pubourethral ligaments and the

uterosacral ligaments must be intact to provide the proper support needed so that the forces of contraction function properly. In addition, isometric contraction of the external anal sphincter is also necessary to effect the contraction of the longitudinal muscle of the anus. Continuing with the idea that a lax vagina is the source of incontinence, the Integral Theory speculates that if the pubourethral and uterosacral ligaments do not adequately support the horizontal vagina, the forces produced by the contractions of the pubococcygeous muscle, the levator plate and the longitudinal muscle of the anus will be dissipated and as a result the bladder neck will not be tugged down sufficiently to effect the kinking of the urethra.[9-11]

Both of the first two mechanisms of continence are described as being under sympathetic control. A third voluntary mechanism centers around the contraction of the three muscle groups associated with the puborectalis muscle. The contraction of one or more of these muscle groups pulls the ventral and dorsal walls of the vagina and the rectum in an anterior direction. It is thought that this contraction effectively stimulates the contraction of the pubococcygeous muscle which reflexively causes the first two continence mechanisms to activate.[9-11]

The above discussion presents the anatomy, and physiology underlying "The Integral Theory of Continence." The question that now must be answered is how the functional anatomy is altered in the case of stress urinary incontinence. Petros and Ulmsten in the case of the first mechanism speculate that vaginal laxity caused by either trauma suffered during vaginal birth or as result of tissue stiffening due to aging can cause ineffective contraction of the pubococcygeous muscle which in turn leads to insufficient tension in the vagina, which results in the inefficient contraction of the

periurethral sphincter.[9-11] In other words the laxity of the vagina causes incomplete closure and sealing of the urethra which results in the achievement of lower urethral pressures in the distal urethra. As a result, a positive pressure gradient may develop in response to increased abdominal pressure that will allow urine to flow through the distal urethra.

In the second mechanism of continence Petros and Ulmsten cite defects in the ligamentous supports or in the connections of the muscles to the vagina as potential anatomical changes that can result in stress urinary incontinence. They specifically cite defects to the pubourethral ligament as one of the primary causes of stress urinary incontinence. Petros and Ulmsten speculate that damage to this ligament will result in the proximal urethra not being restrained as a result of the contraction of the pubococcygeous muscle. They further theorize that if the proximal urethra is not restrained, then the contraction of the levator plate dorsally will actually cause funneling in the bladder neck instead of kinking in the urethra as the proximal urethra will move in a dorsal direction as a result of the levator plate contraction. [9-11]

Petros and Ulmsten also site laxity in the uterosacral ligaments as a potential contributor to stress urinary incontinence. They theorize that if the uterosacral ligament is lax then the vagina is not adequately supported and also lax, as a result, the contraction of the longitudinal anal muscle will be dissipated and the bladder neck will not be pulled downward with sufficient force to pull it into a position that will effect the closure of the bladder neck. Tears in the external anal sphincter are also identified as a potential cause of ineffective longitudinal anal muscle contractions.[9-11]

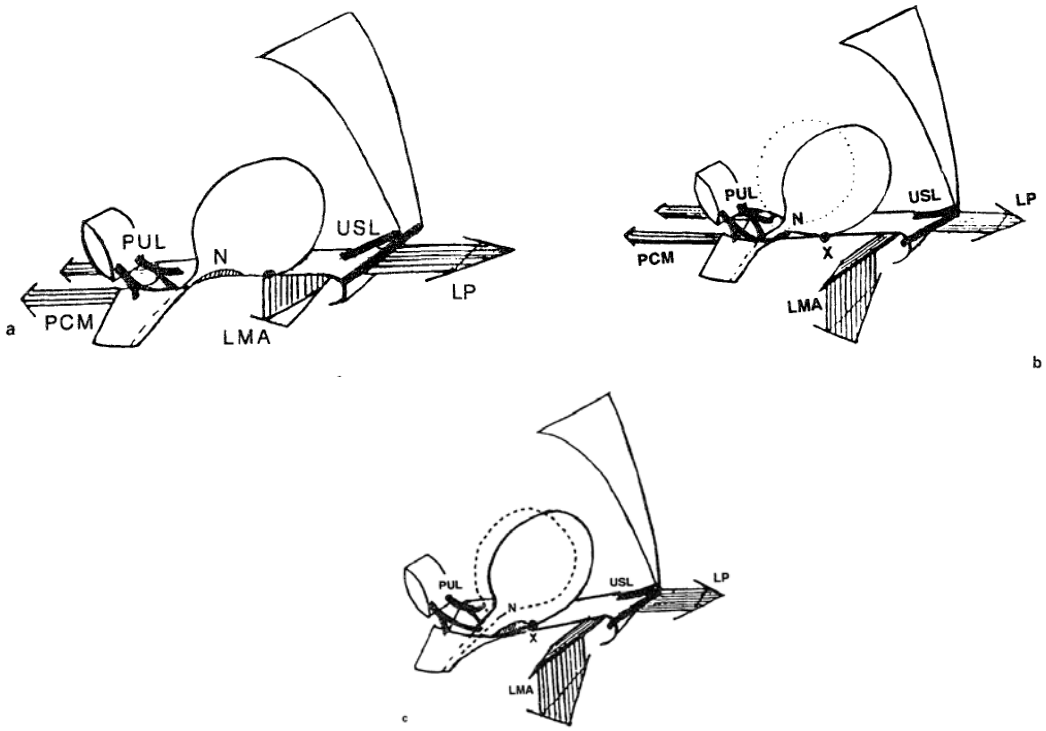

Figure 3: Integral Theory of Continence a) First mechanism of continence illustrating the contraction of the pubococcygeous muscle responsible for immobilizing the distal urethra b) First and Second mechanism of Continence c) Second Mechanism of continence illustrating the contractions of the levator plate and longitudinal muscle of the anus that result in the kinking of the proximal urethra. (PUL = Pubo-urethral ligaments, PCM = Pubococcygeous Muscle, USL = UteroSacral Ligament, LP = Levator Plate, LMA = Longintudinal Muscle of the Anus) (Reprinted from International Urogynecology Journal Volume No. 8 Authors: PEP Petros and U Ulmsten Title: Role of Pelvic Floor in Bladder Neck Opening and Closure II: Vagina 69-73 1997 with kind permission from Springer Science and Business Media)

3.4.3 Hammock Theory:

Similar to the theory proposed by Petros and Ulmsten, the hammock theory focuses on the supporting structures of the pelvic floor in order to understand the continence mechanism.[4-8] Two major differences exist between the two theories. The

first major difference is that Delancey and Ashton-Miller propose that the urethral sphincter (periurethral sphincter in Integral Theory) plays a major role in the maintenance of continence. The second major difference is that the Hammock Theory does not even mention the pubourethral ligaments in its description of the functional anatomy of the pelvic floor and lower urinary tract.[4-8] The following presents an overview of The Hammock Theory proposed by Delancey and Ashton-Miller to explain how continence is maintained during episodes of increased abdominal pressure.

In the case of stress urinary incontinence, Delancey and Ashton-Miller speculate that during a hard cough the inferior abdominal contents are forced due to increased abdominal pressure in a caudal direction. Ultrasound scans have been used to show that the proximal urethra can be displaced up to 10 mm in a caudal dorsal direction while the bladder neck is displaced in a caudal ventral direction. In response to this motion, it is thought that either the pelvic floor, the abdominal wall or both must stretch in order to accommodate and arrest this motion. Delancey and Ashton-Miller hypothesize that this motion is arrested due to the inertial forces occurring as the pelvic floor is stretched. They speculate that these inertial forces cause a caudal cranial pressure gradient to occur in the abdominal organs. However, before this motion can be arrested, the Hammock Theory suggests that the proximal intra-abdominal portion of the urethra is compressed against the support structures of the pelvic floor by the increased abdominal pressure. It is further hypothesized that the abdominal pressure acts in a transverse manner on the urethra meaning that the anterior wall is pressed against the posterior wall while the lateral walls are pressed against each other. If this supporting structure is damaged by injuries like those often seen during child birth, Delancey and Miller suggest that the

supportive layer will be more compliant and the compression of the urethra by abdominal pressure will not be as effective. To illustrate this point, they cite the example of stepping on a garden hose while it is lying on concrete versus when it is lying on a trampoline. The levator ani muscle is cited as being the primary support structure responsible for allowing this compression to take place. During a cough, the levator ani muscle contracts simultaneously with the diaphragm which contributes to the elevation of abdominal pressure. This contraction also tenses the suburethral fascial layer which in turns provides the support necessary to compress the urethra [4-8]. In short, under normal healthy circumstances, the urethra is supported by a hammock like structure consisting of the endopelvic fascia and the anterior wall of the vagina. When a cough occurs, the levator ani muscle contracts causing a tensile load to be placed on both ends of the hammock which draws the structure taught. The rising abdominal pressure then forces the urethra into this now tight hammock compressing the anterior wall against the posterior wall which is supported by the hammock. In addition because pressure acts uniformly on a surface, the lateral walls are compressed towards one another. While in stress urinary incontinent women, due to injuries or aging, the contraction of the levator ani muscle can no longer effect the tightening of the hammock as a result the support structure is not held as taught and as a result the compression of the urethra is not as effective as the hammock deforms due to this compressive force.

Both the Integral and the Hammock theory cite break downs in the support structures as the cause of stress urinary incontinence [4-11]. However, the theories disagree as to which structures are involved and the failures of which structures actually cause the condition. The Hammock Theory focuses primarily on the levator ani muscle

as the primary structure needed to provide the necessary support to prevent incontinence. This theory stresses that if this muscle cannot produce an effective contraction then the support of the urethra will be insufficient to cause it to be compressed effectively which will allow for the leakage of urine [4-8].

The Integral Theory cites inadequate support of the vagina as the primary cause of incontinence as without this support, the kink cannot form in the bladder neck This support is primarily dependent on the pubourethral ligaments [9-11].

The fact that this theory centers on the pubourethral ligaments as the primary support structure necessary to maintain continence is not without controversy as it has been reported in an anatomic study of female pelvic floor anatomy that these ligaments do not exist or that thin flimsy strands of smooth muscle tissue with none of the physical properties or mechanical strength associated with ligaments have been mistakenly named as ligaments [21,32,33].

3.5 Bladder Models:

Modeling of the bladder follows bladder function and can be split into two separate parts, the modeling of bladder filling and the modeling of bladder contraction. Models of bladder filling frequently make the assumption that the process can be modeled as a passive quasi-static process where the increasing liquid volume within the bladder causes the pressure within the bladder to increase in a step wise fashion. This increase in pressure causes the walls of the bladder to deform outward in order to accommodate an increasing volume of urine.

The earliest studies of bladder mechanics made the assumptions that the bladder was made of an isotropic, homogenous, incompressible material and that it was spherical in shape in order to extract the constitutive equations to predict bladder deformation during filling [36,37]. In a study by Damaser and Lehman, the spherical assumption of the bladder was tested using stress-strain constitutive relationships and the thin shell assumption to model stretching in hypothetical spherical, oblate spheroidal and prolate spheroidal bladders. Their findings indicate that for most regular shapes, the shape of the bladder does not greatly affect the compliance. Severely oblate spheroidally shaped bladders are the most compliant and therefore allow for the greatest volume of urine to be stored in the bladder at the lowest pressure. However, when compared to physiological data there was no evidence of this being the case in humans. This led them to conclude that the sensation of bladder fullness is likely not solely dependent on bladder pressure. As a result of this study, it can be concluded that the shape of the bladder is not as important in the modeling of the bladder as are the actual mechanical properties of the wall [38].

In a study published by Chi et al, the finite element method (FEM) was used to model the deformation of the walls of three organs, the bladder, the rectum, and the prostate.[39] The goal of this study was to perform a sensitivity analysis on the FEM solutions in order to understand how varying the material properties assigned to the modeled structures would affect the FEM solutions describing the deformations of the organs under specified loads. The authors found that in their simulations varying the material properties did not greatly impact the FEM predictions of the deformation of thin walled hollow organs such as the bladder and the rectum. However, in the case of a solid

model such as the prostate gland, varying the material properties significantly affected the FEM prediction of the deformation of the prostate. In order to validate their findings, and to demonstrate that the accuracy of the FEM solver used, the authors of this study constructed simplified models that could be solved analytically in order to compare the deformation predicted by the FEM models to the deformation predicted by the closed form solution. In this case, the authors found that the deformations calculated by hand and those calculated by FEM were in close agreement demonstrating the validity of their methods and increasing the authors confidence in the accuracy of the results generated from the more complex models [39].

3.6 Urethra Models

Several studies have focused on modeling the urethra either mechanically or mathematically in both males and females. In the early mathematical studies, such as those conducted by Backman and Ritter et al, the urethra is modeled as a straight rigid tube since little information was available at the time regarding flow in elastic tubes. The main focus of these early studies was to establish a relationship that would enable prediction of the effective diameter of the urethra. These studies concluded that, because urine flow was turbulent, the Bernoulli principle could be used in conjunction with pressure and flow rate data to determine the effective diameter of the urethra [40,41].

Griffiths was the first to construct mathematical models of both male and female urethras with elastic walls [42-44]. In his first model of the female urethra, he assumed that during micturition the urethra was an elastic walled tube with a circular cross section whose radius varied gradually over the length of the urethra with a minimum cross

section at the midpoint, simulating the constriction seen at the bladder neck. The elastic walls in this model were assumed to obey Hooke's law of linear elasticity and have uniform elastic properties. This allowed Griffiths to establish a relationship between pressure and radius of the urethra during micturition. Fluid flow in this model was governed by the Bernoulli equation which was used to calculate the flow rate through the urethra. Although this model made several simplifying assumptions regarding shape as well as elastic properties and urine flow properties in the urethra, it was the first to actually take into account urethral elasticity [42].

Griffiths then extended this work by creating a model for an elastic walled male urethra, in which energy losses due to friction are accounted for due to the greater length of the male urethra [43,44]. In addition, the elastic properties of the wall varied along the length of the model urethra. The end result was that the male model of the urethra is more physiologically realistic than the female model since fewer simplifying assumptions were made. Spangberg and colleagues furthered Griffiths initial work by using the models proposed by him to quantify urethral function. They conclude that changes in the minimal opening pressure of the urethra and physiological changes which limit the ability of the urethra to distend during micturition are both possible causes for bladder outlet obstruction [45].

Horak and Kren have produced one of the most complex finite element models of the male urethra to date.[46] They modeled urine as a Newtonian fluid and its flow as non-stationary, isothermal and turbulent. The urethral wall was modeled in the opened position as an isotropic and linearly elastic material that is subject to large displacements and strains. The authors incorporated this into a transient finite element model to solve

the flow and wall displacement problems. The difficulty in assessing this model comes from the fact that their publication focuses mainly on the construction and solution methods and while providing minimal results [46].

3.7 Models of Stress Urinary Incontinence

To date only a small number of finite element models focusing on stress urinary incontinence have been published. The first of these was published as part of a doctoral dissertation by Kyu-Jung Kim. In the dissertation Kim outlined two dimensional models that could be used to study urethral closure during stress events[47].

In his first model, Kim constructed a very simplified axis-symmetric model of the urethra and the pelvic floor utilizing literature values to specify the dimensions of the structures. This model also included a representation of a 7 French catheter inserted into the lumen of the urethra. The model was discretized using shell elements and incorporated linearly elastic material properties to define the mechanics of the structures[47].

In this first model Kim modeled two states, a resting state and a state corresponding to elevated abdominal pressure. In the resting state the model was run with a resting abdominal pressure obtained from literature applied to the model. In this state he adjusted the Young's moduli used to describe the tissues and the urethral loads applied to the exterior surface of the urethra until the closure pressure predicted by the model matched a resting closure pressure obtained from the literature. In the elevated pressure state an abdominal pressure corresponding to that observed during a cough was

applied and the same parameters were varied until the urethral pressure closure pressure in the stressed state matched that reported in the literature[47].

The goal of the first model was to predict the degree to which urethral closure is caused by active (muscle contractions) and passive (pressure transmission) forces. The relative active and passive contributions were determined by predicting the amount of pressure that would act on the modeled catheter when the loads placed on the model were varied. The difference between the predicted pressures then allowed him to determine the active and passive contributions to urethral closure. The results of the models indicated that passive mechanisms dominated in affecting closure in the region of the bladder neck whereas active mechanisms dominated in the more distal regions of the urethra. From these results he concluded that active contraction of the sphincter muscles and the pelvic floor play a key role in the maintenance of continence.[47]

In the second model in order to characterize the role of urethral support structures a second model was constructed based on a sagital section of a specially prepared cadaver. This two-dimensional plain strain finite element model incorporated the bladder, urethra, endopelvic fascia and the levator ani muscles. The model in this case was evaluated based on the predicted urethral closure pressure generated when forces designed to simulate the active contraction of the urethral sphincter and levator ani muscles were applied to the model. The models findings indicated that properly timed levator ani contractions and support of the endopelvic fascia could potentially play a role in the maintenance of continence.[47]

A more recent model by Zhang et al constructed a very complex finite element model of the lower urinary tract and pelvic floor with the intention of studying the

feasibility of using a finite element model to study mechanics of stress incontinence that can occur in female athletes when landing a jump.[48] This model incorporated idealized representations of the intestine, uterus, rectum, pelvis, pelvic diaphragm , vagina, urethra, uro-genital diaphragm, bladder and abdominal muscles. In addition, urine was also included in this model in order to allow for the simulation of leakage. The model incorporated sagital symmetry meaning that only half of the above listed structures were simulated. The jump was modeled by assigning an initial velocity to all the structures that was reduced to zero to simulate the landing over a short period of time[48]. The velocity and time until zero velocity was reached was specified based on experimental data. All structures with the exception of the fluid were modeled as linearly elastic structures using the Lagrangian kinematic descriptions and discretized using hexahedral elements. The fluid in this case was modeled using the Eulerian kinematic description as a "viscosity material model". It is interesting to note that in this study what constitutes a leakage of urine is not clearly defined. From the illustrations, it appears that a leakage of urine is defined as urine exiting the bladder and entering the urethra, all figures only show urine entering the proximal urethra and no figures are included that show full transit of the urine through the entire length of the urethra[48].

The main finding of this work was that it is feasible to model stress incontinence induced by a jump using the finite element method. In addition, this study also found that for low height jumps (less than 1 foot) the amount of urine contained within the bladder does not affect the volume of leaked urine and that increasing jump heights increased the predicted leaked volume of urine. This study also found that the urethra does indeed

funnel at the level of the bladder neck during a jumping stress event which allows for urine to enter into the proximal urethra[48].

Haridas et al has also proposed utilizing a finite element model with which to model the biomechanics of the lower urinary tract and pelvic floor[49]. In their initial publication, a finite element model of the uterus, cervix, bladder, vagina, levator ani, endopelvic fascia and rectum was created from MRI scans of a single subject. MRI scans were also acquired during a filling study and during the inflation of a transvaginal balloon which were then used to define deformations of the structures in a finite element model. The inverse finite element method was used to define the hyper-elastic material properties of the vagina, urethra and the bladder wall. The model was then validated by simulating the inflation of a transvaginal balloon within the model and comparing the deformations predicted by the model to those observed in ultrasound images of the same event. Good correlation was reported between the deformations predicted by the model and the deformations observed in the ultrasound images[49].

3.8 Summary

As stated above the feasibility of utilizing the finite element method to model the lower urinary tract and pelvic floor has been demonstrated. The models focusing on modeling stress incontinence show that it is possible to model the fluid structure interactions that occur during stress events as well. The current work expands on the previously published models in that this work focuses not only on modeling the mechanics of the bladder and urethra during a stress events (cough and valsalva maneuver) it also focuses on incorporating clinical urodynamics into the models and

attempting to determine if a model can show mechanical differences between continent and stress incontinent women. In the previous models the modeling effort has focused on modeling a specific mechanical aspect of the continence mechanism (urethral closure) or demonstrating that the finite element model can simulate the leaking situation. This work focuses on trying to determine under what conditions or parameters will a leak occur or not occur in order to gain insight into how the mechanics of continence may differ between continent and stress incontinent women.

CHAPTER IV

FINITE ELEMENT METHODS

4.1 Introduction

It is beyond the scope of this dissertation to provide an in depth description of the finite element method (FEM) and the derivation of the equations utilized as this would only duplicate the work of several excellent resources available on the subject.[50-53] As a result, this section will focus on providing a general overview of the finite element method and focus on the specialized techniques and methods that were used to construct the models presented in this dissertation. In this work the explicit finite element solver LS Dyna (LSTC Corporation Livermore, CA) was used to run all of the simulations presented. Therefore, the description of the FEM techniques presented in this section will also focus on how these methods have been incorporated into this particular software package.

4.2 Finite Element Method

In continuum mechanics problems, the main goal is to determine the value of the field variable (pressure, temperature, stress, displacement etc.) at various points within the continuum. However, a continuum is defined as having an infinite number of points contained within the boundaries of that continuum.[54] Therefore the only way the value of the field variable can be calculated at each point in the continuum is if a closed form solution exists for that particular continuum. With the exception of very simple problems this closed form solution does not exist and as a result, the solution must be approximated. The finite element method (FEM) is a mathematical technique specifically formulated to generate these approximate solutions. FEM accomplishes this by representing the continuum with a finite number of simple shapes known as elements and calculating the field variable at a finite number of points, known as nodes, corresponding to each element.[50-52]

The finite element solution to a problem involves a seven step process. The first step is to discretize the continuum using a number of simple shapes known as elements. There are a variety of shapes that these elements can take however; the most common shapes used to discretize three dimensional problems are hexahedrals or tetrahedrals. The next step then is to select interpolation functions for the problem. Interpolation functions are typically polynomials that define how the field variable varies within an element. Once the continuum has been discretized and the interpolation functions have been chosen, the next step is to define the matrix equations that will determine the behavior of an element in a given situation. The matrix equations for a given element are determined by the direct method, the variational method or the method of weighted

residuals. Once the matrix equations are determined, the next step is to assemble the matrix equations for each individual element into a system of equations. In other words just as the individual matrix equations define the behavior of an individual element, the assembled system of equations which combines all of these equations for all the elements in the continuum, will define how the system behaves under a given set of conditions. The assembly of the individual element matrix equations into the system of equations is based on the connectivity of the elements as each element shares nodes with neighboring elements. Therefore, when the system of equations is generated, this sharing of nodes must be accounted for in order to define the interconnectivity of the elements. After the system of equations has been constructed the next step is to impose boundary conditions on the problem. It is during this phase that loads are assigned to the appropriate nodes and the value of the field variable at nodes where this value is known are defined. After the boundary conditions have been established, the next step is to solve the system of equations for the unknown values of the field variable at each node. After solving for the field variable, it is then possible to use these values in the final step of calculating other parameters that are important to defining the behavior of the system as a whole.[50-52]

It should be noted that when using commercial finite element solvers, most of the above steps are performed automatically by the software package with little input from the user. However, the steps involving the discretization of the continuum and the assignment of boundary conditions, material properties and loads require significant user input to define and troubleshoot each unique problem being considered.

4.3 Dynamic Finite Element Method

During a stress event such as a cough, the forces acting on the bladder and urethra vary rapidly with time. As a result, static finite element modeling where the loads and deformations are modeled as being constant with respect to time is not sufficient to model the rapidly changing forces acting on the model or the resulting rapidly changing displacements.

In static finite element modeling the equation relating force and displacement has the following form[50-52,55,56].

$$\{F\} = [K]\ \{\delta\} \qquad \text{Eq. 1}$$

Where {F} is the nodal force vector, {δ} is the nodal displacement vector and [K] is the global stiffness matrix. It should be noted that the formulation of [K] varies based on the shape and type of elements used and the material properties used to describe the modeled structures. As can be seen from this equation the forces and displacements in this case do not vary with time. In the case of dynamic finite element modeling the equations relating forces and displacement have the following form based on Newton's second law. Which states that the total force applied on a body is equal to the time derivative of linear momentum of the body [50,51,55,56].

$$[M]\{\ddot{\delta}\} + [C]\{\dot{\delta}\} + [K]\{\delta\} = \{F(t)\} \qquad \text{Eq. 2}$$

Where [M] is the global mass matrix, [C] the global damping matrix, $\{\ddot{\delta}\}$ is the second derivative of the nodal displacement vector with respect to time (acceleration) and $\{\dot{\delta}\}$ is the first derivative of the nodal displacement vector with respect to time (velocity). Due the fact that the displacement vector and its derivatives vary with time during a dynamic

event, the equations of motion must be solved in which an incremental time stepping scheme is utilized. In this scheme the dynamic equations are solved at instantaneous moments in time during the event that are separated by a fixed interval of time. The techniques used to solve these equations incorporate one of the following approaches, the implicit approach or the explicit approach which will be discussed in the following section [50,51,55,56].

4.4 Implicit vs. Explicit Aproaches to Solving Dynamic Finite Element Problems

As mentioned above finite element solutions to problems involving time dependent forces and displacements incorporate either an explicit or implicit approach to obtain the solution, with each approach having its own advantages and disadvantages. The main difference between the approaches is that the explicit approach utilizes only historical or known data to calculate the value of the field variable for each time increment. This means that the value of the displacement vector at the time point ($t + \Delta t$) will be a function of the value of the displacement vector and its derivatives at the current time point (t) and the time point ($t-\Delta t$).[50,51,55,56] Symbolically this can be written as:

$$\{\delta\}_{t+\Delta t} = f(\{\delta\}_t, \{\dot{\delta}\}_t, \{\ddot{\delta}\}_t, \{\delta\}_{t-\Delta t}, \{\dot{\delta}\}_{t-\Delta t}, \{\ddot{\delta}\}_{t-\Delta t} \ldots.) \qquad \text{Eq. 3}$$

In other words by definition in the explicit approach only one unknown in this case the value of $\{\delta\}$ at $t = t+\Delta t$, is solved for, which means all of the rest of the terms on the right hand side of Eq. 3 must be known. The explicit method incorporates a marching type of solution in which the value of the unknown is calculated at each time increment and subsequently used to calculate the value of the unknown in the next time increment. This differs from the implicit method in that in the implicit method the value of $\{\delta\}$ at the

time point (t + Δt) is a function not only of the historical values of {δ} and its derivatives but also the value of {δ} and its derivatives at the time point (t + Δt) [50,51,55,56]. Symbolically, this can be written as:

$$\{\delta\}_{t+\Delta t} = f(\{\dot{\delta}\}_{t+\Delta t}, \{\ddot{\delta}\}_{t+\Delta t}, \{\delta\}_t, \{\dot{\delta}\}_t, \{\ddot{\delta}\}_t, \{\delta\}_{t-\Delta t}, \{\dot{\delta}\}_{t-\Delta t}, \{\ddot{\delta}\}_{t-\Delta t}, ...) \qquad \text{Eq. 4}$$

In the above equation it can be seen that there are three unknowns indicating that in the implicit approach an iterative scheme would need to be incorporated in which the value of {δ} at all time points would need to be solved as a systems of equations [50,51,55,56].

By applying the explicit approach and a half step central difference method to Equation 3, and solving for the displacement vector {δ} at the time point (t+Δt) the following equation is obtained [50,51,55,56]

$$\frac{1}{\Delta t^2}[M]\{\delta\}_{t+\Delta t} = \{F\}_t - [K]\{\delta\}_t + \left[\frac{2}{\Delta t^2}[M] - \frac{1}{\Delta t}[C]\right]\{\delta\}_t - \left[\frac{1}{\Delta t^2}[M] - \frac{1}{\Delta t}[C]\right]\{\dot{\delta}\}_{t-\Delta t} \qquad \text{Eq. 5}$$

When the mass matrix [M] is a diagonal matrix the solution of the above equation even with the inversion of the mass matrix is relatively straight forward. However, it should be noted that the above equation is conditionally stable in that increment Δt must be small enough to prevent the calculations from becoming unstable. In order prevent this from occurring, Δt is set based on the characteristic length of the smallest element divided by the dialational wave speed of the material [50,51,55,56]. As a result of the above condition, the explicit approach generally requires the use of very small time increments to maintain solution stability which significantly increases the computational cost of utilizing the explicit approach [50,51,55-60].

When the implicit approach is applied to Equation 4 and the Newmark method is used to calculate the values of nodal acceleration and velocity using the factors γ and β to control accuracy, numerical stability and damping, and the resulting equation is solved for the displacement vector {δ} at the time point (t+Δt) the following equation is obtained.[50,51,55,56]

$$[K^*]\{\delta\}_{t+\Delta t} = \{F\}_{t+\Delta t} + [M]\left\{\frac{1}{\beta\Delta t^2}\{\delta\}_t + \frac{1}{\beta\Delta t}\{\dot{\delta}\}_t + \left(\frac{1}{2\beta}-1\right)\{\ddot{\delta}\}_t\right\} + [C]\left\{\frac{\gamma}{\beta\Delta t}\{\delta\}_t + \left(\frac{\gamma}{\beta}-1\right)\{\dot{\delta}\}_t + \Delta t\left(\frac{\gamma}{\beta}-1\right)\{\ddot{\delta}\}_t\right\} \quad \text{Eq. 6}$$

Where

$$[K^*] = \frac{1}{\beta\Delta t^2}[M] + \frac{\gamma}{\beta\Delta t}[C] + [K] \quad \text{Eq. 7}$$

Due to the fact that [K*] contains the stiffness matrix [K] the resulting matrix will not be diagonal and as a result the computation of {δ} at the time point (t+Δt) requires the inversion of a non-diagonal matrix which significantly increases the computational cost of utilizing the implicit approach.[50,51,55,56]

The implicit approach is considered to provide a more accurate solution than the explicit approach.[50,51,55-60] The main draw back to using the implicit approach stems from the fact that, the inversion of the stiffness matrix remains very computationally expensive and in the case of complex problems this computational expense can be prohibitive in that a solution may not be achieved. The explicit method is considered despite the large number of time steps required to maintain stability the computationally less expensive of the two approaches [50,51,55-60]. In addition, the explicit approach has

been shown by others to be able to effectively solve and generate useful solutions to problems with similar complexity to the ones faced in this dissertation [46,48,61-66].

4.5 Finite Element Modeling of Fluid Structure Interactions

In the above discussion, the basics of utilizing the finite element method to solve dynamic structural mechanics problems were summarized. In modeling SUI, it is not sufficient to model only the structures of the bladder and urethra. One must also account for the fluid (urine) contained within the bladder and the fact that during an event in which the abdominal pressure rises, that fluid may be forced into and through the urethra. As a result, the associated fluid structure interactions must be accounted for. In terms of the finite element method modeling the fluid in this case is not trivial as in order to enter and transit the urethral lumen the fluid as a whole must undergo large deformations. In order to account for this, the bladder, urethra and the fluid can be modeled using a Lagrangian Formulation, an Eulerian Formulation or an Arbitrary Lagrangian Eulerian Formulation (ALE). Each of the above techniques as well as the associated pros and cons of utilizing each formulation to model the fluid structure interactions will be summarized in the following sections.

4.5.1 Lagrangian Formulation:

The Lagrangian Formulation is the most commonly used formulation in structural mechanics to model the deformation of structures [65-70]. This formulation was designed so that the finite element mesh deforms in the same manner as the continuum that it represents and that the elements of the mesh always represent the same portion of the

continuum. In the Lagrangian description of motion/deformation, all motion and deformation is defined by comparing the location of a particular point in the new/deformed configuration to its original location in the undeformed configuration. As a result, the location of a particular point in the deformed structure is dependent on its location in the original structure. Defining deformation in this manner offers several advantages, due to the fact that each element represents the same portion of the continuum at all times makes the tracking of interfaces and free surfaces relatively straight forward. In addition, this definition of deformation is very useful when modeling materials that have history dependent behaviors as it is easy to follow and keep track of the deformations and loads acting on a particular part of the continuum at a given time.[65-70] The main disadvantage to using this approach occurs in situations where large deformations occur. In these cases, the Lagrangian based algorithms tend to produce less accurate results [65-69]. In addition, large deformations can result in the computational mesh becoming twisted or developing negative volume elements which in both cases will cause the simulation to fail. In certain cases where unstructured meshes are used it is possible to work around this problem by performing frequent remeshing steps at regular intervals during the simulation [50-52,65-67,70].

4.5.2 Eulerian Formulation

The Eulerian description was developed to compensate for some of the shortcomings of the Langrangian description [50-52,65-67,70]. In the Eulerian description which is popular in modeling fluid mechanics, the computational mesh is fixed in space and the continuum moves with respect to the grid. The basic idea of this method is that

the modeler is solely interested in the physical quantities associated with only that portion of the moving continuum that is present within a given element at any given instant of time. For example, in fluid mechanics, one might be interested in the flow patterns and velocity of flow in a given region. In these cases, one does not need to follow the particles throughout the geometry as one is only interested in their behavior in a given region. The Eulerian algorithms are based on the conservation equations which are formulated in terms of spatial coordinates and time. As a result, the Eulerian description of motion only accounts for those variables and functions having an instantaneous significance in a fixed region of space. Deformations and distortions in the Eulerian method are defined relative to the deformed orientation of the continuum rather than the original orientation. The advantage of using the Eulerian method is that large deformations and distortions can be handled with ease. The disadvantages of this method include the fact that because the nodes of the computational mesh are dissociated from the material particles, convection effects must be accounted for. The non-symmetric character of the associated convection operators frequently causes numerical difficulties in these methods. Another drawback associated with the use of this method is that it is difficult to track and find interfaces between materials and mobile boundaries. This stems from the fact that the continuum moves through the mesh, meaning that at any given time a moving boundary will not always be in the same place. Further complications can also arise when the boundary lies within an element which means that at a given time, that particular element may contain two or more different materials that will need to be accounted for [50-52,65-67,70].

4.5.3 Arbitrary Lagrangian Eulerian (ALE) Formulation:

The Arbitrary Lagrangian Eulerian method was designed to take advantage of the best parts of both the Lagranagian and Eulerian methods while eliminating or minimizing the problems of each of these methods.[50-52,65-73] This method is designed to handle larger deformations than the ones that can be handled by the Lagrangian method while at the same time allowing for the tracking of interfaces and boundaries that is impossible in the Eulerian method. The main advantage of the ALE method is that the nodes of the computational mesh can either move with the continuum as they would in the Lagrangian description or be fixed as they would in the Eulerian description with the continuum moving through the fixed elements. In order to accomplish this, the ALE method does not use the undeformed or deformed configuration in order to define motion (deformations / distortion). Instead it uses a third configuration, referred to as the referential configuration. By defining the location based on the referential configuration, it is possible to relate motion to either the material (undeformed) or spatial (deformed) domain as required [50-52,65-73].

The ALE algorithms used to handle large deformation problems can be thought of as automatic rezoning algorithms[50-52,65-73]. Prior to the introduction of ALE algorithms, FEM problems involving large deformation had to be stopped at regular intervals in order to smooth the distorted mesh to prevent mesh entanglements and extreme distortions. The smoothing step had to be done manually by removing the distorted mesh and generating a new mesh for the deformed geometry while mapping the solution to the new geometry. The ALE algorithms handle these same problems by processing a Lagrangian time step, followed by a remap or an advection time step. During the advection step, an

incremental rezone is performed where the nodes of the mesh are moved a fraction of the characteristic length of the elements to which they are associated. In this advection step the topology of the mesh remains constant. The advantage of using ALE algorithms over manual rezoning algorithms lies in the fact that ALE algorithms are often more accurate as the ALE rezoning and remapping algorithms are second order accurate whereas the manual algorithms are only first order accurate[50-52,65-73].

It is during the advection step that the Eulerian calculations are also carried out since it is during this step that the amount of material transported between neighboring elements is calculated as is the momentum transport and the velocity of the nodes. The advection step usually dictates the computational cost of the solution as this step is usually much more computationally expensive than the Lagrangian step}. It is also during this step when most failures occur due to rezoning difficulties if no smooth mesh is possible due to the large deformations of the Lagrangian defined boundary mesh[50-52,65-73].

In terms of modeling SUI, each of the above formulations has pros and cons associated with it. The Lagrangian formulation would be the preferred formulation in regards to the tracking of the interfaces between the bladder wall, the urethra and the urine. However, the large deformations that the fluid must undergo when modeling incontinence and the large number of remeshing steps that would have to be incorporated make this formulation unsuitable for modeling the leakage of urine. The Eulerian formulation would allow for the modeling of the fluid deformations associated with urine leakage without the need for the remeshing steps, unfortunately, the difficulties arising from not being able to track the boundaries between the urine and the structures make

this formulation less than ideal in this case. This leaves the arbitrary Lagrangian Eulerian which has been the method of choice in the field for fluid structure interaction problems [65,66,69,70,72,74,75]. This method would allow for both the tracking of the fluid structure interfaces as well as the modeling of the large deformations associated with the leakage of urine. However, the remeshing steps associated with the pure ALE method would still present problems in this case as the automatic rezoning algorithms would not be able to reolve the large deformations of the fluid mesh necessary to model the fluid being forced into the urethra. As a result, a simplified form of the ALE method known as the operator split method which eliminates the need to perform the remeshing may provide a solution. This method has been used in the past to model similar situations such as the fluid structure interactions that occur during left ventricle contraction and to model blood flow in the aortic root where the large distortions of the fluid continuum also present difficulties in terms of the remeshing step used in traditional ALE methods. [61-64]

4.5.4 Operator Split Method

In the operator split method the Lagrangian mesh is embedded within an Eulerian mesh that is fixed in space meaning that the both the Lagrangian and Eulerian mesh are co-located within the same spatial domain. [61-64,70] Similar to the ALE method, a Lagrangian step is performed in which the deformation of the Lagrangian structures is calculated. This step is then followed by an Eulerian calculation or advection step in which the motion of the fluid that occurs in response to the calculated Lagrangian deformation is mapped onto the Eulerian mesh which does not move. The main difference between this method and the traditional ALE method is that during the

advection step, the Eulerian mesh does not move therefore there is no need for a remeshing or a mesh updating step.[61-64,70]

One of the main issues that arises from utilizing the operator split method is that there is no time step associated with the Eulerian steps of the solution[70]. The Eulerian step in this method serves only to project the solution of the Lagrangian mesh onto the Eulerian mesh. As a result, time only evolves in the Lagrangian step which due to the fact that an explicit solver is being used in this case is not fully second order accurate in time. This in turn indicates that the operator split method will generate a solution that is less than second order accurate[70]. However, due to the complex fluid structure interactions that must occur during SUI, it remains the most attractive option.

In LS Dyna the Lagrangian and Eulerian domains in the split operator method are coupled through the use of the penalty coupling method.[76-78] In this method, the materials defined by the Eulerian mesh are categorized as the master materials and the materials defined by the Lagrangian mesh as slave materials. During a time step after the nodal forces are calculated for both the structure and the fluid, fluid coupling forces are calculated at the fluid structure interface based on the predicted penetration of the slave material nodes into the master material elements. This can be thought of as assigning springs to couple the master and slave material to one another to resist the penetration of the slave material into the master material (Figure 4) by applying forces to return the penetrating slave material back to the interface between the two meshes. The magnitude of the coupling force is proportional to the depth of penetration with a higher resisting force being applied for a deeper penetration and is defined as follows

$$F = kd \qquad \text{Eq. 8}$$

Where F is the coupling force, k the spring constant and d the predicted depth of penetration of the slave material into the master material.

The spring stiffness is defined by the following equation

$$k = p_f \frac{KA}{V} \qquad \text{Eq. 9}$$

Where K is the bulk modulus of the fluid, A the area of the master segment, V the volume of the master element and p_f the scale factor for interface stiffness. The default value of p_f in LS Dyna 0.1.[76-78]

As the penalty coupling factor functions by coupling the Lagrangian and Eulerian meshes together through the use of springs there is the potential for numerical dissipation to occur at the interface due to the vibrations of the springs.[76-78] To compensate for this LS Dyna allows the user to specify the degree to which the coupling system is damped. Damping can range from a completely undamped system to a critically damped system.

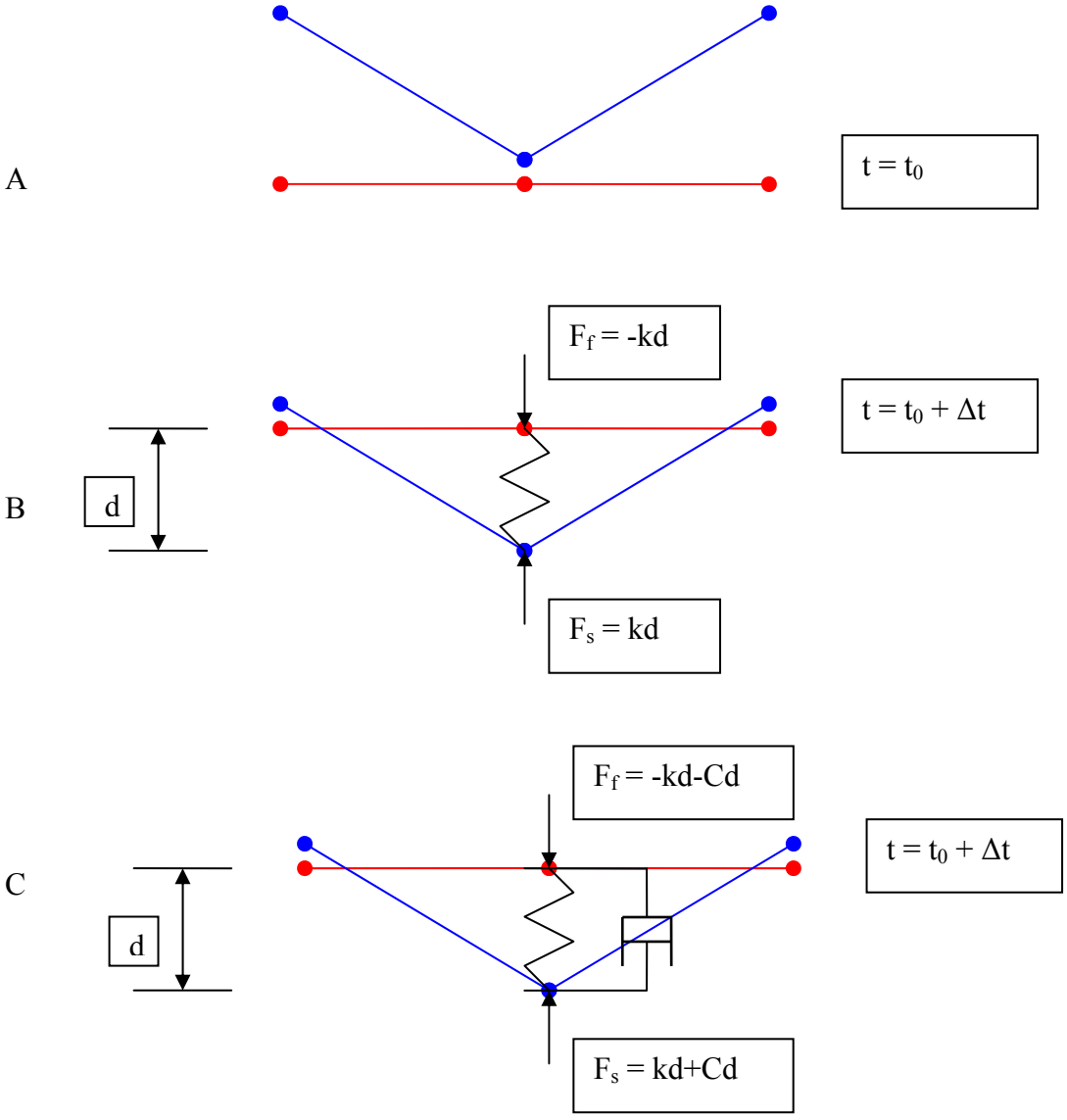

Figure 4: Schematic of Penalty Coupling Method. In the above drawing the blue structure represents the slave surface and red the master surface. A illustrates the undeformed configuration. B illustrates the penalty coupled surfaces in which the slave surface has penetrated the master where a spring has been added and the corresponding forces applied to return the slave node to the interface. C represents a damped version of the penalty coupling method

4.6 Material Properties

In continuum mechanics, the behavior of a continuum is often affected by the type of material that the continuum is composed of. FEM takes account for this by incorporating the material properties of the continuum into the interpolation functions that describe the distribution of the field variable across the element. In the case of deformation modeling in response to a load this typically involves fitting a mathematical relationship to an experimentally acquired stress strain curve [50-52].

As of this writing there have only been two studies that have published material property data specifically for the structures associated with the lower urinary tract and pelvic floor. Yamada, assumed that the constitutive relation is linearly elastic (Equation 10) and published a modulus of elasticity for several of the structures in Table I[48,79].

$$\sigma = E\varepsilon \qquad \text{Eq. 10}$$

Where σ = stress
E = modulus of elasticity
ε = strain

Table I: Published linear material properties of the structures of the lower urinary tract and pelvic floor. [79] (Note a Poisson's Ratio of 0.45 was assumed in this study)

Tissue	Modulus of Elasticity (E) (MPa)	Density (kg/m^3)
Bladder	0.05	1030
Urethra	0.3	1030
Uterus	0.05	1030
Vagina	0.005	1030
Rectum	0.1	1030
Intestine	0.1	1030
Muscle (contracted)	2.4	1040
Fascia	1.2	1010
Ligament	1.2	1010

Haridas et al also published material property data for several structures of the pelvic floor and lower urinary tract [49]. However, they did not assume linear elastic material properties for all structures. For certain structures, the Blatz Ko and Mooney Rivlin constitutive equations were assumed to define the material properties. In making this assumption, Haridas et al assumed that these structures were isotropic hyper-elastic materials, i.e. the materials are structurally uniform with no variation throughout the structure[49,80]. The mechanical properties of a hyper-elastic material are completely dependent on a scalar strain energy density function associated with the free energy per unit undeformed volume of the material (Equation 11).

$$s = \frac{\partial W}{\partial E} \qquad \text{Eq. 11}$$

Where s = Second Pioloa Kirchoff Stress Tensor
W = Strain Energy Density Function
E = Lagrangian Strain Tensor

Haridas et al used two different constitutive relationships Blatz Ko and Mooney Rivlin to describe hyper-elastic materials based on the results of their experiments [49]. The main difference between these two constitutive relations lies in the strain energy density function used to describe each material[80]. The strain energy density functions for a Blatz Ko and Mooney Rivlin type material are shown in equation 12 and 13 respectively.

$$W = \frac{\mu}{2}\left(\frac{I_2}{I_3} - 3 + \left(\frac{1-2\upsilon}{\upsilon}\right)\left(I_3^{\upsilon/1-2\upsilon} - 1\right)\right) \qquad \text{Eq. 12}$$

Where μ = Shear Modulus
υ = Poisson's Ratio
I_2 = Second Strain Invariant
I_3 = Third Strain Invariant

$$W = A(I_1 - 3) + B(I_2 - 3) \qquad \text{Eq. 13}$$

Where A = Experimentally Determined Constant
B = Experimentally Determined Constant
I_1 = First Strain Invariant
I_2 = Second Strain Invariant

Table II: Published linear and non-linear material properties for structures of the lower urinary tract and pelvic floor [49]. (Note a Poisson's Ratio of 0.45 was assumed in this study)

Tissue	Constitutive Equation	Constants
Vesico Vagina Layers	Blatz Ko	Shear Modulus (μ) 2.5kPa
Recto Vagina Layers	Blatz Ko	Shear Modulus (μ) 1.25 kPa
Bladder Wall	Mooney-Rivlin	Constant A: 7.5 kPa Constant B: 2.5 kPa
Rectum	Linearly Elastic	Modulus of Elasticity (E) 900 kPa
Uterus	Linearly Elastic	Modulus of Elasticity (E) 50 kPa
Urethra	Blatz Ko	Shear Modulus (μ) 100 kPa

In this study urine was defined as an elastic fluid and assumed to have material properties of water. The modeled mechanics of the elastic fluid are determined by the bulk modulus (K) of the material which was set to 2.2 x 10^9 Pa for all models presented in this dissertation.[81,82]

CHAPTER V

MODELING THE BLADDER AND URETHRA DURING A CONTINENT COUGH

One of the main challenges faced in constructing a model of the lower urinary tract and pelvic floor is the lack of sufficiently detailed material properties of the relevant tissues due to the extreme difficulty in acquiring in-vivo values.[48,49] Therefore, the main goal of the first objective was to validate a simplified finite element model with clinical urodynamic data of a subject coughing and use it to determine the effects of variations in material properties.

5.1 Methods

5.1.1 Urodynamics

Following IRB approval, urodynamic data was obtained from six continent women between the ages of 28 and 79 during coughs at maximum cystometric capacity. Maximum Cystometric Capacity is defined as the maximum valume of fluid a patient can

store within their bladder with out having to void. To be included in this study, the women had to have no history of incontinence, pelvic floor surgery, or neuromuscular disease. Women were also excluded from the study if they had given birth vaginally within six months prior to the urodynamic testing. Cystometry was performed using sterilized water at a fill rate of 80 mL/min with the subject in a birthing chair reclined at 45 degrees until the patient's maximum cystometric capacity was reached. To estimate abdominal pressure (Pabd), an 8 French micro tipped catheter (Millar Instruments, Houston, Texas) was placed in the subject's vagina. Urethral pressure profilemetry was performed through the use of an 8 French dual-micro tipped catheter with an infusion port (Millar Instruments, Houston, Texas). Urethral pressure profiles (UPP) were acquired by initially placing the catheter so that both tips were located within the bladder, once inserted; the catheter was then withdrawn at a rate of 1 mm per second with pressure measurements being acquired at 0.2 second intervals (Figure 5). The catheter was then reinserted so that the distal tip was located within the bladder to measure vesical pressure (Pves) and the proximal tip was located within the urethra at the position corresponding to the maximum urethral pressure measured during the UPP facing the 9 o'clock position to measure the urethral pressure (Pura). Abdominal, vesical and urethral pressure data were then acquired at 0.2 second intervals both while the patient was at rest and during cough and valsalva events (Figure 6).

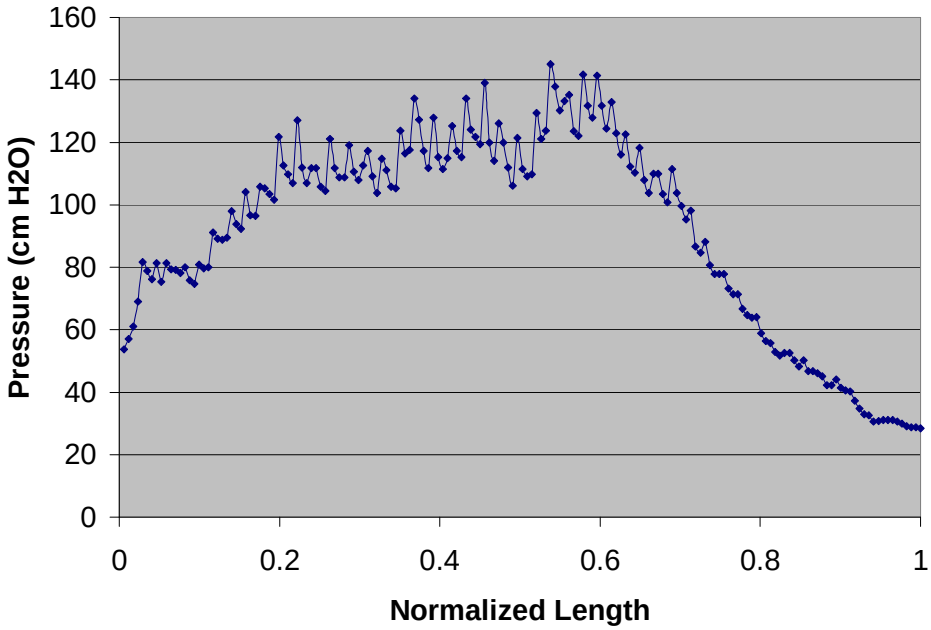

Figure 5: Example of a UPP obtained from a 28 year old continent female. Normalized length = 0 corresponds to the location where the urethra attaches to the bladder. Normalized length =1 corresponds to the urethral outlet. Pressure readings were acquired at 0.2 s intervals as the catheter was withdrawn at a rate of 1mm/s (Urethral Length = 34 mm).

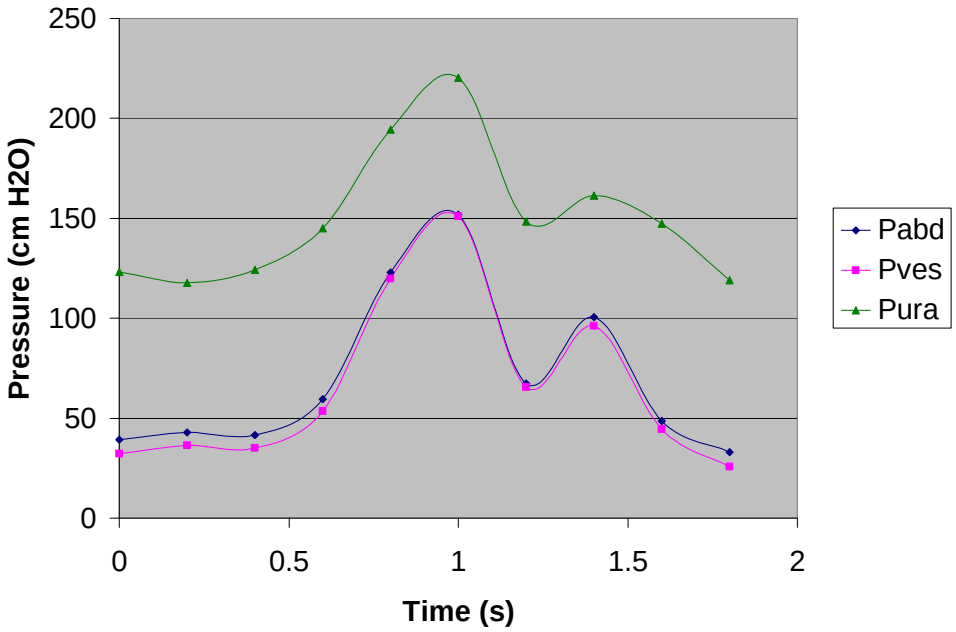

Figure 6: Example of urodynamic pressure measurements acquired during a 1.8 second cough in a 28 year old patient at maximum cystometric capacity (536 mL) (Blue = Pabd, Pink = Pves and Green = Pura)

5.1.2 MODELING

The initial model for this study incorporated urodynamic data including Pabd and Pves obtained from a 28 year old continent subject during a 1.8 second cough (Figure 7). This initial model was then used to determine both which set of material properties (linear or non-linear) when incorporated in the model would result in the most accurate prediction of Pves and what effect varying these material properties would have on the predicted Pves. Once the material properties that produced the most accurate prediction of Pves were identified, an additional 5 models were constructed utilizing urodynamic data from 5 additional patients to test whether the results obtained in the original model could be replicated in these additional models.

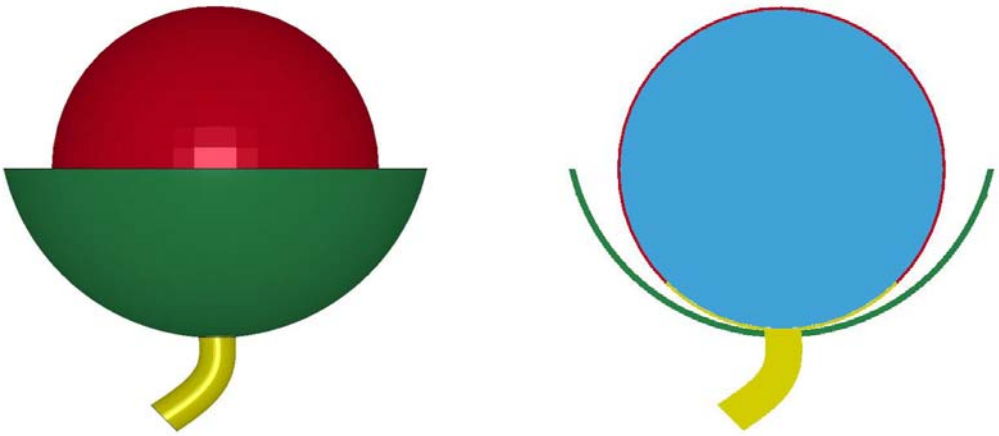

Figure 7: FEM model based on urodynamic data acquired from a 28 year old continent female (Right). Cross Section of Model (Left) Patient Specific Dimensions: Bladder ID = 100.8mm, Bladder OD = 102.6mm Urethra Length = 34mm

Several simplifying assumptions were made to create the geometry of the models. The bladder was modeled as a sphere, consistent with several previous studies that have also used a spherical shape to study the mechanics of the bladder.[36-38,83-86] In the initial model, the inner diameter of the bladder was set to 100.8 mm, based on the maximum

cystometric capacity of 536 mL for this subject, at which the cough occurred. The thickness of the wall was calculated based on the findings of Chan et al, who found that in a cohort of 42 women with normal urodynamics, the average bladder wall thickness was 1.7mm when 200 cc of fluid was contained within the bladder.[87] We utilized this finding by assuming bladder wall material is incompressible, as has been assumed in previous bladder models giving a wall thickness of 0.9 mm at a volume of 536 mL in the initial model.[38,47] In the five additional models used to validate the findings of the initial model, the bladder inner diameter ranged between 92.2 mm and 108 mm (mean 98.6 mm, std dev = 7.3 mm) while the outer diameter ranged between 94.2mm and 109.6 mm (mean 100.5 mm, std dev = 7.1 mm). The bladder wall thickness in these models ranged between 1.6 mm and 2.0 mm (mean = 1.9 mm, std dev = 0.18 mm).

To simplify the geometry of the urethra, it was modeled as a cylindrical tube, as has been done in several other studies.[40-42,45,84-86] The outer diameter was set to 11.5 mm based on sagital measurements published by Umek et al.[88,89] The length of the urethra was determined based on the UPP obtained during individual urodynamic testing and in the initial model was set to 34 mm. In the additional validation models the urethral length ranged between 15.8 mm and 39.8 mm (mean 27.9 mm, std dev = 10.8 mm). Since the subjects utilized for this study were continent, the assumption was made that in continent patients all of the urine remains in the bladder at all times. This allowed the geometry to be simplified by not including a lumen in the urethra.

The support structure through which the urethra passes and on which the bladder rests was assumed to be bowl-shaped based on drawings observed in anatomy text books.[14,90] The dimensions of the bowl were based on the dimensions of the pelvic inlet

determined by Janda et al who reported the pelvic inlet to be elliptical in shape with a long axis dimension of 140 mm and a short axis dimension of 122 mm.[91] To further simplify the geometry, a circular shape was adopted by taking the average of the two axis values and setting the diameter of the top rim of the support structure to 131mm. The outlet of the bowl was set to be equal to the diameter of the urethra to prevent excessive movement of the urethra. As an initial approximation, the thickness of the bowl was set to 2 mm to equal the thickness of the levator ani muscle reported by D'Aulignac et al.[92] These dimensions were used in all models in this study.

All structures were represented in the models as a mesh of solid eight node hexahedral elements with the exception of the fluid which was represented using eight node hexahedral elastic fluid elements, allowing the fluid to be treated as a quasi solid whose deformation is determined by the bulk modulus of the liquid (Table III).[81,82] All meshes were created using the commercially available software package TrueGrid (XYZ Corporation Livermore, CA).

Table III: Mesh Density

Structure	# of Elements
Bladder	2,880
Fluid	12,096
Bladder Neck and Urethra	26,784
Support Structure	15,488

To prevent rigid body translation, boundary conditions were applied to completely constrain the rim of the support structure and the walls of the urethral orifice. To simulate the support of the vagina, the distal two-thirds of the urethra were also constrained for translation in all axes as well as for rotation about the z-axis. Contact of the bladder, the bladder base, the urethra with the support structure was modeled using a

surface to surface contact algorithm provided with the LS Dyna FEM modeling software that allowed the materials to come into contact and continue deform while preventing the sliding of the materials relative to one another (LSTC Corporation, Livermore California).[81,82]

To date, two sets of material properties one linear, the other nonlinear are available for the bladder and urethra through the work of Yamada and Haridas et al respectively.[49,79,93] Through an inverse finite element model Haridas et al determined that the mechanical behavior of the bladder and urethra can be characterized using hyper-elastic constitutive equations as described in Chapter IV with the bladder being described as a Mooney Rivlin material and the urethra as a Blatz Ko material.[49] Both sets of material properties were evaluated by constructing two versions of the initial model that were identical in every other aspect except the structural material properties assigned to the bladder and the urethra. Due to the fact that neither Haridas nor Yamada published information regarding the Poisson's ratio, a Poisson's ration of 0.45 was assumed for all materials where this value was necessary to fully define the material properties

5.1.3 Simulations

Each model was loaded by applying pressure loads to the top hemisphere of the bladder that corresponded with the rise in Pabd relative to its baseline (Figure 8). Each of the 6 models used in this study was loaded based on a cough event that was recorded for each individual patient. It was assumed in this study that the rise in bladder pressure observed during a cough resulted solely from increased abdominal pressure that occurred in the absence of bladder contractions.

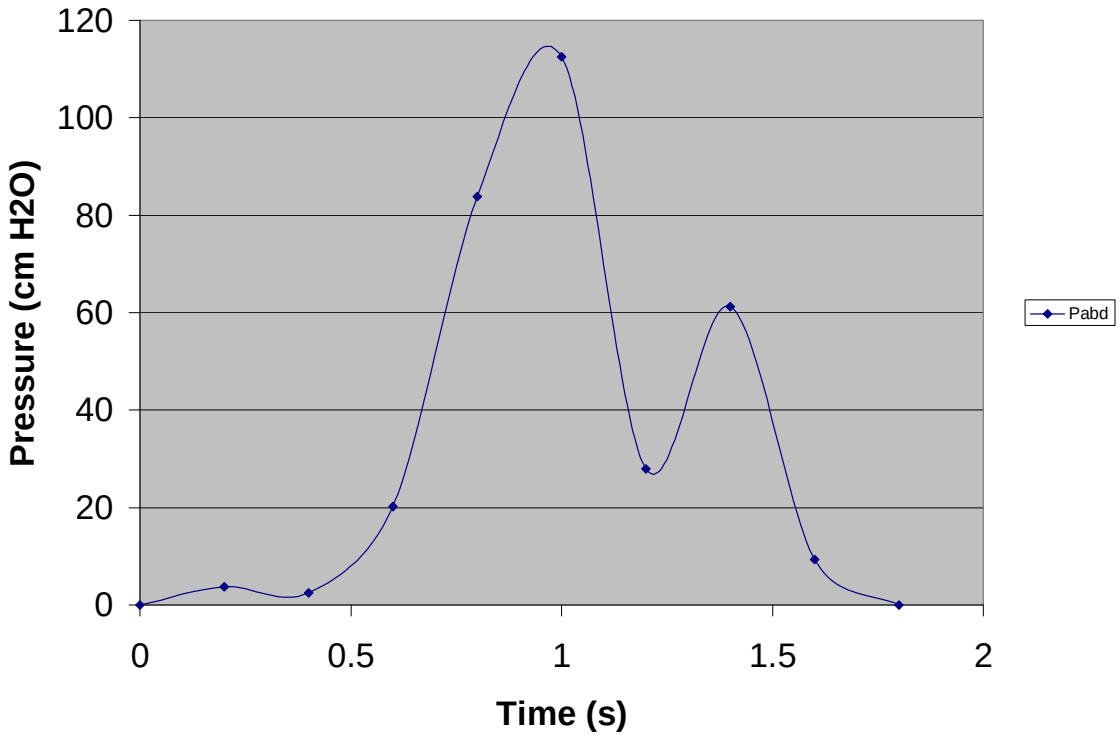

Figure 8: Pabd Loads acquired from the same 28 year old continent patient as modeled in Figure 7, during a cough event and normalized to baseline

Comparison of the two material property sets was performed by comparing Pves measured during urodynamics to the Pves predicted by the model by taking the average of the pressure predicted in four elements located at the center of the model when non-linear and linear material properties were incorporated. To further evaluate the effects of the material properties on the vesical pressure predicted by the model, a series of simulations were run in which the materials incorporated in these two models were made more compliant or more stiff by either decreasing or increasing the coefficients by which the material properties were defined by a factor of 0.75 or 2.0 respectively (Tables IV & V). The effects of these changes was evaluated by comparing the resultant Pves and resultant displacements to the Pves and displacements predicted by the models using published data. All models were solved using the explicit finite element solver LS Dyna

(Livermore CA) on a IBM Cluster 1350 Super Computer (Ohio Super Computing Center Columbus, OH) using the equivalent of 20 processors for each simulation.

Table IV: Simulation Details

Simulation	Description
A	Published Values used for all Structures
B	Stiff Bladder Wall
C	Stiff Support Structure
D	Stiff Urethra & Bladder Neck
E	Compliant Bladder Wall
F	Compliant Support Structure
G	Compliant Urethra & Bladder Neck
H	Stiff values used for all structures
I	Compliant values used for all structures

Table V: Material Properties Used in Non-Linear and Linear Models[49,79]
(Density of Materials defined in Table I, Poisson's Ratio = 0.45)

Structure	Material Type (Non-Linear Models)	Constants(Non-Linear Models)	Constants (Linear Models)
Bladder (Published)	Mooney Rivlin	A=7500 B=2500	E = 5e4 Pa
Bladder (Stiff)	Mooney Rivlin	A=15000 B=5000	E = 1e5 Pa
Bladder (Compliant)	Mooney Rivlin	A=3750 B=1250	E = 3.75e4 Pa
Support Structure (Published)	Linear Elastic	E = 5e6 Pa	E = 5e6 Pa
Support Structure (Stiff)	Linear Elastic	E = 1e7 Pa	E = 1e7 Pa
Support Structure (Compliant)	Linear Elastic	E = 3.75e6 Pa	E = 3.75e6 Pa
Urethra & Bladder Neck (Published)	Blatz Ko	μ = 1e5 Pa	E = 5e6 Pa
Urethra & Bladder Neck (Stiff)	Blatz Ko	μ = 2e5 Pa	E = 1e7 Pa
Urethra & Bladder Neck (Compliant)	Blatz Ko	μ = 7.5e4 Pa	E = 3.75e6 Pa
Urine	Elastic Fluid	K = 2.2e9 Pa	K = 2.2 e9 Pa

To test the repeatability of the model, 5 additional models were constructed utilizing the urodynamic data from 5 additional patients as described earlier (Table VI). In each case a cough was simulated (Figure 9) and the model evaluated by comparing Pves predicted by the model to Pves measured during urodynamic testing . Non-linear material properties were used in these models since our initial results demonstrated that the predicted Pves in models incorporating these material properties more closely replicated the measured Pves in the initial models.

Table VI: Model details for 5 additional subjects

Subject	Subject Age	Bladder ID (mm)	Bladder OD (mm)	Urethra Length (mm)	Type of Event	Duration of Event (s)
1	71	108	109.6	15.8	Cough	2.0
2	38	92.6	94.6	35.3	Cough	1.4
3	79	92.2	94.2	17.2	Cough	1.6
4	29	95.6	97.6	31.2	Cough	1.8
5	28	104.8	106.6	39.8	Cough	1.8

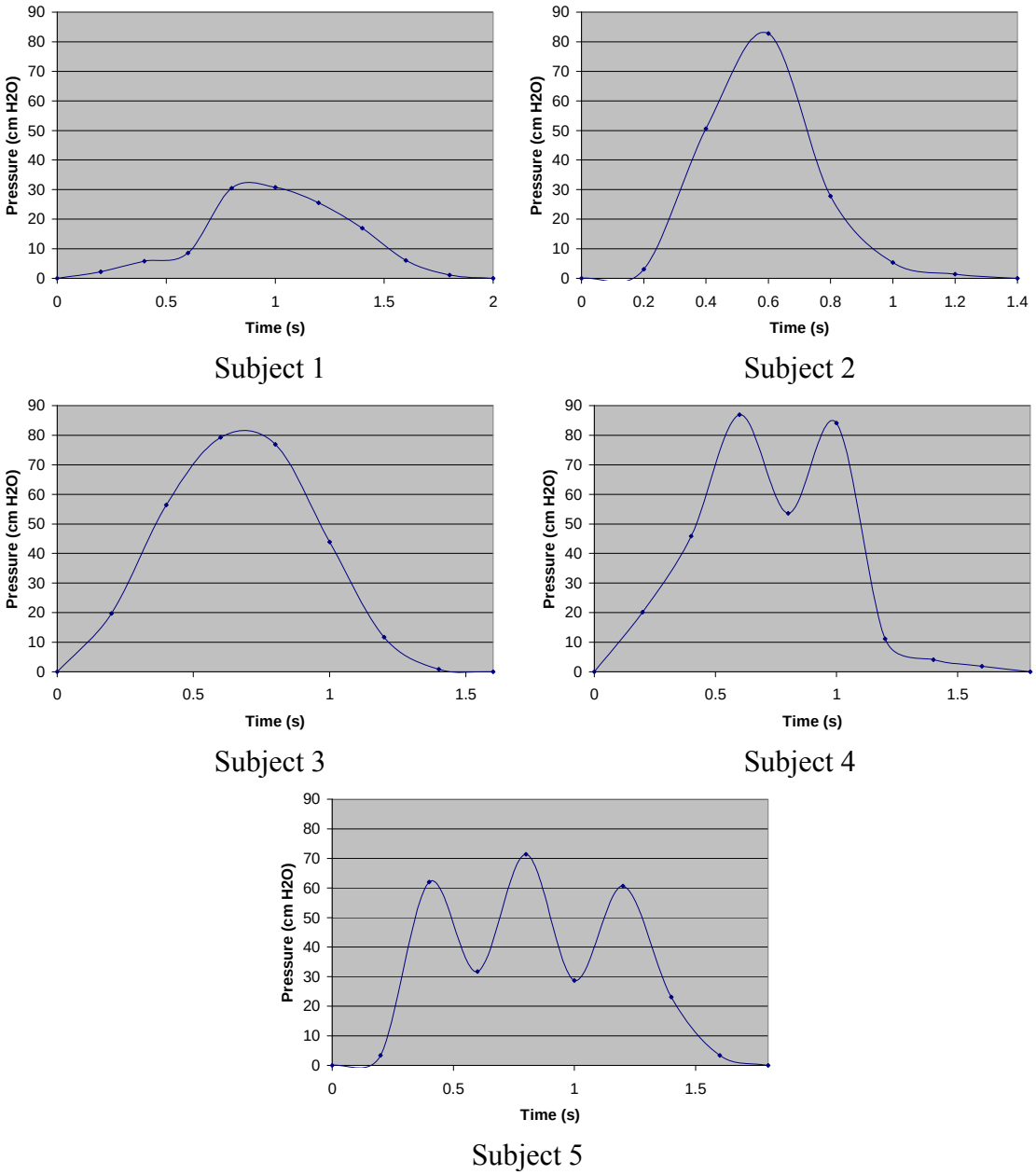

Figure 9: Abdominal Pressure load curves corresponding to the cough event modeled for each of the subjects detailed in Table VI.

5.2 RESULTS

The initial model used to compare the effects of incorporating linear and non linear material properties generally underestimated Pves compared to the measured values of Pves when either set of material properties were incorporated into the model

(Table VII). In the two instances in which Pves was overestimated in the non-linear model and the one instance of overestimation in the linear model, Pves was only overestimated by less than 1 cm H2O. Pves predicted by the model incorporating published non-linear material properties was in closer agreement with measured Pves than those predicted by the model incorporating published linear material properties and never differed by more than 5 cm H2O (Table VII). The least difference between measured and predicted values of the non-linear model was 0.19 cm H2O, which occurred at 0.6s; whereas the greatest difference was -4.63 cm H2O, occurring at 1.0s, the time of peak abdominal pressure (Table VII). In contrast in the model incorporating linear material properties the least difference between predicted and measured Pves was -0.28 cm H20 which occurred at 0.2s while the greatest difference was -7.2 cm H2O which occurred at 0.8s (0.2s prior to peak abdominal pressure).

Table VII: Effect of non-linear and linear material properties on the difference between predicted Pves and measured Pves (Pressure and differences in cm H2O, RMS = Root Mean Squared)

Time (s)	Measured	Predicted Non-Linear	Difference	Predicted Linear	Difference
0.2	36.3	35.6	-0.7	36.0	-0.3
0.4	35	34.3	-0.7	34.6	-0.4
0.6	53.6	53.8	0.2	52.0	-1.6
0.8	119.7	117.4	-2.3	112.4	-7.2
1	151.1	146.5	-4.6	144.4	-6.6
1.2	65.5	61.9	-3.6	60.7	-4.8
1.4	96.1	93.9	-2.2	94.0	-2.1
1.6	44.4	43.1	-1.3	41.8	-2.6
1.8	32.2	32.6	0.4	32.8	0.6
RMS			2.3		3.8
Maximum			-4.6		-7.2
Minimum			0.2		-0.3

Changes in material properties in the initial non-linear model produced changes less than 5.0 cm H2O in the predicted Pves in all simulations at all time points The greatest changes came from increasing compliance of the bladder wall (Simulation E) (Table VIIII). Varying linear material properties in the initial model resulted in increasing the predicted Pves from between 3.0 to 8.2 cm H2O at the 0.8s time point. However, these large increases were limited to this time, since at all other times these changes resulted in Pves changes of less than 2 cm H2O. The largest changes in Pves predicted by the initial linear model were realized by stiffening the bladder neck and urethra (Simulation D) and by stiffening the material properties of all modeled structures with the exception of the liquid (Simulation H) (Table IX).

Table VIII: Effect of varying non-linear material property parameters on predicted Pves. (Pressure Differences in cm H2O compared to Pves predicted by model incorporating published non-linear material properties)

Simulation Time (s)	B	C	D	E	F	G	H	I
0.2	-0.2	0.0	0.2	0.1	-0.2	0.3	-0.3	0.0
0.4	0.6	-0.4	0.2	0.0	-0.2	0.2	-0.1	-0.1
0.6	-1.8	-0.5	1.2	-0.5	-0.6	1.1	0.7	-0.7
0.8	-0.5	-0.5	-2.5	5.0	-3.1	-0.8	1.9	1.5
1.0	0.1	-0.8	0.4	-0.9	-0.4	-2.1	4.5	0.7
1.2	-1.4	0.0	-0.6	1.4	1.1	-0.6	-0.5	-0.9
1.4	0.7	0.5	-1.6	0.3	-0.4	0.3	2.8	-1.9
1.6	-0.7	-0.8	0.0	0.8	0.7	-0.9	0.1	-0.5
1.8	-0.1	0.1	0.0	-0.4	0.5	-0.5	0.3	-0.1
RMS	1.4	1.6	1.3	0.9	1.2	0.9	1.0	1.7
Maximum	-1.8	-0.8	-2.5	5.0	-3.1	-2.1	4.5	1.5
Minimum	0.1	0.0	0.0	0.0	-0.2	0.2	0.1	0.0

Table IX: Effect of varying linear material property parameters on predicted Pves. (Pressure Differences in cm H2O compared to Pves predicted by model incorporating published linear material properties)

Simulation Time (s)	B	C	D	E	F	G	H	I
0.2	-0.5	0.0	-0.5	-0.1	0.1	-0.2	-0.9	-0.3
0.4	0.0	0.1	0.2	0.1	0.1	0.0	0.4	0.1
0.6	0.9	1.8	-0.3	0.3	-0.3	-0.4	0.1	0.2
0.8	5.8	4.5	8.2	3.9	4.4	3.0	8.2	4.1
1	0.2	-1.7	-0.3	1.9	1.4	1.7	-0.4	-1.2
1.2	0.8	-0.6	0.1	-1.6	-0.7	0.1	-0.5	-1.4
1.4	-0.1	0.0	-1.1	-0.1	-1.7	-1.1	1.0	-0.3
1.6	0.0	0.3	0.2	0.2	-0.1	0.2	0.1	0.9
1.8	0.1	0.1	-0.3	-0.1	0.1	-0.0	-0.1	0.0
RMS	2.0	0.7	2.8	1.6	1.7	1.2	2.1	1.5
Maximum	5.8	4.5	8.2	3.9	4.4	3.0	8.2	4.1
Minimum	0.0	0.0	0.1	0.1	0.1	0.0	0.1	0.1

In all simulations involving non-linear material properties, resultant displacements in all structures was less than 2cm (Figure 10). The overall distribution of displacement was also similar in all simulations. However, notable differences in displacement distribution were observed when the compliance of the support structure was increased (Simulation F) and when all structures were made more compliant (Simulation I). In both cases, there is an asymmetric increase in deformation toward the anterior side of the bladder (Figure 10). This increased deformation is also observed, though not as extreme, in the simulations in which the bladder was stiffened (Simulation B) or the bladder neck and urethra were made more compliant (Simulation G). Similar results were also noted in simulations involving linear material properties in which the resultant displacement in all structures was 2cm or less (Figure 10). The overall displacement distribution was also similar in all simulations. Reduced displacement was observed in the simulations in which the support structure was stiffened (Simulation C)

as well as in the simulation where all structures were stiffened (Simulation H). In both of these cases, displacement in the center of the top half of the bladder was reduced.

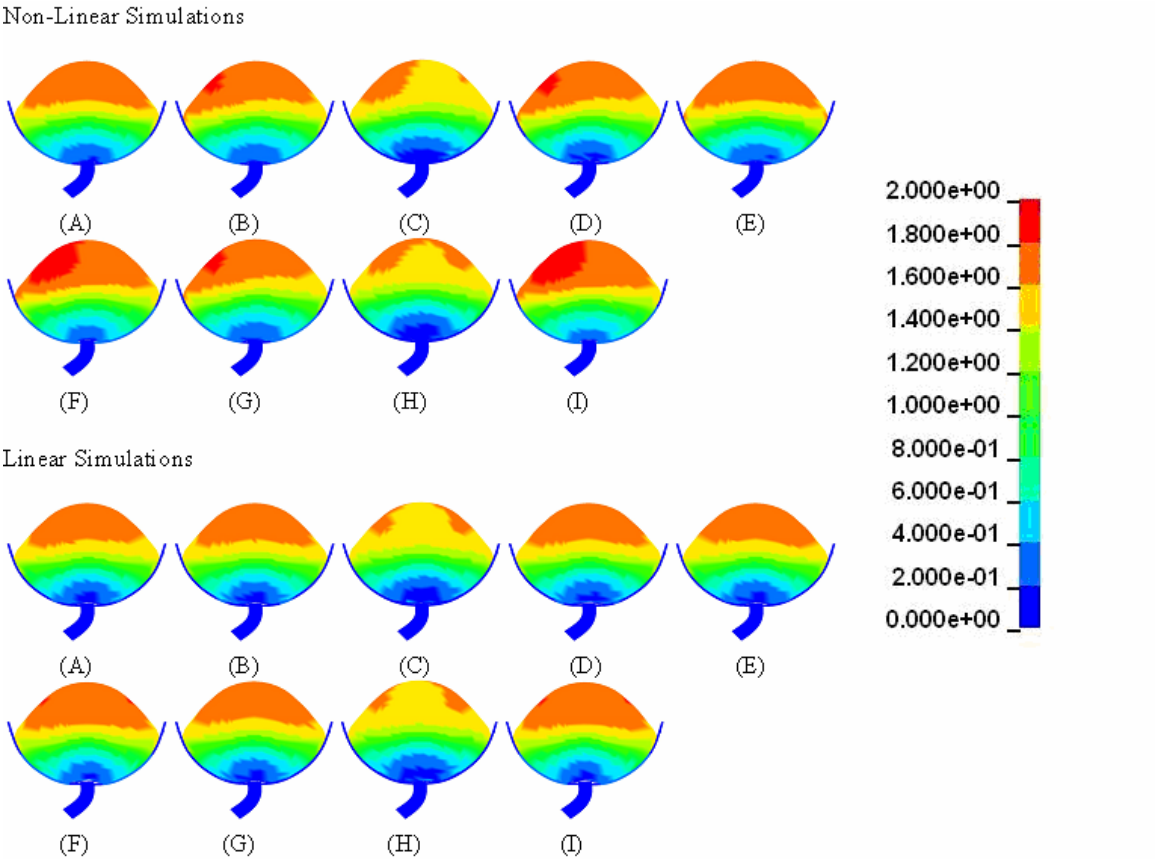

Figure 10: Displacements at peak abdominal pressure in models incorporating non-linear material properties (top) and linear material properties (bottom). Letters denote simulation parameters identified in Table 1. (Displacements in centimeters)

In addition, similar results were obtained in the models generated using urodynamic data from 5 additional subjects incorporating published non-linear material properties. In all models the maximum difference between predicted Pves and measured Pves was less than 6.2 cm H2O, with 3 out of the five producing maximum differences of 3.3 cm H2O or less (Table X). In the two cases in which the difference between measured Pves and predicted Pves exceeded 5 cm H2O the time of this difference

corresponded to an increase in detrusor pressure (Pves-Pabd) which would indicate a small bladder contraction that was not incorporated in the model. Deformation distribution was similar in all models with maximum displacements of less than 2cm in all models. Figures 11-15 and Tables XI – XV provide detailed results of the Pves and displacements predicted by these models.

Table X: Maximum and Minimum Pressure Differences between predicted and measured Pves (cm H2O)

Subject	RMS	Maximum	Minimum
1	1.3	3.3	-0.1
2	3.7	5.9	1.2
3	1.6	-2.4	0.5
4	1.1	1.6	0.4
5	3.1	-6.2	0.2

Subject #1 Results

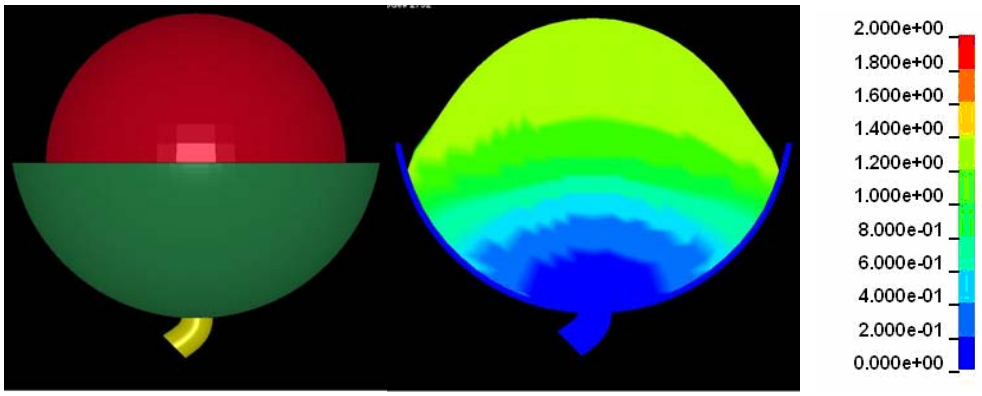

Figure 11: Model of subject 1 in undeformed configuration (Left). Cross section of model in deformed configuration at peak pressure illustrating resultant displacements in centimeters (Right)

Table XI: Comparison of predicted Pves to Measured Pves for Subject 1

Time (s)	Measured Pves (cm H2O)	FEM Pves (cm H2O)	Difference (cm H2O)	Detrusor Pressure (cm H2O)
0.2	36.6	36.6	0	1
0.4	38.6	38.5	-0.1	0.7
0.6	42.2	41.8	-0.4	0.7
0.8	45	45.4	0.4	0.7
1	65.8	67.5	1.7	-0.2
1.2	67.2	66.8	-0.4	0.7
1.4	60.2	63.5	3.3	-0.8
1.6	53	53.4	0.4	0.5
1.8	42.5	43.0	0.5	0.7
2	37.2	37.8	0.6	0.5

Subject #2 Results

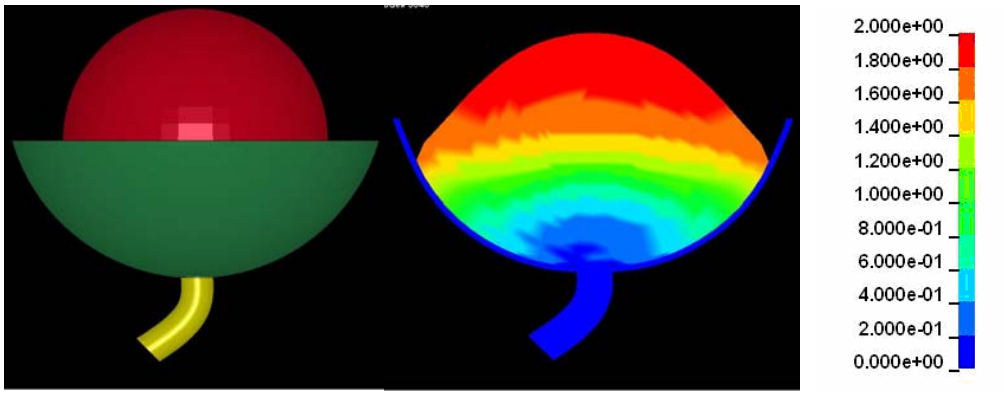

Figure 12: Model of Subject 2 in undeformed configuration (Left). Cross section of model in deformed configuration at peak pressure illustrating resultant displacements in centimeters (Right).

Table XII: Comparison of predicted Pves to Measured Pves for Subject 2

Time (s)	Measured Pves (cm H2O)	FEM Pves (cm H2O)	Difference (cm H2O)	Detrusor Pressure (cm H2O)
0.2	38.6	38.6	0	0.5
0.4	40.5	41.7	1.2	-0.5
0.6	83.3	89.1	5.8	-5.2
0.8	114.7	120.6	5.9	-6.1
1	63.9	66.4	2.5	-1.9
1.2	42.5	44.3	1.8	-0.7
1.4	38.3	40.3	2.0	-1.1

Subject #3 Results

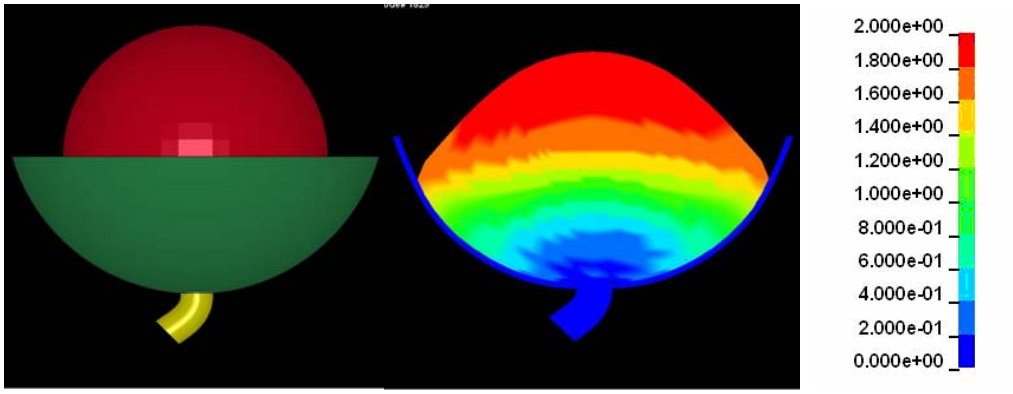

Figure 13: Model of Subject 3 in undeformed configuration (Left). Cross section of model in deformed configuration at peak pressure illustrating resultant displacements in centimeters (Right).

.

Table XIII: Comparison of predicted Pves to Measured Pves for Subject 3

Time (s)	Measured Pves (cm H2O)	FEM Pves (cm H2O)	Difference (cm H2O)	Detrusor Pressure (cm H2O)
0.2	22.6	22.6	0	-1.6
0.4	42.8	42.2	-0.6	-1.1
0.6	79.3	81.3	2.0	-1.2
0.8	103.1	100.7	-2.4	-0.3
1	101.7	103.3	1.6	0.5
1.2	69.5	70.0	0.5	1.4
1.4	36.5	34.4	-2.1	0.5
1.6	25.3	24.2	-1.1	0.2

Subject #4 Results

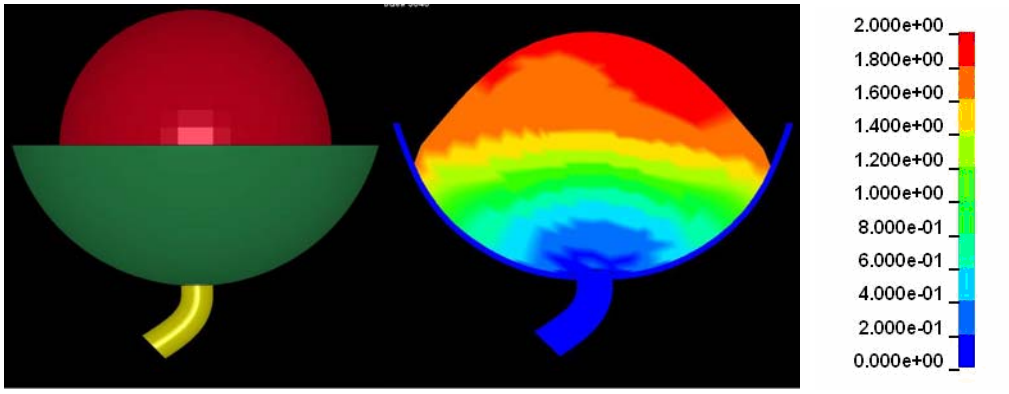

Figure 14: Model of Subject 4 in undeformed configuration (Left). Cross section of model in deformed configuration at peak pressure illustrating resultant displacements in centimeters (Right).

Table XIV: Comparison of predicted Pves to Measured Pves for Subject 4

Time (s_	Measured Pves (cm H2O)	FEM Pves (cm H2O)	Difference (cm H2O)	Detrusor Pressure (cm H2O)
0.2	20.5	20.5	0	-3.3
0.4	39	40.6	1.6	-5
0.6	67.1	67.9	0.8	-2.5
0.8	108	108.7	0.7	-2.8
1	75	75.4	0.4	-2.5
1.2	106.4	105.6	-0.8	-1.5
1.4	33.9	32.7	-1.2	-1
1.6	25.9	24.8	-1.1	-2.1
1.8	23.5	22.8	-0.7	-2.2

Subject #5 Results

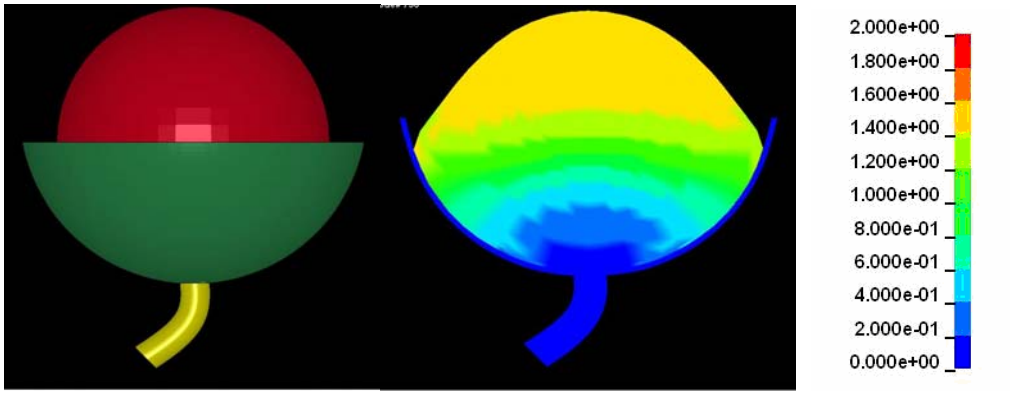

Figure 15: Model of Subject 5 in undeformed configuration (Left). Cross section of model in deformed configuration at peak pressure illustrating resultant displacements in centimeters (Right).

Table XV: Comparison of predicted Pves to Measured Pves for Subject 5

Time (s)	Measured Pves (cm H2O)	FEM Pves (cm H2O)	Difference (cm H2O)	Detrusor Pressure (cm H2O)
0.2	25.2	25.2	0	8
0.4	29.1	28.6	-0.5	8.5
0.6	90	86.9	-3.1	10.8
0.8	58	57.2	-0.8	9
1	100.2	94.0	-6.2	11.5
1.2	55.7	53.9	-1.8	9.7
1.4	85.7	86.0	0.3	7.8
1.6	49.8	47.8	-2.0	9.5
1.8	28.9	29.1	0.2	8.2

5.3 Discussion

In this work, a simplified model of the bladder, urethra, and support structures was used to determine the feasibility of using clinical urodynamic measurements and FEM to simulate the mechanics of these structures during a cough. The goals of this work were to determine if such a model could reproduce urodynamically measured

vesical pressures during a cough event in a continent subject and what effect if any altering the material properties of the model structures would have on predicted vesical pressures. In reality, the female pelvic floor and lower urinary tract are made up of complex structures that are not well characterized from a biomechanical modeling perspective. Most published descriptions of the geometry of these structures are qualitative in nature, focusing on the shape and location of each structure while providing minimal quantitative descriptions of the geometry.[5-11,15,16,25,27,31-33,89,94-100]. Therefore several simplifying assumptions were incorporated into the FEM models.

Three major simplifying assumptions were made with regard to model geometry. Two of these assumptions, the assumption to model the bladder as a sphere and the assumption to model the urethra as a tube have been previously validated. The impact of the spherical bladder shape assumption was studied by Damaser and Lehman, who found that the shape of the bladder was not as important as the mechanical properties of the bladder wall when modeling its mechanics.[38] The assumption to model the urethra as a tube was validated by Bush et al who compared a straight tube model of the urethra to a patient specific model of the urethra and noted minimal differences in the pressure and flow data collected from the two models.[95] Unlike the previous assumptions, the assumption to model the support structure as a bowl has not been validated. The bowl shape geometry was chosen based on drawings of the levator ani muscle and pelvis found in anatomy text books which show that these two structures form a bowl-like shape inside which the bladder rests. [14,90]

This study found that the Pves predicted by the non-linear model more closely matched the Pves measured during urodynamic testing than Pves predicted by the linear

model; however, the difference between predicted and measured Pves never exceeded 8 cm H2O in either model. Biological tissues are known to exhibit non-linear behavior when subjected to outside forces as a result, this outcome was not unexpected as one would assume that the non-linear material properties would more closely replicate the in-vivo behavior of the tissues manifested in the urodynamic measurements.[80,101]

To further investigate the effects of the non-linear and linear material properties on predicted Pves, the material properties in the two initial models were stiffened or made more compliant as described earlier. Varying material properties between 0.75 times and 2.0 times the published values resulted in mean changes to the predicted Pves of less than 1 cm H2O. These results suggest that material properties have minimal impact on Pves predicted by the model. As a result, the models cannot be described as singular when predicting Pves as similar predictions can be obtained with models incorporating different parameters. When coupled with the finding that varying the material properties of the bladder and urethra resulted in differences in deformation patterns predicted by the models, it becomes clear that Pves cannot be used as the sole validation criteria for these models and must be used in conjunction with other validation criteria. However, insensitivity of the predicted Pves to changes in material properties may prove beneficial in evaluating more complex models of the pelvic floor and lower urinary tract such as when studying SUI as this parameter can be utilized in the early stages of model construction to evaluate whether the model is adequately constructed and loaded based on the differences between the predicted Pves and the measured Pves.

The finding that varying the material properties of the model did not appreciably affect the quantitative displacements predicted by the model is in agreement with the

findings of Chi et al who found that increasing or decreasing the linear material properties of the bladder wall did not significantly affect the deformation of the bladder wall in their FEM models studying image guided adaptive radiotherapy.[39] In this study, it was reported that increasing or decreasing the linear material properties of the bladder wall by 30% did not significantly affect deformation of the bladder wall. However, significant differences exist between the two studies. Chi et al assumed that the bladder wall was transversely isotropic whereas in this study the bladder wall is assumed to be fully isotropic. Another major difference stems from the fact that in this study, the bladder is assumed to be completely filled with water at all times which differs from Chi et al's study in which the bladder was assumed to be a hollow structure. [39]

Although, there have been several other studies of the mechanics of the bladder and urethra, most have tended to focus on studying the bladder during filling or during micturition.[38,38,42,42-46,83-86,99,102] Very little has been published regarding the modeling of the bladder, in a passive situation during which outside forces act on the bladder such as during a cough. In a recent paper published by Zhang et al that did focus on modeling the mechanics of the bladder and urethra during such a situation, the bladder is shown to undergo what qualitatively appear to be large displacements when the modeled subject lands a jump.[48] A qualitative comparison indicates that even though two different events were modeled the displacement patterns observed in both models were similar, with the maximum displacements in both models occurring in the top portion of the bladder dome with only minimal displacements occurring in the region of the bladder neck and in the body of the urethra.[48]

In a dissertation published by K.Y. Kim at the University of Michigan at Ann Arbor, a cough was modeled in a 2 dimensional axis-symmetric model of the lower urinary tract, pelvic floor, and support structures in order to evaluate the Pressure Transmission Theory[47]. Several differences exist between the model presented in his work and the one presented in this dissertation due to advances in computers and in FEM software. These advances have allowed for a three dimensional model to be constructed and the entire cough to be modeled as a dynamic event and not just at baseline and max pressure points of the cough which was a necessary limitation at the time. In addition these advances allowed Pabd to be incorporated as an applied load and Pves to be developed as a result of this load in the present work. In Kim's model it was necessary to assume Pves was equal to Pabd and apply the Pves directly as a load to the interior wall of the bladder.[47] It should be noted that Kim's model was used to model the development of Pura which made comparing the resulting models difficult. However, one of the validation criteria for Kim's model, which used linear material properties similar to those used in the present linear models, was that inferior displacement of the pelvic floor should not be greater than 2 cm. This condition was also met in the current model even though coughs generating Pabds as high as 152 cm H2O were modeled in the current study whereas the maximum pressures in incorporated in Kim's model was 56.9 cm of H2O.[47]

5.4 Conclusions

The two main findings of this portion of the work were that the simplified models could replicate the Pves measured during urodynamics within 5 cm of H2O, and that

varying material properties had minimal impact on Pves and displacements predicted by the model. The second finding limits the use of Pves as a validation criterion as this outcome cannot be said to be singular, which precludes the use of Pves as the sole criterion used to validate models in the future. However, its use as a validation criterion in conjunction with other criteria should not be discounted. The insensitivity of this outcome ensures that the outcome of the models is not solely dependent on variables such as tissue material properties, which are not very well characterized. The advantage of using this relatively insensitive variable is that one can get an idea very early in the modeling process if model parameters are within a range that will be appropriate for generating models that are physiologically valid.

CHAPTER VI

MODELING THE BLADDER AND URETHRA IN THE CONTEXT OF STRESS URINARY INCONTINENCE: EFFECT OF GRID DENSITY, MASS SCALING AND TIME SCALING

The second objective expands on the work completed in the first objective and focuses on creating a model in which the modeled urine is no longer constrained to the bladder but free to flow under appropriate circumstances into and through the urethra. The work presented in this chapter focused on evaluating the effects of grid density, mass scaling and time scaling on the mechanics predicted by the model.

6.1 Methods

The modeling techniques outlined in the first objective provided the basis for the construction of the models used in the second objective. In both the first and second objective, urodynamics from the same 28 year old continent woman were used to construct the initial models. However, three main differences exist between the models used in each objective. In the second objective models, the bladder, bladder base and urethra were discretized using shell elements instead of eight node hexahedral elements to reduce computational costs.[81,82] To accommodate the shell discretization of the

structures only the inner wall of the bladder, bladder base and the urethral lumen were included in this model. The urethral lumen was assumed to have a plus (+) shaped orientation with a constant initial cross sectional area of $1.2mm^2$ to provide a channel through which the urine could potentially flow under appropriate circumstances. To further reduce the computation cost of the simulations, the support structure was also eliminated in favor of boundary conditions (Figure 16).

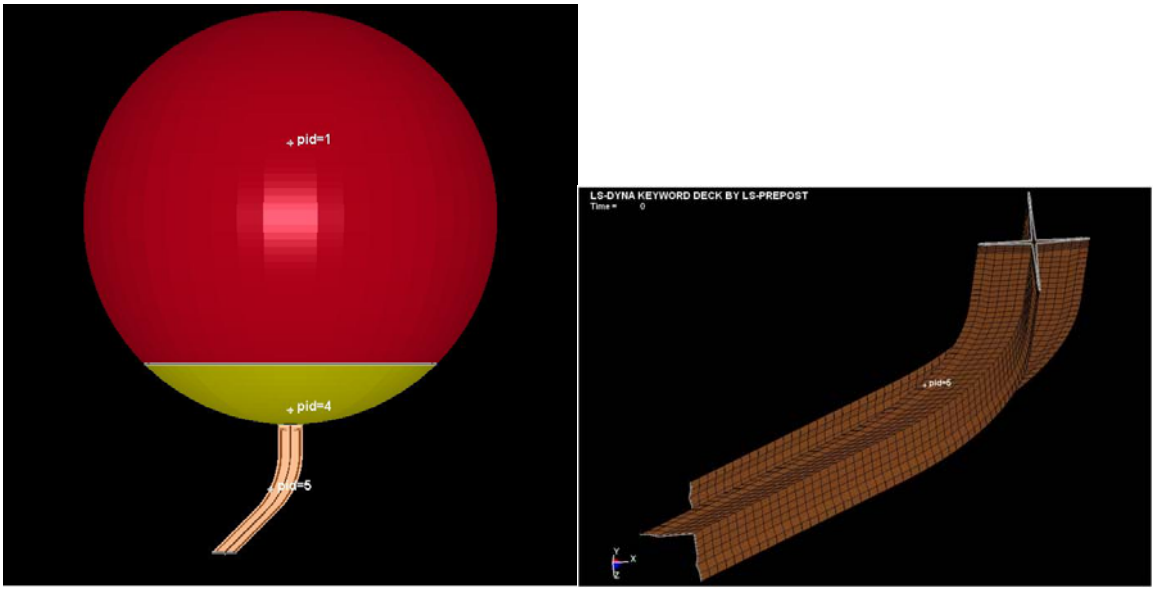

Figure 16: Left: Shell FEM model based on urodynamic data acquired from a 28 year old continent female. Patient Specific Dimensions: Bladder ID = 100.8mm, Bladder Urethra Length = 34mm Right: Close up view of the + orientation of the urethral lumen walls incorporated into the shell model. Urethral cross section = $1.2mm^2$ (Bladder and Bladder Base removed for the sake of clarity)

To model the fluid structure interactions occurring between the walls of the bladder, bladder base, urethral lumen and urine, the split-operator form of the ALE method as described in Chapter IV was incorporated into this model. The Lagrangian structures representing the walls of the bladder and bladder base were discretized using Hughes Liu shell elements (Shell thickness = 2.0 mm for both Bladder and Bladder Base) and were embedded within an Eulerian structure discretized using eight node hexahedral

shells representing the urine.[81,82] The Lagrangian structure representing the walls of the urethral lumen was also discretized using Hughes Liu shell elements (Shell Thickness = 4.0 mm) and were embedded inside an Eulerian structure representing empty space discretized with eight node hexahedral elements to facilitate the flow of urine into and through the urethral lumen (Figure 17).[61,63,64,70,81,82,103]

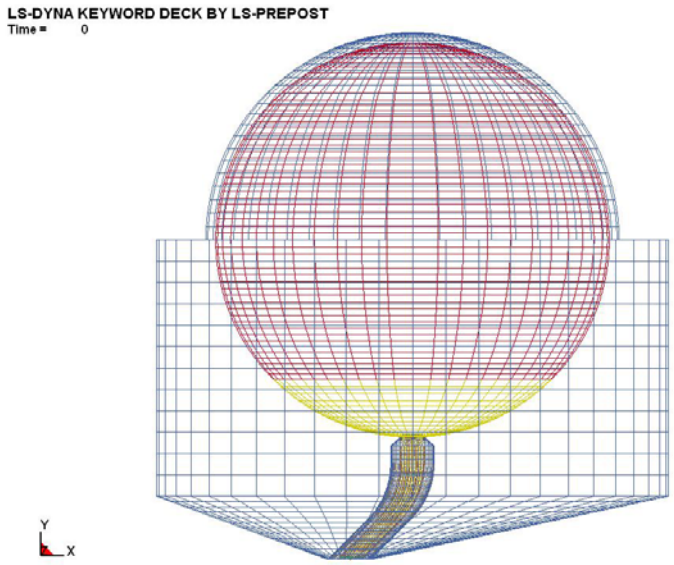

Figure 17: Lagrangian mesh embedded in the Eulerian mesh. Red, Yellow and Brown mesh correspond to the Lagrangian mesh representing the Bladder, Bladder Base and Urethra respectively. Blue mesh corresponds to the Eulereian Mesh representing the fluid.

The material properties in the Lagrangian portion of this model were assigned based on the finding of the first objective that Pves was most accurately predicted when non-linear material properties were assigned to the bladder and urethra. Therefore, the bladder was modeled as a Mooney Rivlin hyper-elastic material and the bladder base and urethra were modeled as Blatz Ko hyper-elastic materials using the parameters listed earlier in Chapter V. The Eulerian portion of the model was split into two regions each defined as a separate material (Figure 18). The region in which the urethra was

embedded was defined as an LS Dyna Vacuum material which allows the region to act as empty space without impeding or facilitating the flow of material into the region.[81,82] The remaining Eulerian region was assigned the material properties of an elastic fluid to model the urine contained within the bladder..

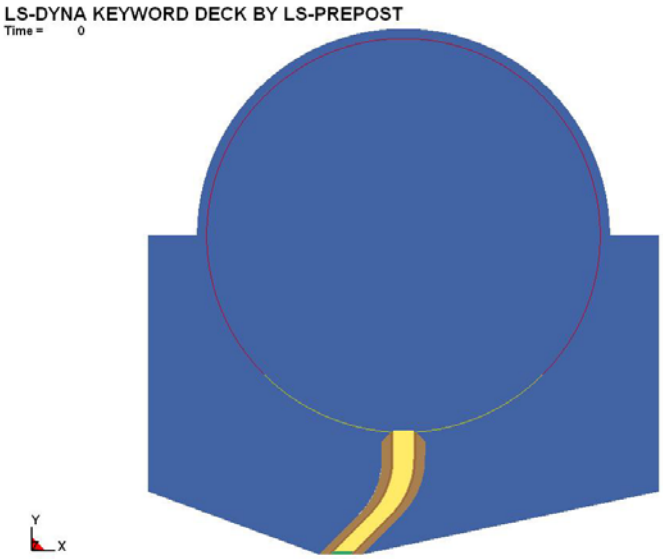

Figure 18: Material Property Definitions. Blue represents the portion of the model defined as an elastic fluid, brown, and yellow portions were defined using the vacuum material description. Green represents the outlet also assigned the vacuum material description

To prevent non-physiologic movement, the upper portion of the bladder base was constrained to prevent downward movement and to simulate the support that would be afforded to the bladder by the bones of the pelvis and the levator ani muscle (Figure 19). Only the top portion of the bladder base was constrained in this manner so as to simulate the opening in the levator ani muscle known as the urogenital hiatus to allow for the bladder neck to descend. The opening of the urethral lumen was constrained to prevent motion in the downward direction to prevent the urethral lumen from turning inside out. The urethral lumen was further constrained along its length to prevent in-plane motion by

constraining the extreme exterior ridges of the (+) geometry. This was done to simulate support of the urethra provided by the vagina through the endopelvic fascia. [4,5,8]

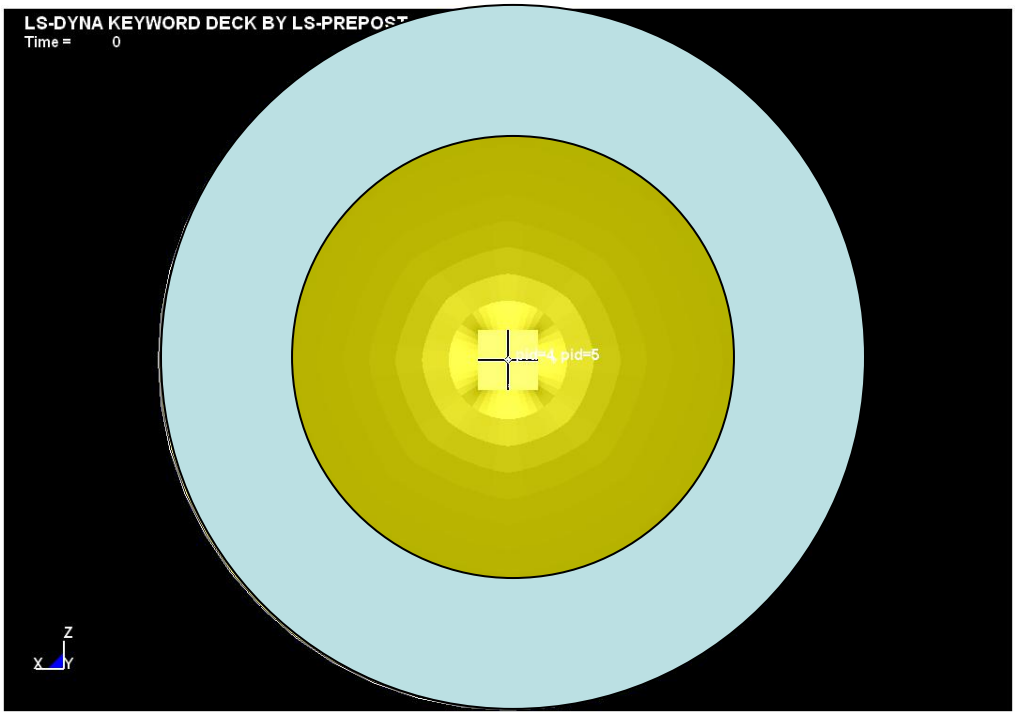

Figure 19: Constraints assigned to the bladder baseThe blue region of the above structure was constained against downward motion to prevent non-physiologic movement while allowing for the decent of the bladder neck

In this portion of the work, the initial models were loaded based on the urodynamic measurements obtained during the same 1.8 second cough event that was used to define the Pabd loads incorporated in the first objective (Figure 20). To avoid shocking the grid the load curve for this event was modified by adding an additional one second to the beginning of the event during which the pressure was applied gradually until baseline pressure was reached at the 1.0 second time point

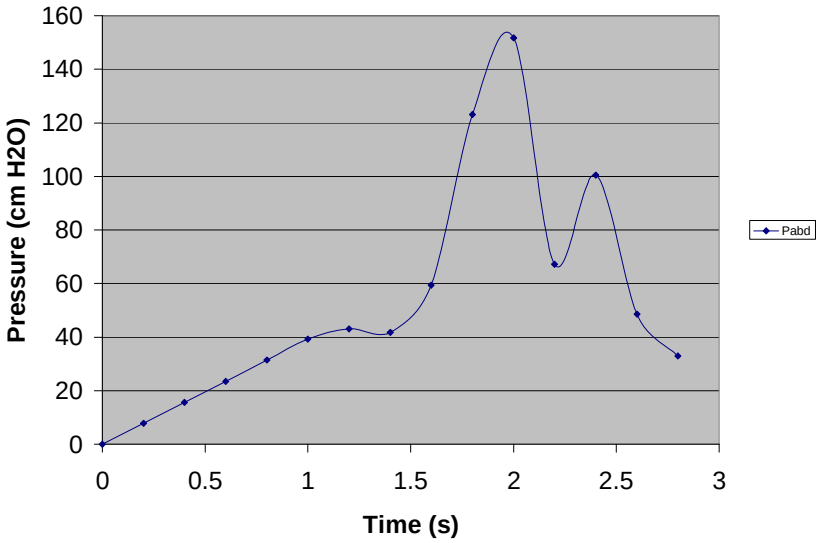

Figure 20: Pabd loads acquired from urodynamic measurements during a 1.8 second cough in a 28 year old continent volunteer. Note the addition of a 1 second interval at the beginning of each event during which pressure was applied gradually until baseline pressure was reached to prevent shocking the grid.

In addition to the Pabd loads applied to the bladder, Pura loads also needed to be incorporated into the model to close the urethra and provide resistance to flow. To account for the fact that Pura varies along the length of the urethra, the urethra was subdivided into 10 regions as was the UPP from this patient. The pressures in the profile corresponding to each region were averaged in order to establish the baseline pressure for each region (Figure 21). After averaging the profiles for each region, it was discovered that the peak Pura in the averaged profile did not match the baseline Pura recorded at the beginning of the cough event. In order to correct for this finding all baseline pressures were reduced by 5% so that the peak Pura in each profile matched the baseline Pura at the start of the cough event while maintaining a similar pressure profile in the remainder of the urethra.

The clinical urodynamic measurement as detailed earlier provides data regarding the Pura at only one location in the urethra during an event. As a first approximation, it

was assumed that in the remainder of the urethra, the Pura increased in the same manner and in the same proportion as the Pura did within the recorded region (Figure 22). In all, twenty Pura loads were applied to the urethra in an opposing fashion in order to close the lumen and provide urethral resistance.

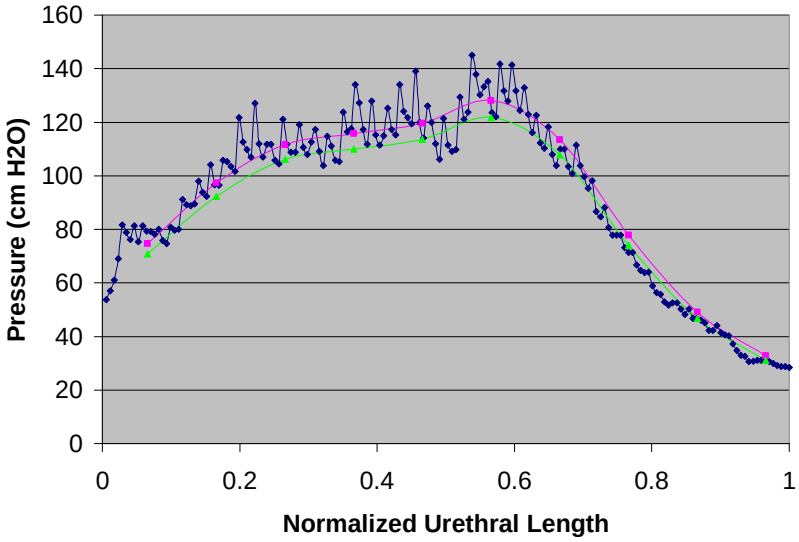

Figure 21: UPP (Blue) measured in a 28 year old continent patient (Urethral Length = 34mm) Averaged UPP (Pink) dividing the urethra into 10 equal regions. Cough Event corrected UPP (Green) corrects the averaged urethral pressure profile so that the peak urethral pressure in the profile matches the baseline urethral pressure at the start of the modeled cough event.

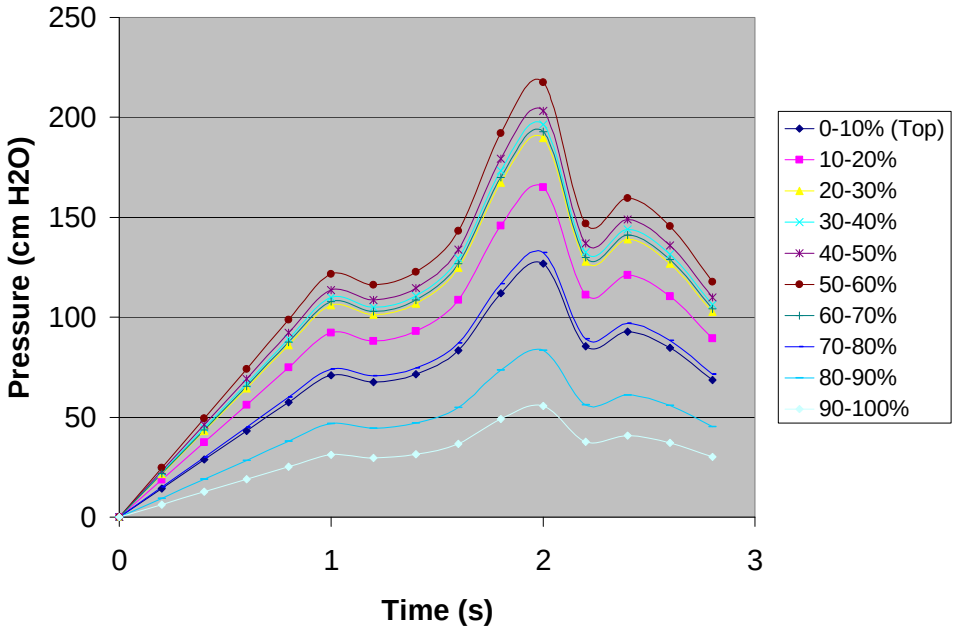

Figure 22: Pura loads applied to the urethra to close urethra and provide resistance to flow during the modeled cough event. Note: 0-10% corresponds to most proximal region of the urethra (closest to the bladder neck) whereas 90-100% corresponds to most distal region (exit)

6.2 Model Characterization

6.2.1 Grid Dependence

In order to determine the grid dependence of the models, three identical models were constructed with the only differences between the models being the number of elements used to discretize the various structures as detailed in Table XVI. In addition, it must be noted that in the case of simulations A and B the mesh comprising the urine and vacuum was modified to cluster additional elements within the urethral lumen to better simulate the flow of urine whereas due to large number of elements this was not necessary in simulation C and all elements were evenly distributed. (Figure 23)

Table XVI: Element distribution in Grid Dependence Simulations

Simulation	Bladder* No. of Elements	Bladder Base* No. of Elements	Urethra* No of Elements	Urine** No of Elements	Vacuum** No of Elements
A	3408	1008	3168	90576	23708
B	8228	3388	5808	90576	23708
C	8228	3388	5808	195264	56544
* Hughes Liu Shell Elements ** 8 Node Hexahedral Elements					

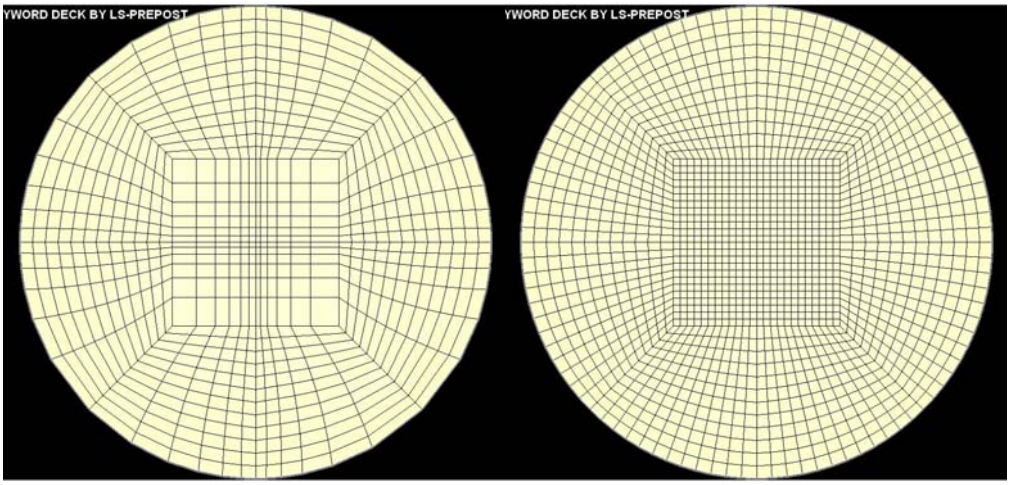

Figure 23: Illustration of clustering of elements designed to place more elements within the urethral lumen when a coarser mesh was used to discretize the Eulerian portion of the model (Left). Un-clustered mesh used when a finer mesh was used to discretize the Eulerian portion of the model (Right)

All simulations modeled the cough described earlier in this chapter with the time of the cough scaled so that 0.05 seconds in model time was equal to 1 second of real time. (Simulations used to determine the effects of this scaling are detailed in the next section.).

6.2.2 Effect of Mass and Time Scaling

In complex finite element problems such as this one, one way to reduce solution times is to scale the model by either scaling the mass or by scaling the time.[57,58,60,104,105] However, when scaling factors are incorporated into explicit FEM models, dynamic effects may be introduced which can cause the solution to become inaccurate especially in regards to stress. [57,58,60,104,105] To test the effects of mass and time scaling, seven simulations were run in which mass and or time were scaled (Table XVII). Mass scaling was accomplished by increasing the density of all of the structures in the problem by a factor of 10,100 or 1000 whereas time scaling was accomplished by reducing the event time to either 0.1 or 0.05 times its actual duration.. It should be noted that the simulations were run using the grid density incorporated in simulation B above. It was necessary to utilize the coarser grid for this work to accommodate the increased computational cost that would be incurred when the time scaling factor was increased towards unity.

Table XVII: Simulations to determine effects of mass and time scaling

Simulation	Mass Scaling Factor	Time Scaling Factor
D	10	1.0
E	100	1.0
F	1000	1.0
G	1.0	0.1
H	1.0	0.05
I	100	0.1
J	1000	0.1

6.3 Results

6.3.1 Grid Dependence

In this part of the project the primary outcome of interest is the depth to which urine penetrates or transits the urethra. In the three simulations used to evaluate the effect of grid dependence on this parameter, it was determined that changing the number of elements used to discretize the modeled structures affected the depth to which the urine was predicted to penetrate (Table XVIII) and Figure 24). The greatest depth of penetration was predicted by the model incorporating the coarsest grid (simulation A) at both the time point corresponding to peak Pabd and the time point corresponding to the second peak in the applied cough loads. Simulations B and C both predicted decreasing penetration depths at the time point corresponding to peak Pabd and identical penetration depths at the time point corresponding to the second peak in the applied cough loads. .

Table XVIII: Effects of varying mesh density on urine penetration depth

	Depth of Penetration	
Simulation	1st Peak	2nd Peak
A	11 mm	14 mm
B	9 mm	11 mm
C	6 mm	11 mm

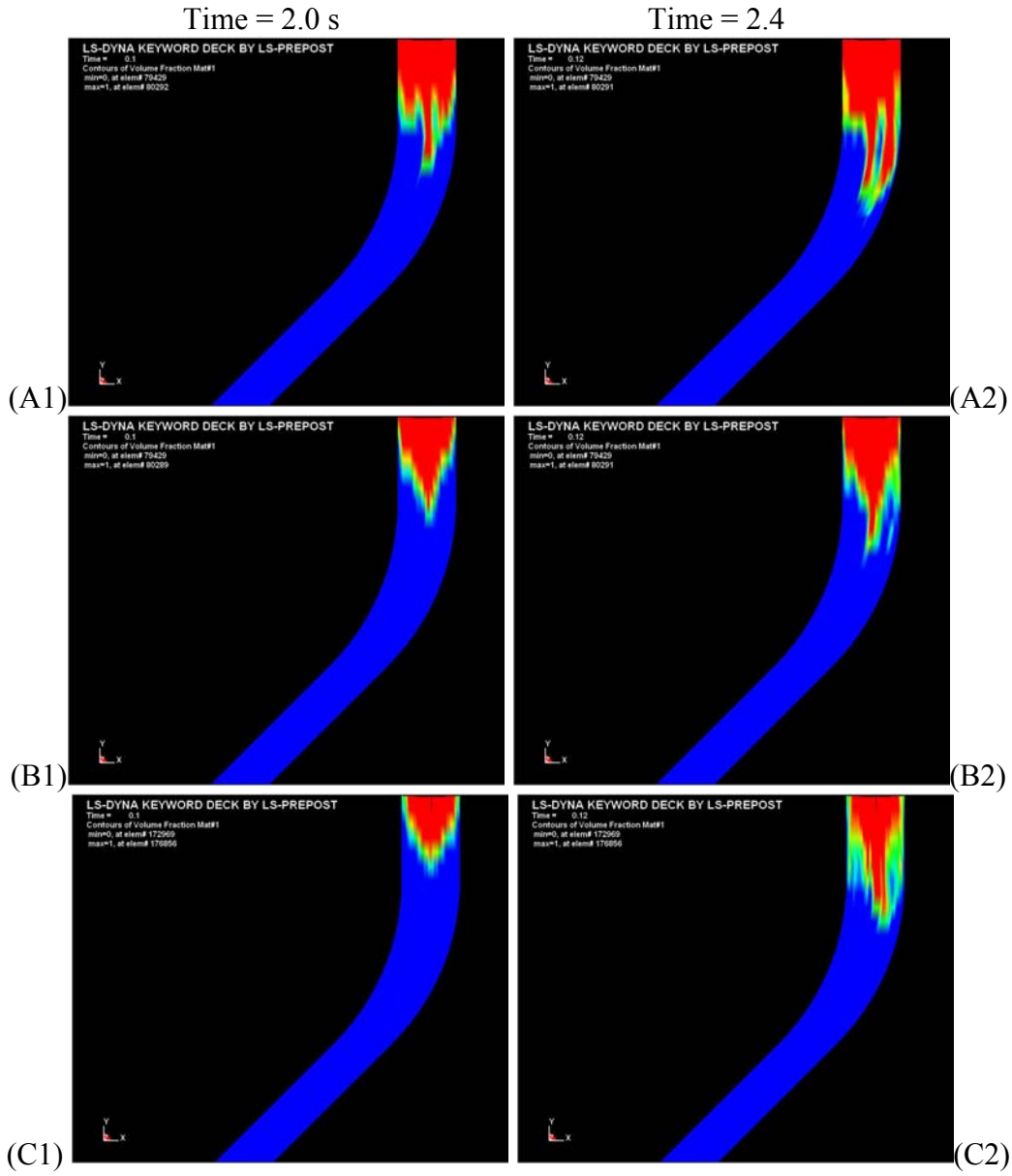

Figure 24: Depth of Penetration seen in simulations testing for grid dependence. A left hand column shows results in models at the2.0 second time point corresponding to peak abdominal pressure. The Right had columns show results at the 2.4 second time point corresponding to the secondary peak in abdominal pressure. A, B & C denote the simulations detailed in Table XVI. Varying grid density produced both qualitative differences as well as quantitative differences in regards to the depth of penetration predicted by the model.

The time required for each simulation to run varied based on the number of elements utilized to discretize the structures and the size of the smallest element utilized. In simulation A, which incorporated the least number of elements, the entire simulation was completed in 67 hours and 25 minutes when run using a total of 32 processors on an IBM Cluster 1350 Super Computer (Ohio Super Computing Center Columbus OH). Simulation B when run using the same number of processors was completed after 87 hours while the simulation in which the finest grid was incorporated was 93% complete after 96 hours of running time on 32 processors. It should be noted that due to the finite computational resources available for this project a simulation was considered complete after the time point corresponding to the second peak of the cough was passed.

6.3.2 Effect of Mass and Time Scaling

In the above work used to determine the effect of grid density on the depth of urine penetration, the time was scaled by a factor of 0.05 which means that the events occurring during one second of real time were compressed to occur within 0.05 seconds in the computational model. To determine the effects of this scaling on the mechanics predicted by the model specifically the depth of urine penetration, several simulations were run in which mass, time or both parameters were scaled as detailed earlier. The models in this set of simulations incorporated the grid used in simulation B in order to accommodate the increased computational cost associated with some of the simulations. Table XIX and Figure 25 detail the effects of mass and time scaling on the depth of urine penetration.

Table XIX: Effect of mass and time scaling on depth of urine penetration depth

Simulation	Mass Scaling Factor	Time Scaling Factor	Depth of Penetration at peak Pabd
D	10	1.0	DNF
E	100	1.0	DNF
F	1000	1.0	4.8 mm
G	1.0	0.1	12.0 mm
H	1.0	0.05	8.4 mm
I	100	0.1	1.2mm
J	1000	0.1	1.2 mm

DNF = Did not finish (Model proved too computationally expensive to solve)

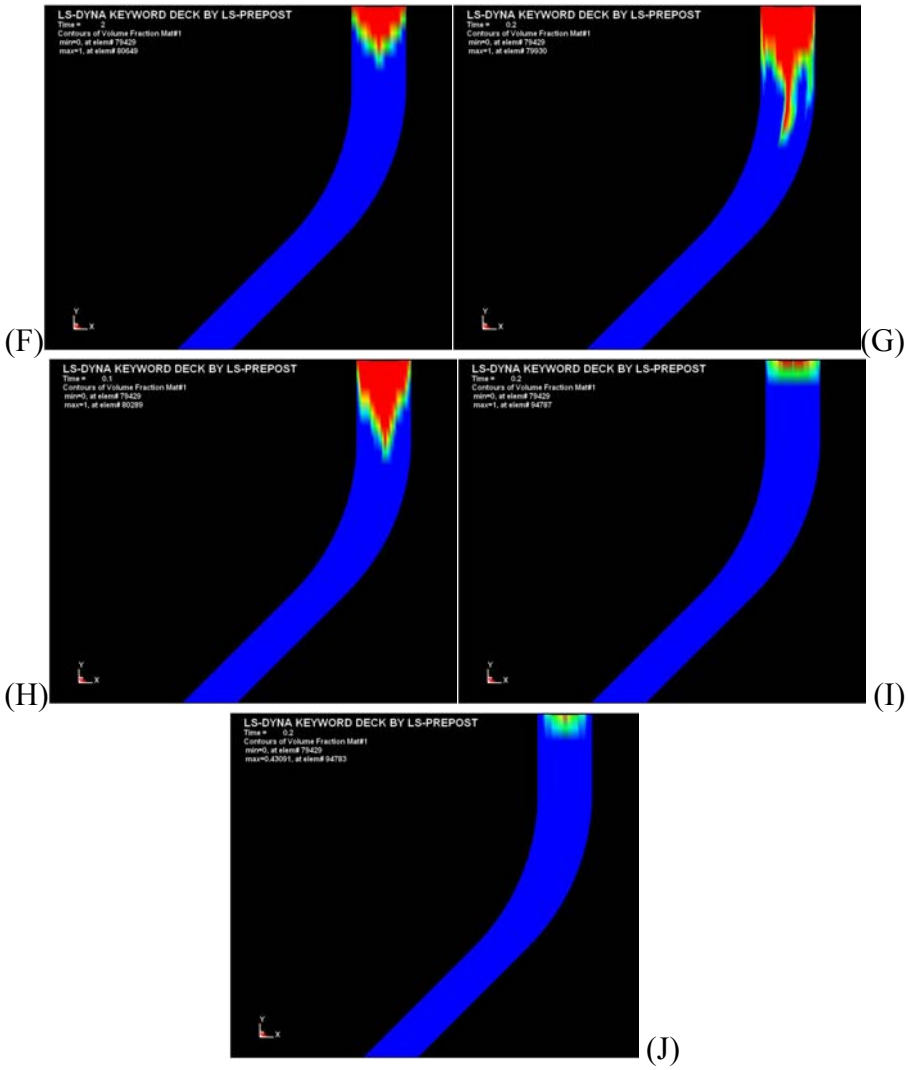

Figure 23: Effect of Mass and Time scaling on depth of urine penetration at peak Pabd (Letters denote simulations defined in Table XVII)

Several authors who have investigated the effects of mass and time scaling on modeled sheet metal forming processes have identified stress magnitude and distribution as key outcomes for evaluating the effects of mass and time scaling.[58,60,104,106] Figure 26 illustrates the effects of mass and time scaling on the stress distributions predicted at peak Pabd.

Simulation G in which the mass was not scaled and the time was scaled by a factor of 0.1 predicted the greatest depth of penetration at peak abdominal pressure. In addition, this simulation also predicted the highest levels of stress at the time point corresponding to peak Pabd when compared to the other simulations. The results indicate that when increased mass scaling is applied to this problem both the predicted stress levels and depth of urine penetration will be reduced. The effect of time scaling on the model was found to have the opposite effect in that when the time scaling factor was increased towards unity, both the predicted stress levels and depth of urine penetration increased. The trends appear to indicate that less severe scaling results in increasing values being predicted for both parameters. However less severe scaling will incur increased computational cost. Simulations D and E in which the mass was scaled by a factor of 10 and 100 while time was not scaled would have required 12 days or more for a solution to be obtained when these simulations would be run on 32 processors. Similarly, of the simulations in which a solution was obtained Simulation G which incorporated the least amount of scaling was also the most computationally expensive requiring a run time of 144 hours on 32 processors.

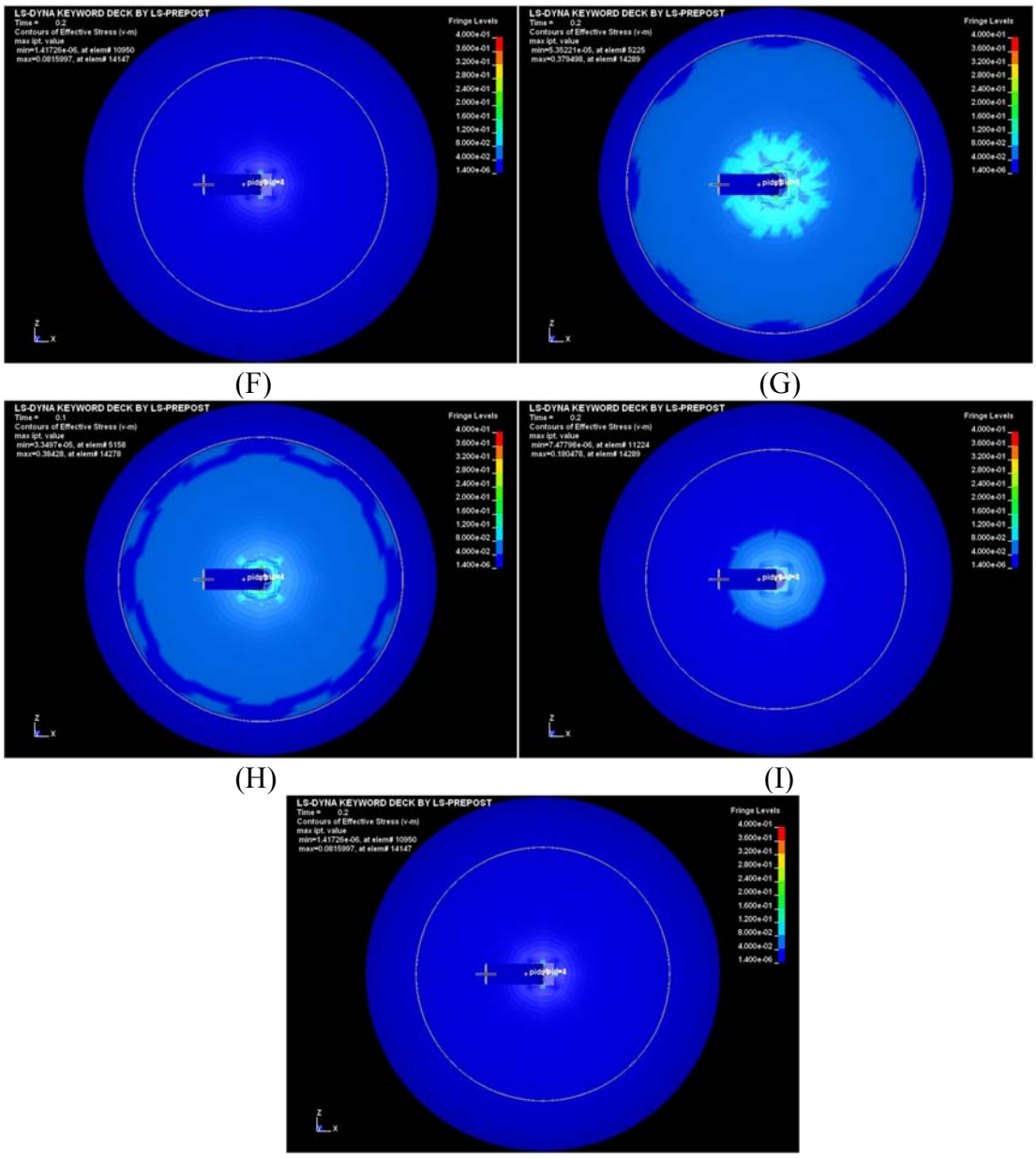

Figure 26: Effects of mass and time scaling on stress distributions Letters denote simulations detailed in Table XVII & XIX.

The above results provide qualitative insight into the effects of mass and time scaling, to quantify the effects of scaling Chung et al, have also proposed an error calculation that can be used to determine the degree to which dynamic effects are present in explicitly solved models and the time at which these effects impact the model through the use of the following equation.

$$e(t) = \frac{1}{W_{\text{int}}^{plastic}(t)} \int_0^t \int_\Omega dE_k = \frac{E_k(t) - E_k(t_y)}{W_{\text{int}}(t)} \qquad \text{Eq. 13}$$

Where W_{int} is the internal strain energy and E_k is the kinetic energy. This equation indicates that when e(t) is low, kinetic energy is also low and dynamic effects are minimized. Therefore a simulation exhibiting low e(t)s would be considered to have minimal dynamic effects present in the solution and would be considered to be more accurate[104].

Figures 27 - 31 show plots of the internal and kinetic energy vs. time for simulations F through J. It is interesting to note that in all of the simulations with the exception of simulation G the internal energy curve has a single peak and does not have a double peak as one would expect based on the applied abdominal pressure and urethral pressure load curves.

Figure 32 shows a comparison of the error (e(t)) associated with dynamic effects for each simulation while Figure 33 shows this comparison for only those simulations that predicted urine penetration of greater than 1.2mm into the urethra. In both cases, it can be clearly seen that simulation G had the lowest amount of error associated with dynamic effects of all of the simulations evaluating mass and time scaling.

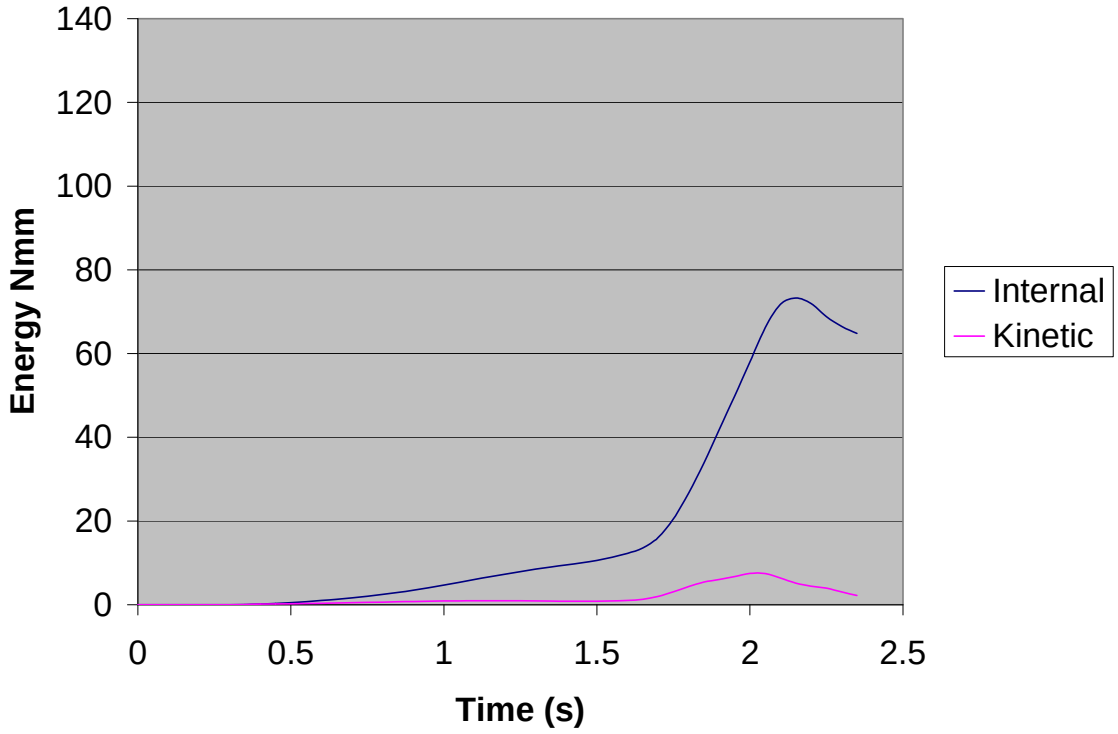

Figure 27: Kinetic & Internal Energy vs. Time for Simulation F (Mass Scaling = 1000, Time Scaling = 1.0)

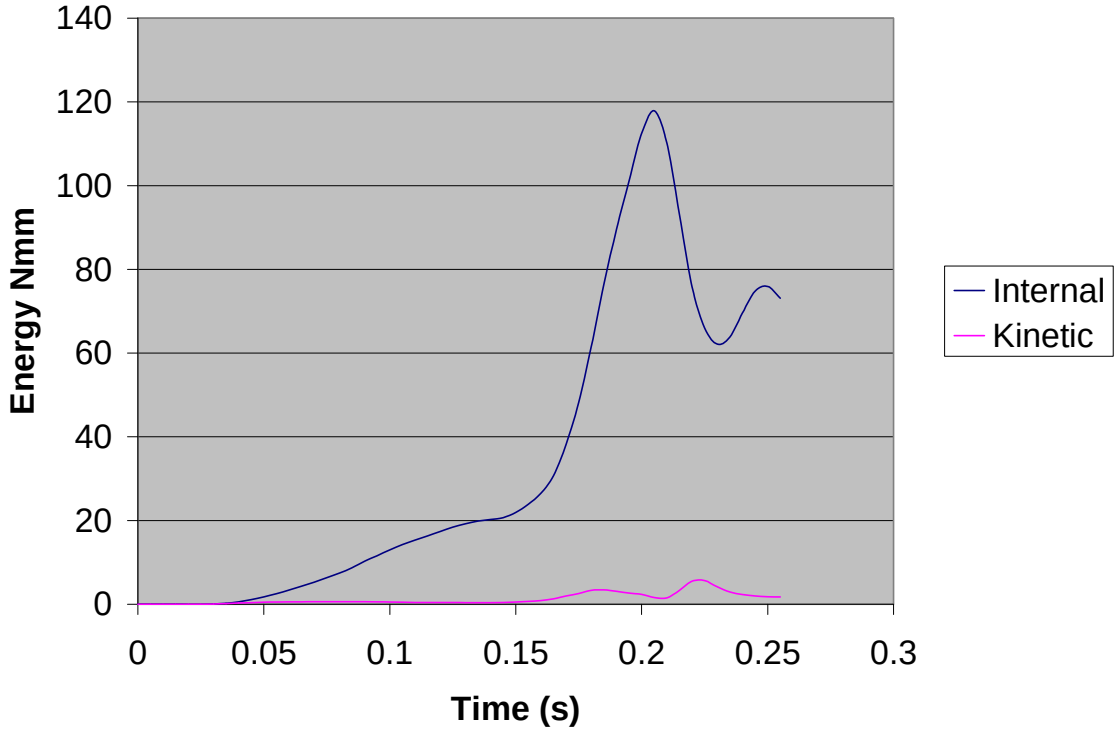

Figure 28: Kinetic & Internal Energy vs. Time for Simulation G (Mass Scaling = 1.0, Time Scaling = 0.1)

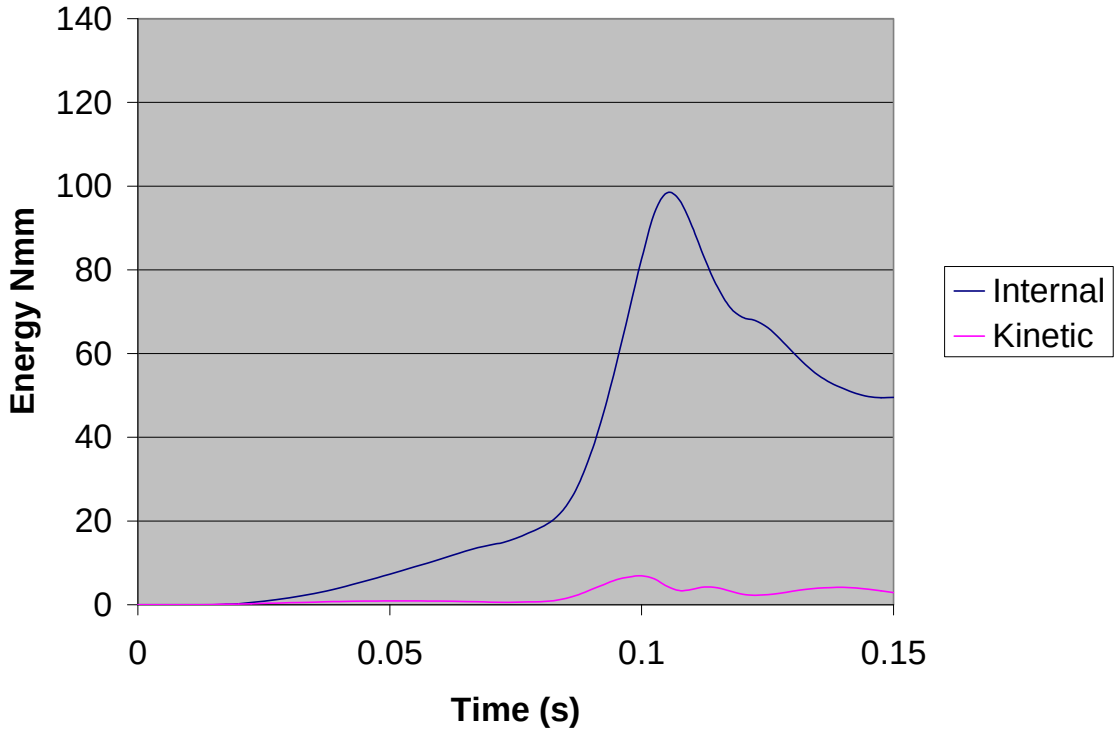

Figure 29: Kinetic & Internal Energy vs. Time for Simulation H (Mass Scaling = 1.0, Time Scaling = 0.05)

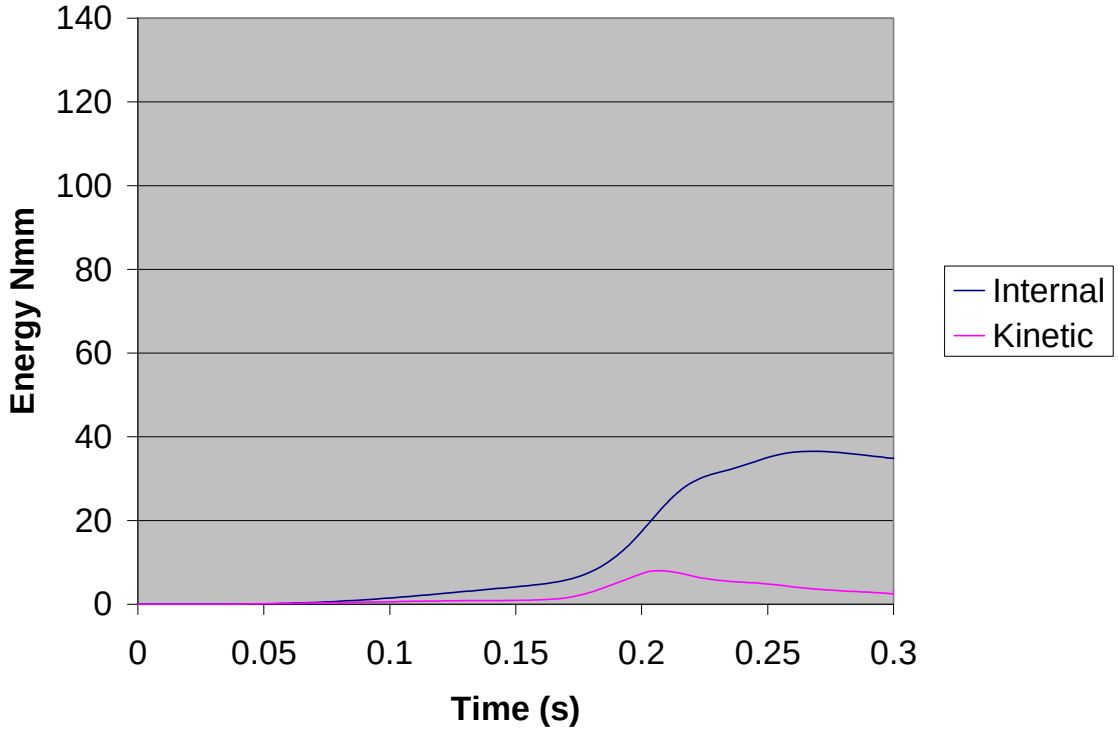

Figure 30: Kinetic & Internal Energy vs. Time for Simulation I (Mass Scaling = 100, Time Scaling = 0.1)

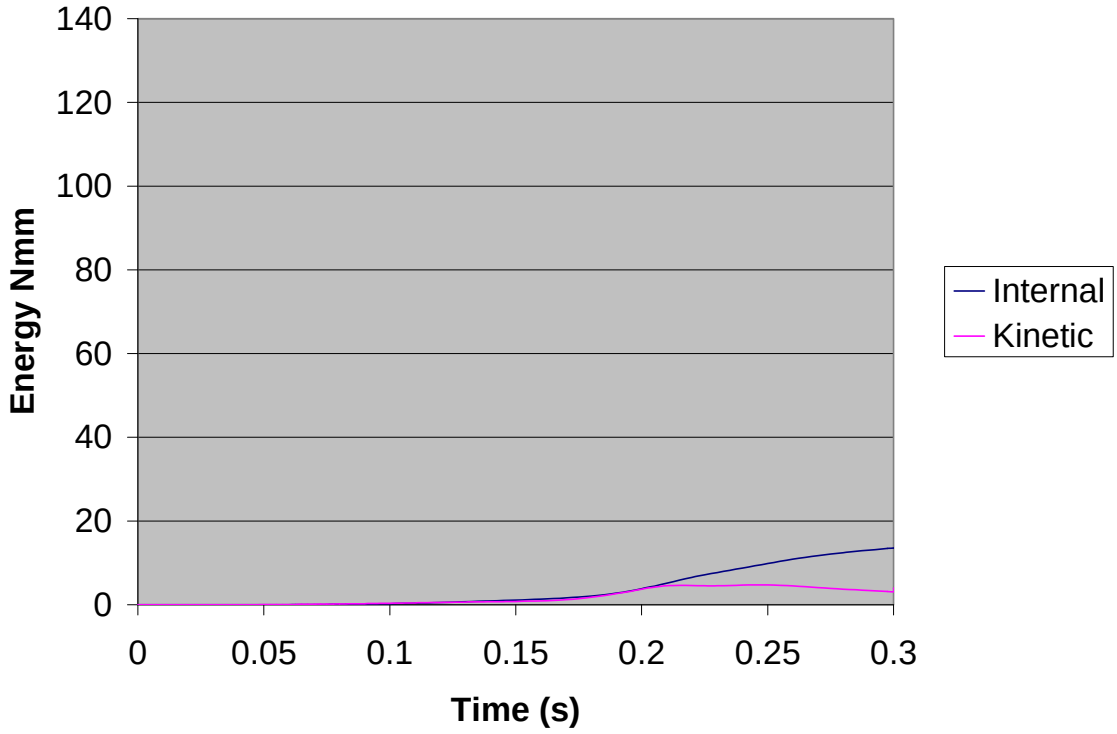

Figure 31: Kinetic & Internal Energy vs. Time for Simulation J (Mass Scaling = 1000, Time Scaling = 0.1)

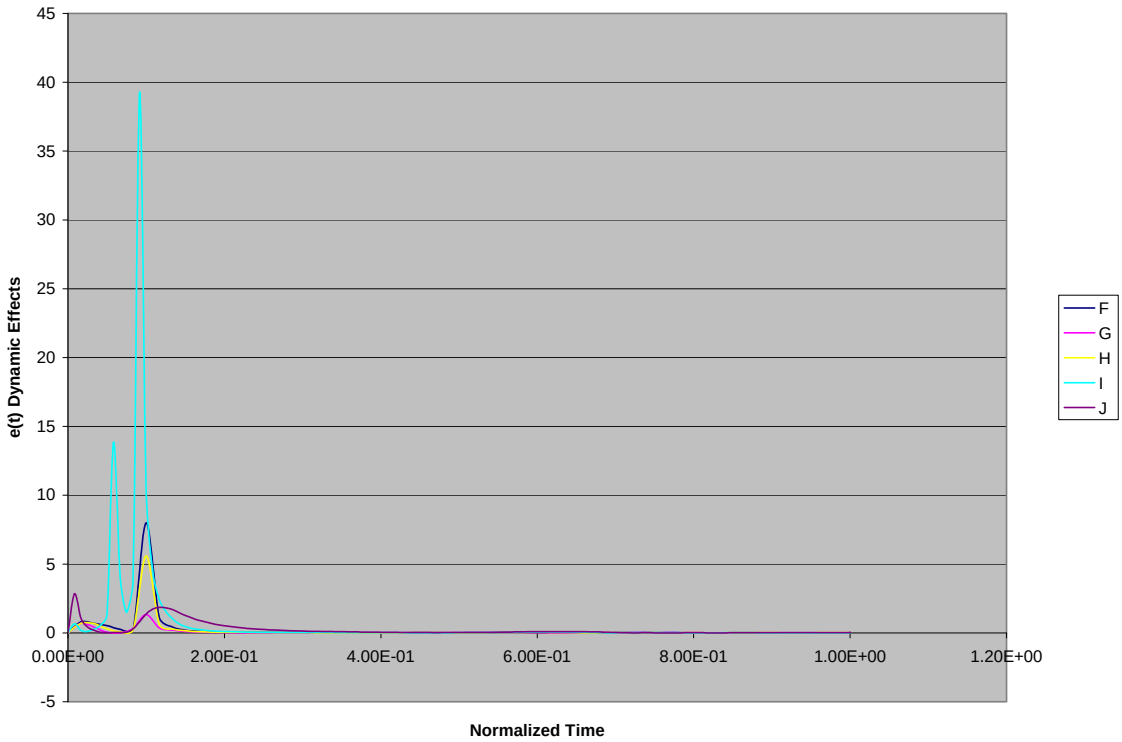

Figure 32: Error associated with dynamic effects in Simulations F through I

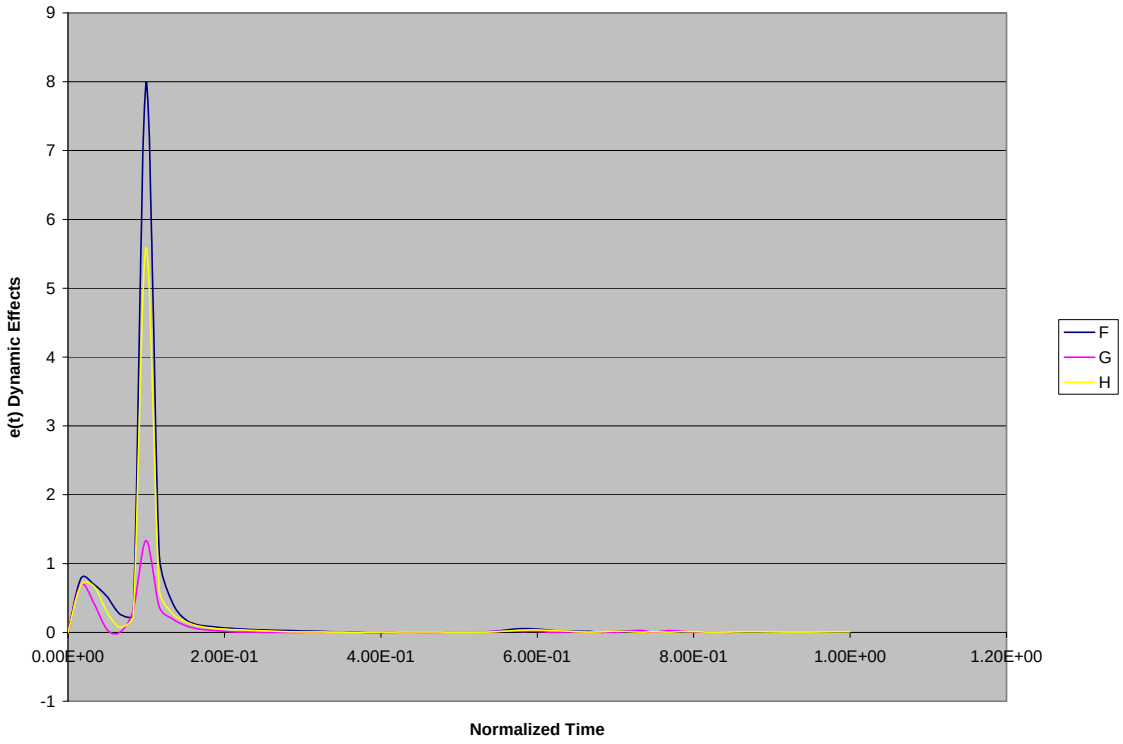

Figure 33: Error associated with dynamic effects in mass and time scale simulations exhibiting urine penetration > 1.2mm. It should be noted that Simulation G had the lowest error associated with dynamic effects and would be considered to be the most accurate solution.

6.4 Discussion

The second objective of this project expanded on the work done in the first objective in that a simplified model of the bladder and urethra was used to determine the feasibility of using clinical urodynamic measurements and finite element models to simulate the mechanics of these structures during a cough. However, the main goal of the second objective was to determine how to model a situation in which the urine was no longer constrained to the bladder but free to flow under appropriate circumstances out of the bladder and into the urethral lumen.

In this work the operator split version of the ALE method as described in Chapter IV was utilized to model the fluid structure interactions that occur between the urine and the walls of the bladder, bladder base and urethral lumen. This method has been used in other studies to model the mechanics of the heart valves as well as to model left ventricular contraction. [61-64] The main reason that this method was chosen for this work and in the works cited above over the pure ALE method is that the Eulerian mesh used to discretize the fluid would have had to undergo large deformations in order to accurately model the coupled fluid structure interactions. These large deformations would have resulted in the failure of the automatic rezoning algorithms employed by the ALE method to smooth the distorted Eulerian mesh. As a result every time the automatic rezoning algorithm failed a time consuming manual remeshing step would have to be completed in which the distorted Eulerian mesh would be removed and replaced by a new undistorted mesh onto which the solution corresponding to the current time step would need to be mapped[63]. In the current models this situation would arise as the Pabd forced the urine which would be represented as an Eulerian mesh into the urethral lumen. The operator

split method handles this problem by embedding the Lagrangian mesh within the Eulerian mesh while fixing the Eulerian mesh in space and coupling the two meshes together through the use of the penalty coupling algorithm described in Chapter IV. In this method a Lagrangian step in which the deformation of the Lagrangian structures is calculated is performed. Through the penalty coupling method, this step is then followed by an Eulerian step in which the transport of the fluid between adjacent elements resulting from the motion of the embedded Lagrangian mesh relative to the fixed Eulerian mesh is calculated.[70,103] In short, because the Lagrangian mesh moves through the Eulerian mesh which is fixed in space without deforming it there is no need to rezone the mesh.

As was the case in the first objective simplified models of the bladder and urethra were utilized in this portion of the study. However, in order to further reduce computational costs Hughes Liu shell elements were utilized instead of eight node hexahedral solid elements. The Hughes Liu shell elements were selected for use in these models because the formulation of this element in LS Dyna allows the user to specify which surface of the structure the shell is representing [81,82]. In this case, this was useful in specifying that the shell as representing the inner wall of the bladder wall, bladder base and urethral lumen.

The decision to model the urethral lumen as a (+) shape was made to simplify the conceptualization of how to load the walls to effect closure of the lumen and how to constrain the urethral lumen based on anatomical descriptions. The urethral opening was sized so that it would fit entirely within a tube having a 11.5 mm diameter which corresponds to the external diameter of the urethra reported by Umek et al.[88] In reality,

the urethral lumen has been reported to be a slit or crescent shaped and its shape and size have been found to affect urine flow during micturition. [107,108] The size and shape of the urethral lumen will need to be evaluated in future models in order to determine if varying these parameters will have an impact on the mechanics predicted by the model.

In determining how to construct this model several factors had to be considered including the grid dependence of the model, the effects of mass and time scaling and computational cost due to the finite computational resources available for this project. Based on the results of the simulations run to evaluate grid dependence, and the effects of mass and time scaling the model can be described as being grid dependent, and not tolerant of scaling. In an ideal situation with unlimited computational resources, the results of these simulations indicate that the model should be run with no time scaling and with a very fine mesh to fully capture the fluid structure interactions that occur as the urine is forced into the urethral lumen. However, the available computational resources dictated that concessions be made in order to obtain a solvable model. As a result, it was decided to utilize the largest time scaling factor possible (0.1) in conjunction with a coarser mesh in order to generate such a model. The time scaling factor of 0.1 was chosen based on the findings that in all of the simulations run to evaluate mass and time scaling the simulation incorporating this time scaling factor generated the least amount of error associated with dynamic effects. Furthermore this was also the only simulation in which the internal energy predicted by the model matched what was expected based on the applied pressure loads. The one drawback to utilizing this scaling factor is the computational cost associated with it as the simulation required 144 hours when run on 32 processors. As computer technology improves and computational resources become

more readily available this result should be reevaluated to determine if increasing the time scaling factor towards unity further alters the mechanics predicted by the model.

6.5 Conclusions

The split operator form of the ALE method shows potential for modeling the fluid structures interactions that occur during stress events. However, the computational expense associated with this method and the necessary concessions required to achieve a solution must be taken into account when evaluating the physiological realism of models created utilizing this method and the solutions these models generate.

CHAPTER VII

MODELING THE BLADDER AND URETHRA IN THE CONTEXT OF STRESS URINARY INCONTINENCE: EFFECT OF URETHRAL STIFFNESS, APPLIED URETHRAL PRESSURE AND URETHRAL SUPPORT

In the previous chapter, it was determined that the fineness of the mesh used to discretize the model and the mass and time scaling factors incorporated to reduce solution times affected the mechanics predicted by the model. In this chapter, the effects of varying urethral stiffness, applied Pura and urethral support on the mechanics predicted by the model are presented. The goal of this portion of the work was to examine if the physiological parameters assigned to the urethra could impact the mechanics predicted by the model.

7.1 Methods

7.1.1 Modeling

Based on the findings reported in the previous chapter and the computational resources available, the models used in this portion of the study were identical in terms of

dimensions and grid density to the model utilized in Simulation B to evaluate grid dependence as described in Chapter VI. In all of the models described in this chapter, a time scaling factor of 0.1 was incorporated to ensure that solutions could be obtained in a timely fashion based on the findings reported in the previous chapter.

7.1.2 Simulations

To gain a better understanding of how the mechanics predicted by the model would be altered by varying the physiological parameters used to define the model, the simulations detailed in Table XX were run.

Table XX: Simulations utilized in sensitivity analysis

Simulation	Urethral Pressure	Urethral Stiffness
K	Non-Leaking Cough	Published
L	Leaking Cough	Published
M	None	Published
N	Non-Leaking Cough	2x Published
O	Leaking Cough	2x Published
P	Non-Leaking Cough	0.5x Published
Q	Leaking Cough	0.5x Published
R	Non-Leaking Cough	0.25x Published
S	Leaking Cough	0.25x Published
T	Non-Leaking Valsalva	Published
U	Leaking Valsalva	Published
V (Dorsal Support of Urethra Removed)	Non-Leaking Cough	Published
W (Dorsal Support of Urethra Removed)	Leaking Cough	Published

In the above simulations, simulations K through S evaluated the effect of varying the stiffness of the urethra by increasing or decreasing the value of the shear modulus of the urethral material published by Haridas et al by a factor 0.25, 0.5 and 2.[49] Simulations K,N,P and R were run utilizing Pura acquired from urodynamic data and applied to the

urethra in the same manner described in the previous chapter to incorporate variations in Pura along the urethral length. The Pura incorporated in these models fulfilled the urodynamic definition of continence in that at all times during the event the Pura in at least one region of the urethra exceeded the expected Pves based on the urodynamic measurements (Figure 34 & 35). In simulations L,O,Q and S the Pura incorporated into the model in all regions of the urethra and at all time points was reduced to half of the value indicated by the measured urodynamic data (Figure 34 and 35). This was done to force a situation in which the applied Pura would be insufficient to prevent the leakage of urine based on the urodynamic definition of incontinence which asserts that a leakage of urine will occur if the Pves developed in response to increased abdominal pressure during an event exceeds the Pura in the entire urethra at a any time during an event. In short, simulations K,M,O and Q were used to investigate the effects of varying urethral stiffness during a continent (non-leaking) event while simulations L,N,P and R were used to investigate the effects of varying urethral stiffness during an incontinent (leaking) event.

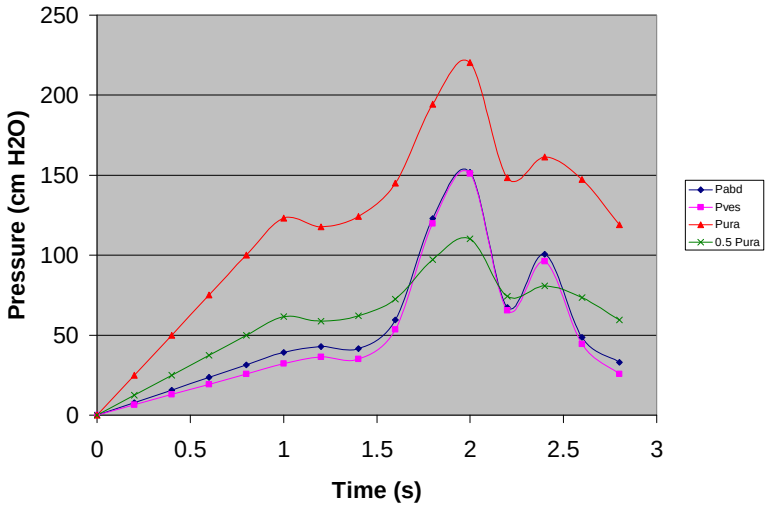

Figure 34: Pressure Loads associated with modeled cough; Blue = Pabd, Pink = Pves, Red = Non-Leaking Pura, Green = Leaking Pura. In this figure the values of the Pabd, Pves and non-leaking Pura were all obtained from measured urodynamic data. The leaking Pura was obtained by reducing the non-leaking Pura to one half of its measured value to force a leaking situation to occur in the model.

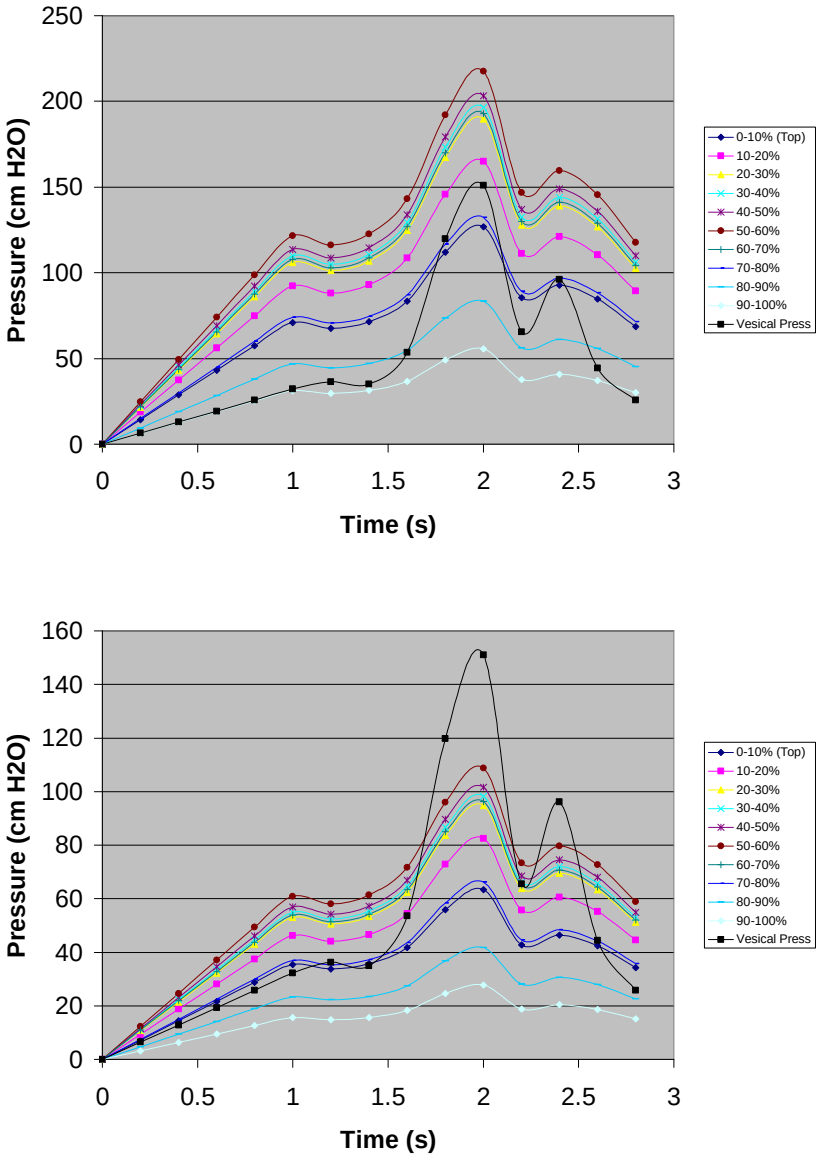

Figure 35: Illustration of the relationship between the measured Pves and the applied Pura loads along the urethra. Top graph illustrates a non-leaking event in which the urethral pressure is greater than vesical pressure (black line) in the regions located in the between the 10th and 70th percentile of the urethras length (Note 0th percent corresponds to the bladder neck region). Bottom graph illustrates a leaking event in which the vesical pressure (black line) exceeds the applied urethral pressure along the entire length of the urethra at the 1.8 2.0 and 2.4 second time points during the cough event

To get a clearer understanding of the effect of Pura on the mechanics of the model, an additional three simulations were run. In simulation M, the Pura was completely eliminated from the model. This simulation was used to gain insight as to the

intrinsic resistance to flow that would be supplied by the tube itself when the urethra stiffness was set to the published values.

Simulations T and U were utilized to investigate how the mechanics of the model would be altered if Pabd loads were increased and sustained over a period of time rather than increased and decreased in an abrupt fashion that is typical of a cough. To accomplish this, urodynamic data corresponding to a valsalva maneuver in which the subject is instructed to strain and hold the strain for as long as possible were acquired from the same 28 year old continent patient from whom the urodynamic cough data was obtained (Figure 36)

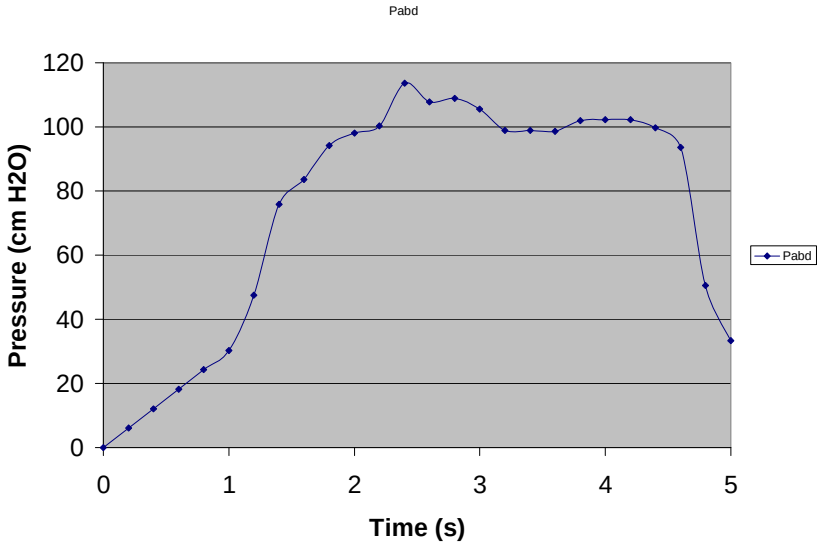

Figure 36: Pabd loads acquired from urodynamic measurements during a 4.0 second valsalva maneuver in a 28 year old continent subject. Note the addition of a 1 second interval at the beginning of each event during which pressure was applied gradually until baseline pressure was reached to prevent shocking the grid.

The Pura loads in the case of the valsalva maneuver were applied in the same manner as the Pura loads obtained for the cough. The only difference between the two was that in the case of the valsalva maneuver it was necessary to decrease the initial UPP

by 13% so that the peak Pura in the profile matched the baseline Pura at the start of the valsalva event while maintaining a similar pressure profile in the remainder of the urethra (Figure 37). As was the case with the cough simulations both a continent (non-leaking) and incontinent (leaking) simulations were run in which the Pura was specified in the same manner as was described earlier (Figure 38 and 39).

Simulations V and W investigated the effect of altering the urethral support on the mechanics predicted by the model. In all of the previous simulations the urethra was constrained against in-plane motion by constraining the outer most ridges of the (+) geometry to prohibit motion in the x and z plane. In models V and W these constraints were removed from the anterior and dorsal ridges of the (+) geometry but were left in tact on the lateral ridges. In both simulations the Pabd loads corresponding to the cough event modeled in simulations K through S was incorporated. Simulation V incorporated Puras corresponding to the continent cough event while simulation W incorporated Puras corresponding to an incontinent cough event as was described earlier.

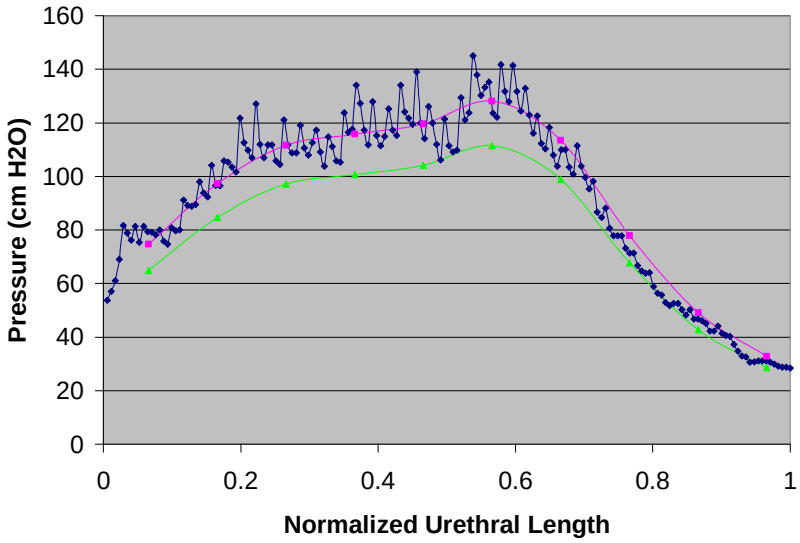

Figure 37: UPP (Blue) measured in a 28 year old continent patient (Urethral Length = 34mm) Averaged UPP (Pink) dividing the urethra into 10 equal regions. Valsalva Event corrected urethral pressure profile (Green) corrects the averaged urethral pressure profile so that the peak urethral pressure in the profile matches the baseline urethral pressure at the start of the modeled cough event.

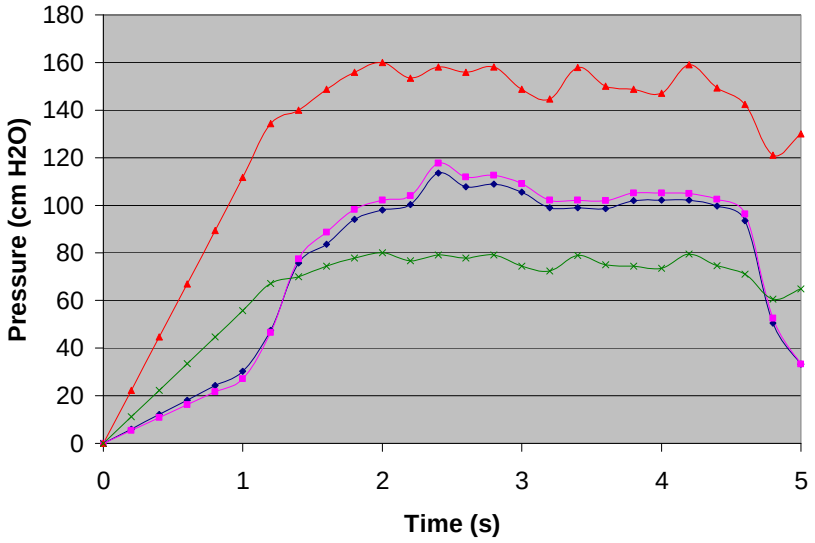

Figure 38: Urodynamic Pressure Loads associated with modeled valsava maneuver; Blue = Abdominal Pressure, Pink = Vesical Pressure, Red = Non-Leaking Urethral Pressure, Green = Leaking Urethral Pressure. In this figure the values of the abdominal, vesical and non-leaking urethral pressures were all obtained from measured urodynamic data. The leaking urethral pressure was obtained by reducing the non-leaking urethral pressure to one half of its measured value in order to force a leaking situation to occur in the model.

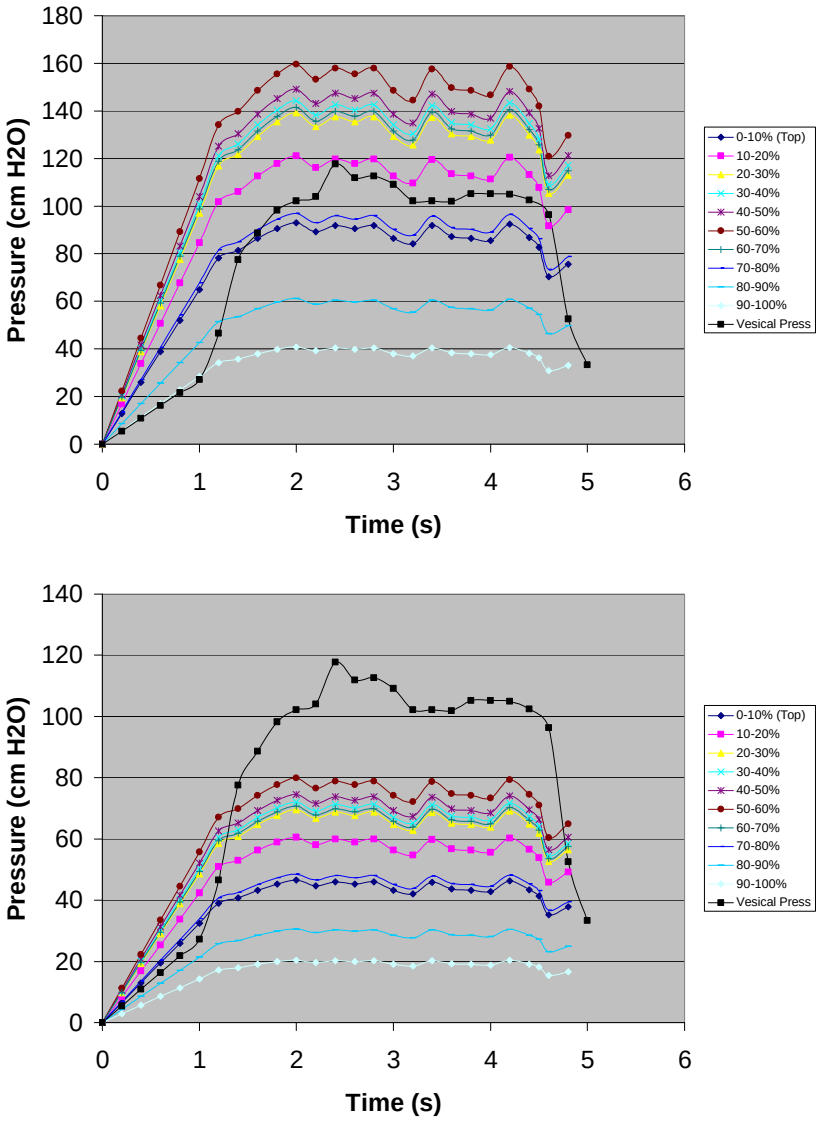

Figure 39: Illustration of the relationship between the measured vesical pressure and the applied urethral pressure loads along the urethra. Top graph illustrates a non-leaking event in which the urethral pressure is greater than vesical pressure (black line) in the regions located in the between the 10th and 70th percentile of the urethras length (Note 0th percent corresponds to the bladder neck region). Bottom graph illustrates a leaking event in which the vesical pressure (black line) exceeds the applied urethral pressure along the entire length of the urethra for almost the entire duration of the valsalva event

7.2 Results

Based on the findings of the simulations utilized to evaluate grid dependence and the effects of mass and time scaling, a sensitivity analysis was run utilizing a grid detailed in Simulation B with the time of the simulation scaled by a factor of 0.1. As was the case in evaluating grid dependence, the parameter of greatest interest in the sensitivity analysis simulations was the depth of urine penetration. Table XXI provides a summary of the results for all of the simulations run during the sensitivity analysis. Figures 40 - 51 illustrate the penetration depth observed at two time points in each simulation. In simulations in which a cough was modeled data is provided regarding the penetration depth at the time corresponding to peak Pabd and to the time corresponding to the second peak in Pabd during the cough event. In the case where a valsalva maneuver was modeled penetration depth is provided at the time points corresponding to peak Pabd and at the 3 second time point of the event.

Simulations K through R focused on evaluating the effects of urethral stiffness and applied urethral pressure on the depth to which urine was able to penetrate into the urethra. As the urethra was modeled as a Blatz Ko material, the effects of stiffness were tested by running simulations in which the shear modulus of this material was varied between 0.25 and 2x its published value. To evaluate the effects of applied Pura each simulation was run twice once utilizing the clinically obtained urodynamic Pura measurements and once utilizing these values at half their measured values to simulate a leaking condition as was described earlier. The results indicate that urethral stiffness will impact the depth to which urine will be able to penetrate. When the urethral stiffness was increased as was the case in simulations N and O where the urethra was stiffened to

2 times its published value the shallowest depth of urine penetration were predicted when both the continent and incontinent Pura loads were applied at both time points. In the simulations P, Q, R and S where the urethra was made more compliant the effects of urethral stiffness are not as clear. When the depth of penetration at the point of peak Pabd is considered, increasing the compliance of the urethra increased the depth of urine penetration when both the continent and incontinent Pura loads were applied. With the lone exception being simulation R in which the continent Pura loads were applied and the urethral stiffness was reduced to 0.25 times its published value. In this case the depth of penetration was equal to simulation P in which the same Pura loads were applied but the urethral stiffness was only reduced to 0.5 times its published values.

When the depth of penetration at the time point corresponding to the second peak in Pabd is considered, it was noted in simulations P and R that the penetration depth is reduced when the urethra is made more compliant and when the continent Pura loads are applied. However, when the incontinent Pura loads are applied as was the case in simulations Q and S the depth of urine penetration is approximately equal in both simulations regardless of urethral stiffness.

To further investigate the effects of applied Pura on the depth to which urine can penetrate a simulation (M) was run in which no Pura was applied to a model incorporating published values to define the urethral material. In this case the model predicted a slightly greater depth of penetration than simulation K in which the measured Pura loads were incorporated in an identical model and slightly shallower depth of penetration than simulation L when the reduced Pura loads were incorporated in an identical model.

Simulations V and W focused on determining if altering the constraints placed on the urethra would affect the depth of urine penetration. In both simulations as described earlier the anterior and dorsal in-plane motion constraints were removed. Both simulations predicted reduced depths of urine penetration when compared to the corresponding fully constrained simulations K and L respectively. However it should be noted that the funneling in the bladder neck region predicted in simulations V and W differed from that observed in simulations K and L (Figure 52).

Simulations T and U focused on determining if incorporating the Pabd and Pura loads consistent with a valsalva maneuver as described earlier would impact the models performance. Overall the models predictions for the depth of urine penetration were very similar to the simulations K and L which incorporated the same parameters but modeled a cough instead. Both models indicated that at peak Pabd the depth of penetration is equal when either the continent or incontinent Pura loads are incorporated. It is only at a later time point in the event that differences are observed as the simulations in which incontinent Pura loads were incorporated predicted an increased depth of penetration.

Table XXI: Summary of Sensitivity Analysis Results

Cough Simulation (Stiffness x Published)	Depth of Urine Penetration Peak Pabd (mm)	Depth of Urine Penetration 2nd Peak (mm)
K (1x)	10	17
L (1x)	10	19
M (1x)	10	18
N (2x)	7	11
O (2x)	7	13
P (0.5x)	12	15
Q (0.5x)	14	19
R (0.25x)	12	13
S (0.25x)	15	19
V (1x)	7	12
W (1x)	8	13
Valsalva Simulation	Depth of Urine Penetration Peak Pabd (mm)	Depth of Urine Penetration after 3 seconds
T (1x)	15	15
U (1x)	15	19

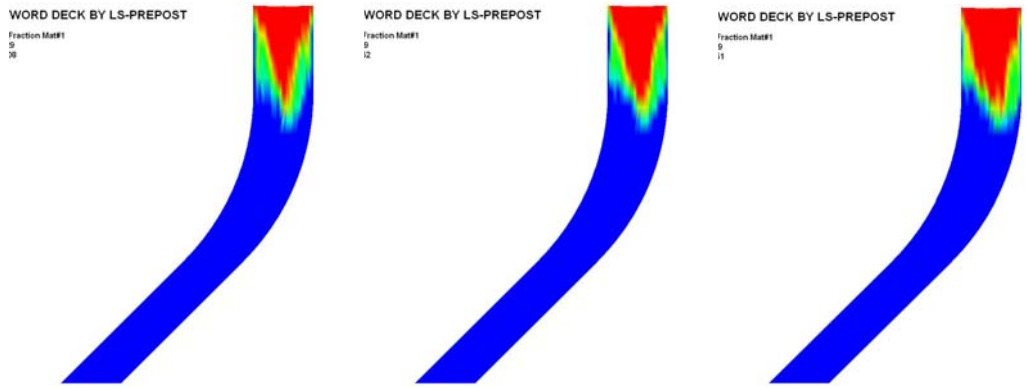

Figure 40: Depth of urine penetration at Peak Pabd during a cough for models incorporating published material properties to define the urethra. The left figure represents simulation K in which the non-leaking measured Pura loads were incorporated into the model. The middle figure represents simulation L in which the measured Pura loads were decreased to half their measured values to simulate a leaking simulation. The right figure represents simulation M in which no Pura loads were applied to the model.

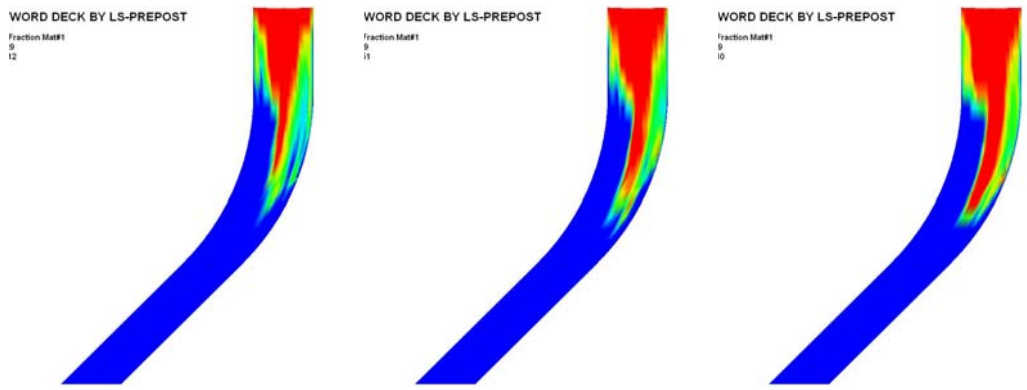

Figure 41: Depth of urine penetration observed at the time point corresponding to the second peak in the applied cough pressure loads for models incorporating published material properties to define the urethra. The left figure represents simulation K in which the non-leaking measured Pura loads were incorporated into the model. The middle figure represents simulation L in which the measured Pura loads were decreased to half their measured values to simulate a leaking simulation. The right figure represents simulation M in which no Pura loads were applied to the model.

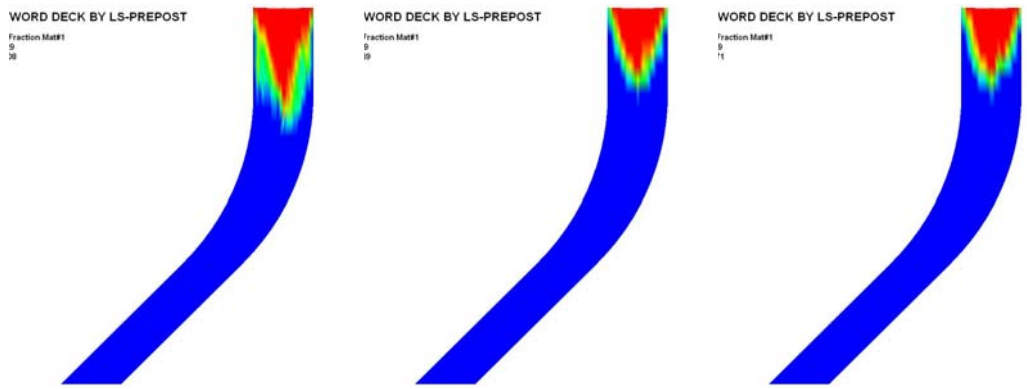

Figure 42: Effect of increasing the urethral material properties to 2 times the published value at the time point corresponding to peak Pabd. The figure on the left represents Simulation K which incorporated measured Pura loads and published material properties. The middle figure represents simulation N in which the shear modulus of the Blatz Ko material defining the urethra was increased to 2 times the published value while incorporating measured Pura loads. The right figure represents simulation O in which the shear modulus of the Blatz Ko material defining the urethra was increased to 2 times the published value while incorporating Pura loads reduced to half their measured values.

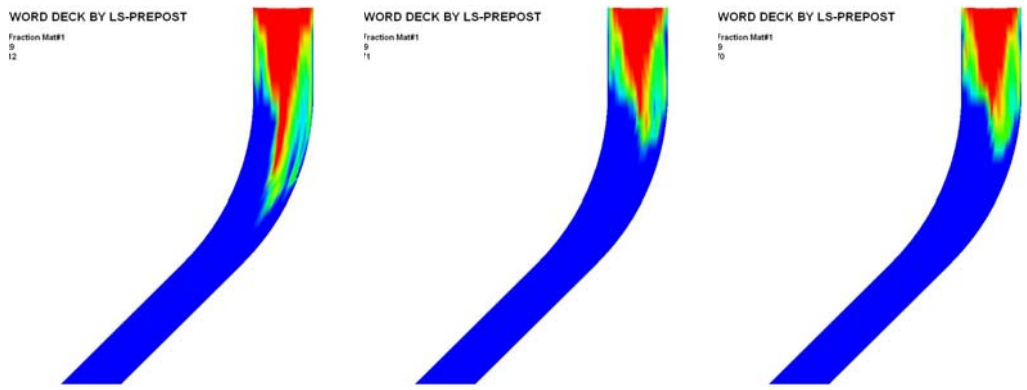

Figure 43: Effect of increasing the urethral material properties to 2 times the published value at the time point corresponding to the second peak in Pabd. The figure on the left represents Simulation K which incorporated measured Pura loads and published material properties. The middle figure represents simulation N in which the shear modulus of the Blatz Ko material defining the urethra was increased to 2 times the published value while incorporating measured Pura loads. The right figure represents simulation O in which the shear modulus of the Blatz Ko material defining the urethra was increased to 2 times the published value while incorporating Pura loads reduced to half their measured values.

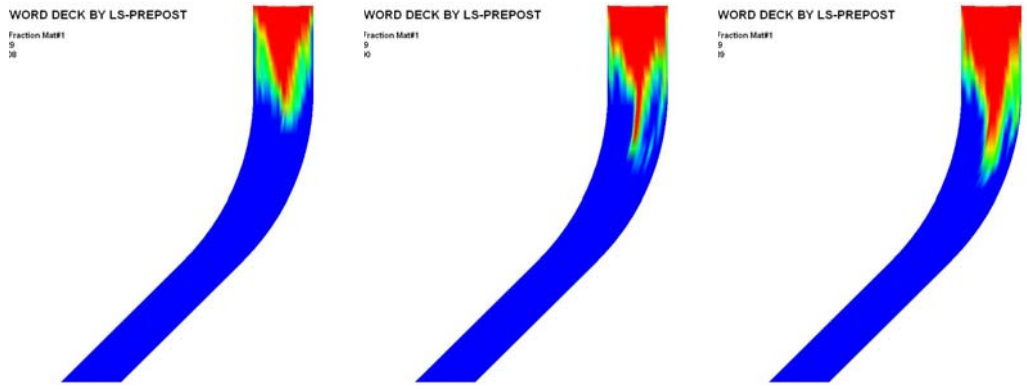

Figure 44: Effect of reducing the urethral material properties to 0.5 times the published value at the time point corresponding to peak Pabd. The figure on the left represents Simulation K which incorporated measured Pura loads and published material properties. The middle figure represents simulation P in which the shear modulus of the Blatz Ko material defining the urethra was reduced to 0.5 times the published value while incorporating measured Pura loads. The right figure represents simulation Q in which the shear modulus of the Blatz Ko material defining the urethra was reduced to 0.5 times the published value while incorporating Pura loads reduced to half their measured values.

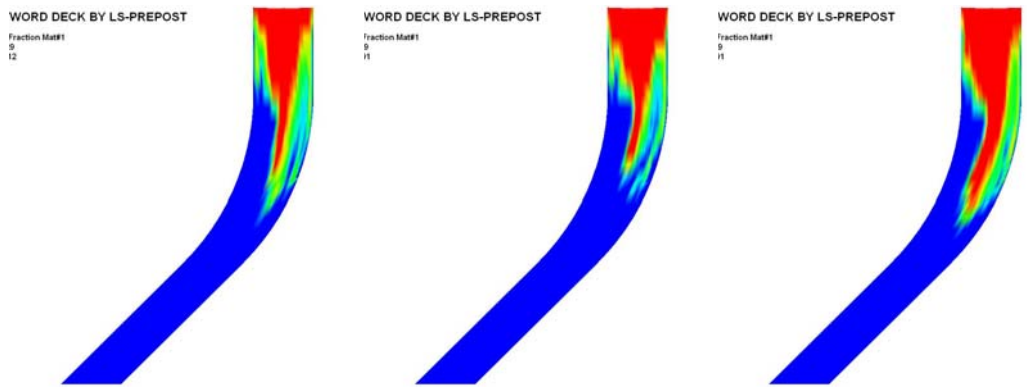

Figure 45: Effect of increasing the urethral material properties to 0.5 times the published value at the time point corresponding to the second peak in Pabd. The figure on the left represents Simulation K which incorporated measured Pura loads and published material properties. The middle figure represents simulation P in which the shear modulus of the Blatz Ko material defining the urethra was reduced to 0.5 times the published value while incorporating measured Pura loads. The right figure represents simulation Q in which the shear modulus of the Blatz Ko material defining the urethra was reduced to 0.5 times the published value while incorporating Pura loads reduced to half their measured values.

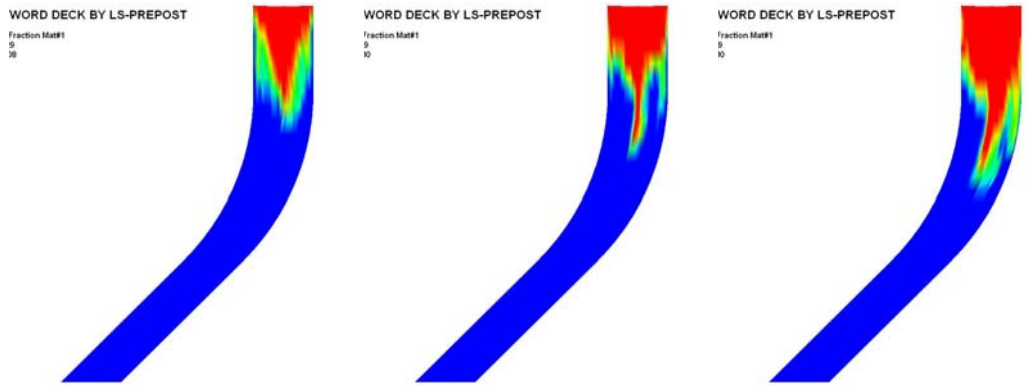

Figure 46: Effect of reducing the urethral material properties to 0.25 times the published value at the time point corresponding to peak Pabd. The figure on the left represents Simulation K which incorporated measured Pura loads and published material properties. The middle figure represents simulation R in which the shear modulus of the Blatz Ko material defining the urethra was reduced to 0.25 times the published value while incorporating measured Pura loads. The right figure represents simulation S in which the shear modulus of the Blatz Ko material defining the urethra was reduced to 0.25 times the published value while incorporating Pura loads reduced to half their measured values.

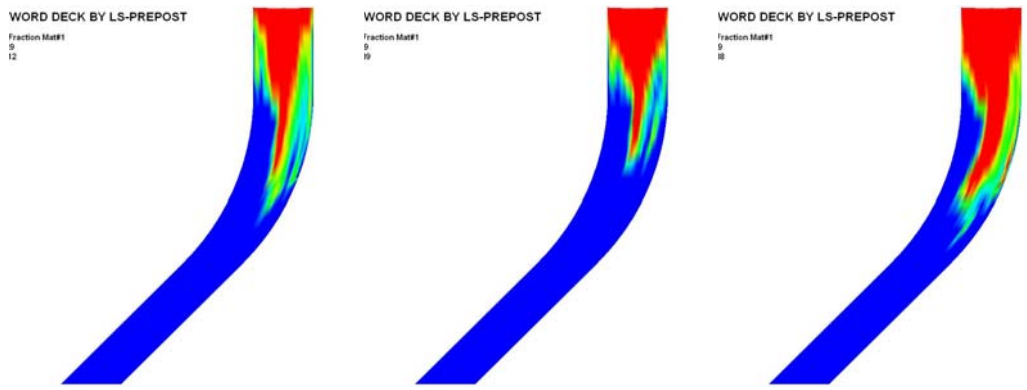

Figure 47: Effect of reducing the urethral material properties to 0.25 times the published value at the time point corresponding to the second peak in Pabd. The figure on the left represents Simulation K which incorporated measured Pura loads and published material properties. The middle figure represents simulation R in which the shear modulus of the Blatz Ko material defining the urethra was reduced to 0.25 times the published value while incorporating measured Pura loads. The right figure represents simulation S in which the shear modulus of the Blatz Ko material defining the urethra was reduced to 0.25 times the published value while incorporating Pura loads reduced to half their measured values.

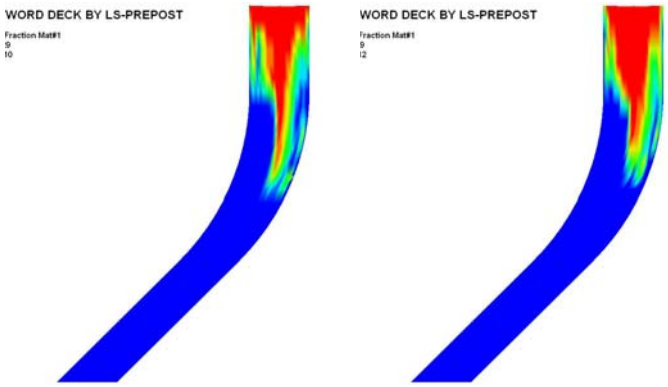

Figure 48: Depth of urine penetration at Peak Pabd during a valsalva maneuver for models incorporating published material properties to define the urethra. The left figure represents simulation T in which the non-leaking measured Pura loads were incorporated into the model. The right figure represents simulation U in which the measured Pura loads were decreased to half their measured values to simulate a leaking simulation.

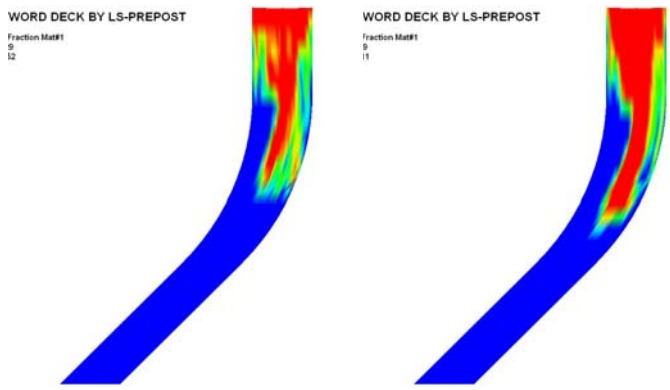

Figure 49: Depth of urine penetration at the 0.3 second time point during a valsalva maneuver for models incorporating published material properties to define the urethra. The left figure represents simulation T in which the non-leaking measured Pura loads were incorporated into the model. The right figure represents simulation U in which the measured Pura loads were decreased to half their measured values to simulate a leaking simulation.

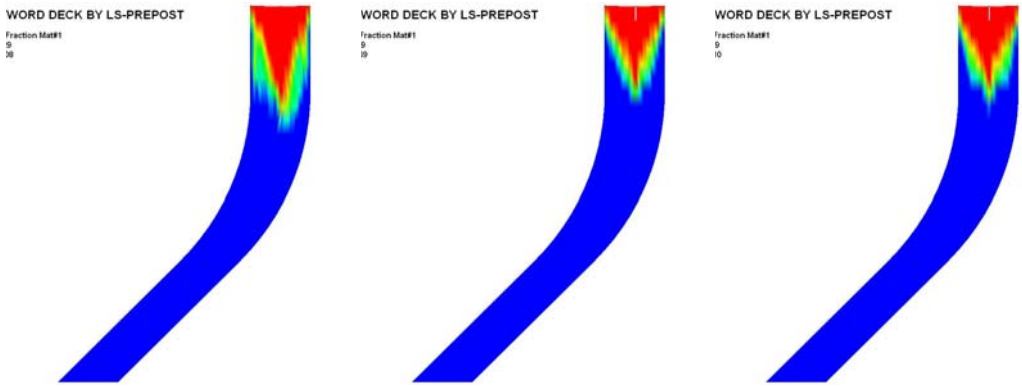

Figure 50: Effect of altering urethral support on the depth of urine penetration at peak Pabd during a cough. Right figure represents simulation K in which all of the exterior ridges of the urethral geometry were constrained against in plane translation and measured Pura loads were applied. Middle figure represents simulation V in which the only the lateral ridges of the urethral geometry were constrained against in plane motion and measured Pura loads were applied. Right figure represents simulation W in which Pura values were reduced to half their measured values. The model in this case was constrained in the same fashion as the model in simulation V.

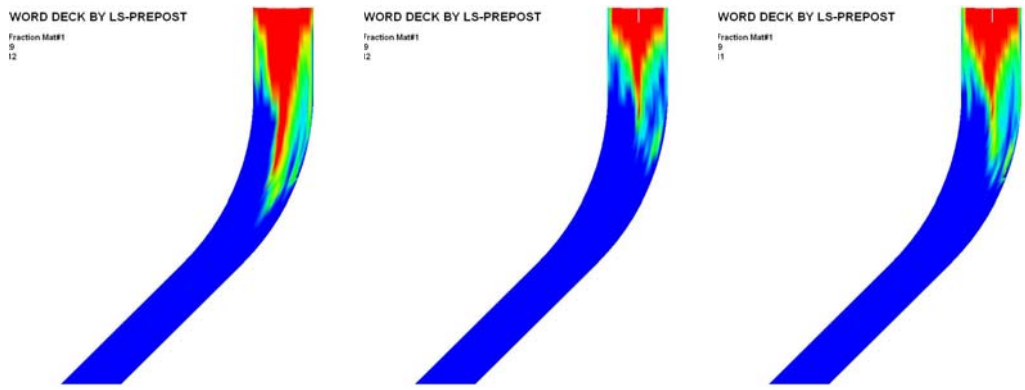

Figure 51: Effect of altering urethral support on the depth of urine penetration at the time point correspond to the second peak in Pabd during the applied cough loads. Right figure represents simulation K in which all of the exterior ridges of the urethral geometry were constrained against in plane translation and measured Pura loads were applied. Middle figure represents simulation V in which the only the lateral ridges of the urethral geometry were constrained against in plane motion and measured Pura loads were applied. Right figure represents simulation W in which Pura values were reduced to half their measured values. The model in this case was constrained in the same fashion as the model in simulation V.

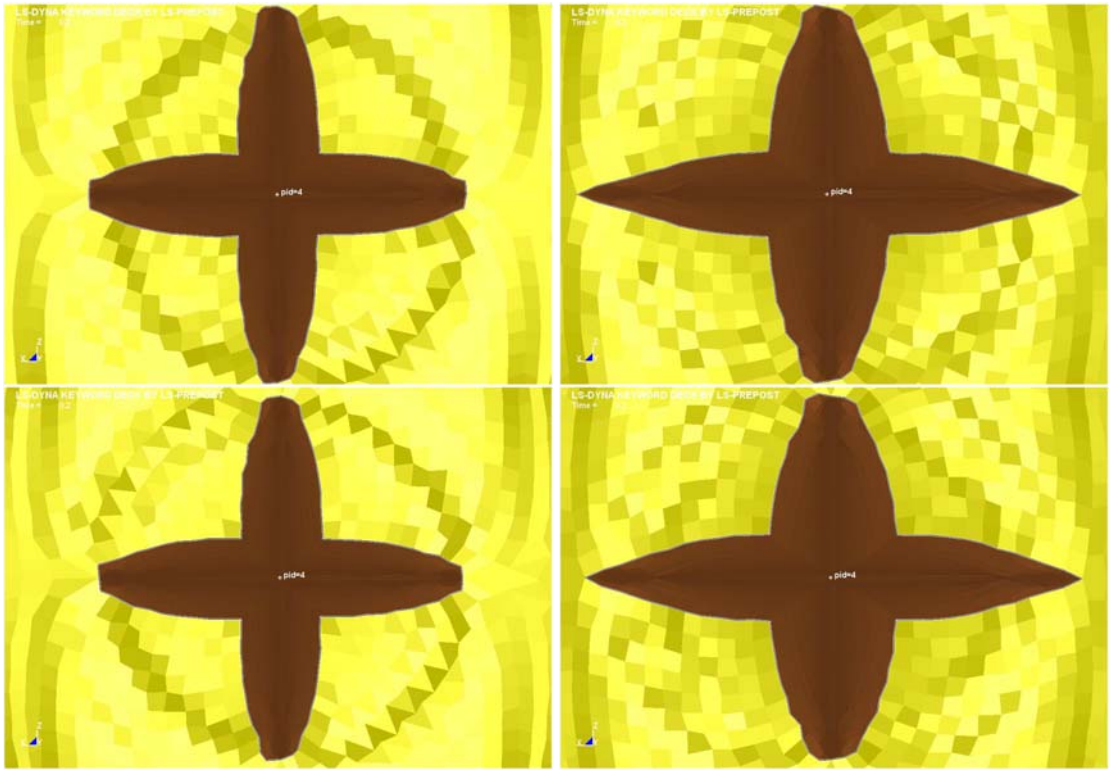

Figure 52: Effect of varying urethral constraints on funneling in the region of the bladder neck. Top Left illustrates funneling predicted in Simulation K in which the non-leaking urethral pressure loads were applied and the urethra was fully constrained for in-plane motion. Top Right illustrates the funneling predicted in Simulation V in which the non-leaking urethral pressure loads and the urethra was only constrained along its lateral ridges. Bottom Left illustrates funneling predicted in Simulation L in which the leaking urethral pressure loads were applied and the urethra was fully constrained for in-plane motion. Bottom Right illustrates the funneling predicted in Simulation W in which the non-leaking urethral pressure loads and the urethra was only constrained along its lateral ridges

7.3 Discussion

The goal of this portion of the dissertation was to utilize the model developed and characterized in Chapter VI to gain insight into how urethral stiffness, applied urethral pressure and urethral support would impact the mechanics predicted by the model.

In attempting to model the bladder and urethra in the context of stress urinary incontinence at this point in time the modeler is faced with a situation in which there are many unknowns with regard to the constitutive behavior, boundary conditions and

important physical processes. When attempting to model such a situation the modelers focus should be to utilize sensitivity analyses to gain insights into the mechanics of the modeled system [109] As a result, the models in this portion of this study focused on trying to understand how the mechanical response of a simplified model of a fluid filled bladder and urethra when subjected to fast acting pressure loads would be altered when the pressure acting on the tube, the compliance of the tube and the support of the tube were varied. In other words, the results of the sensitivity analysis are valid for this model alone and their physiological implications should be treated with great care as the modeled situation and the physiological situation are not the same.

In this model, the applied Pura, the stiffness of the material properties assigned to the urethra and the support of the urethra all affected the depth to which urine could penetrate into the urethral lumen. The impact of the urethral stiffness on the depth of penetration and the increased effectiveness of the measured Pura loads in reducing the depth of urine penetration when the urethral material was made more compliant indicates that one must take into account the material that is being moved out of the way or acted on by the external muscles of the urethra in constructing future models of the urethra. In this model the walls of the lumen were considered to be an isometric material with the material properties being assigned based on the work of Haridas et al who determined the material properties of the urethra while considering the entire structure of the urethra.[49] In reality it is known that the urethra consists of many structures including the urethral sphincters, the vascular plexus, the smooth muscle tube of the urethra and the submucosal layer.[4-8,15,17,19] Future models will need to take into account the role each of these

structures plays in preventing leaks and determine which of these structures are displaced by the urine being forced into the urethral lumen.

The loading of the urethral walls with Pura loads extracted from urodynamic pressure measurements is controversial as the Pura measured during urodynamics of a stress event is actually a measure of the pressure exerted by the wall of the urethral lumen on the pressure transducer of the microtip catheter and may not be an accurate indicator of urethral resistance. [110] However, at this point in time another widespread method for measuring urethral resistance to flow does not exist. In addition, in the above models as an initial approximation, it was assumed that the pressure rose in a uniform fashion along the entire length of the urethra due to the fact that the Pura measurement was only available at one location during the event. In future models, it will need to be determined if non-uniform rises in Pura in different portions of the urethra will affect the mechanics predicted by the model. The difficulty that arises in assigning these loads stems from the fact that while most anatomical descriptions provide information regarding the location of the structures like the external urethral sphincter that can exert pressure on the urethra it is difficult to infer from these descriptions how the pressure will vary from location to location during a stress event.[4-8]

The theories that have been proposed to conceptualize the continence mechanism have all focused on the support of the urethra as being critical to the maintenance of continence. [3,9,12] The models finding that the manner in which the urethra is constrained can affect the depth of urine penetration indicates that the support of the urethra must also be considered in future models. However, in order to accurately gauge the affect of

support on the predicted mechanics, more complex models of the bladder and the urethra that also incorporate the structures that support these organs will need to be considered.

To date, only Zhang et al have published a model of a fluid filled bladder and urethra during a stress event. [48] In this model the authors modeled these structures in a situation where a female subject lands a jump and assume that a leak will occur if any fluid enters into the urethra. In the images published the fluid is only seen in the upper portion of the urethra and does not fully transit the urethra. In the present work urine was found to enter into the urethra in all of the events modeled indicating that this may not be a suitable criterion for evaluating if a leak will or will not occur. Similar to the model published by Zhang et al the current models did not predict full transit of urine through the urethra. However, in the case of the current models this is most likely due to the time scaling that needed to be imposed on the model that modeled a 3 second cough event and a 5 second Valsalva maneuver as occurring in 0.3 and 0.5 seconds respectively.

7.4 Conclusions

The solutions reported above indicate that the applied Pura, the urethral stiffness and urethral support all impact the depth to which urine can penetrate into the urethra. However, a significant amount of work must be done to improve the models to make the models more physiologically realistic and to fully determine the impact and importance of each of these parameters on the mechanics by which continence is maintained.

CHAPTER VIII

OVERALL CONCLUSIONS AND FUTURE WORK

The focus of this study was to address the challenges associated with modeling the bladder and urethra in the context of stress urinary incontinence. The main challenges encountered in this study were how to utilize clinically obtained urodynamic data in FEM models of the bladder and the urethra and how to model the fluid structure interactions that occur within the bladder and the urethra during stress events. In the previous chapters, the construction of a simplified model of these structures in which the spilt operator form of the ALE method incorporating urodynamic pressures as loads to model these structures during stress events was detailed. The models as described in this work should be looked on as a starting point for the construction of future models that can be used to gain insight into the mechanics of SUI

Future work will need to focus on making the models more physiologically realistic. One of the first steps that should be taken in attempting to achieve this reailism would be to re-solve the models using an implicit solver. The utilization of an implicit

solver should allow for larger time steps to be used allowing for a reduction in the computational cost required to solve each model. The reduction in computational cost could potentially eliminate the need to incorporate a time scaling factor to achieve a solvable model.[50,51,55,56] The removal of the time scaling factor would result in a more realistic model as the urodynamic pressures used to specify the loads acting on th model would be applied over the same time interval in which they were measured during urodynamic testing thereby eliminating one abstraction from the model.

In addition to eliminating the time scaling utilized in the model the use of more realistic geometries and more realistic boundary conditions would also contribute to a more physiologically realistic model. A first step to achieving this realism would be to utilize medical images to construct physiologically realistic geometries of the bladder and the urethra and re-run the simulations detailed in this dissertation to determine if the more realistic geometries would have an impact on the mechanics predicted by the model. Future models will also need to incorporate more realistic boundary conditions to simulate the physiologic support provided by the structures of the pelvic floor and connective tissue. It is at this point that the use of the split operator form of the ALE method will be limited due to the fact that the support structures will need to be embedded within the Eulerian mesh representing the fluid which may impact the deformations predicted for these structures during stress events. One potential way to overcome this challenge would be to construct two models, in which a complex Lagrangian model based on medical images is used to determine the deformations of the structures and provide insight into how to constrain the bladder and urethra with equivalent geometries in a split operator model used to investigate the fluid structure

interactions. Both models will be needed as any deformation or stress information that can be generated by the complex Lagrangian model will not provide a great deal of insight into SUI unless it can be determined how these parameters will affect the fluid structure interactions that will indicate if a leak will or will not occur.

In order to evaluate the physiological realism of the above model it will be necessary to obtain medical images of the lower urinary tract and the pelvic floor detailing the deformation of these structures during a stress event. The medical images may be in the form of cine-magnetic resonance images of a stress event or Doppler ultra-sound images of a stress event. In either case it will be necessary to obtain urodynamic data that is acquired at the same time as the images. The urodynamic data will be critical to incorporating realistic loads into the model while the medical image data will be needed to evaluate if the deformations predicted by the model. In addition, it should be recorded as to whether a visivle leakage of urine was observed or not during a given stress event as this information will will be critical to evaluating the fluid mechanics predicted by the model. Determing if the model can predict when leaks should or should not occur will be critical to establishing the usefulness of future models in investigating the mechanics of SUI.

BIBLIOGRAPHY

1. Wilson L, Brown JS, Shin GP, Luc KO, and Subak LL. Annual Direct Cost of Urinary Incontinence. Obstetrics and Gynecology 98[03], 398-406. 2001.

2. Norton P and Brubaker L. Urinary Incontinence in Women. Lancet 367, 57-67. 2006.

3. Enhorning G, Miller ER, and Hinman F. Simultaneous recording of intravesical and intraurethral pressure. Acta Chirurgica Scandinavica 276[Supplement], 1-68. 1961.

4. Delancey JOL. The Patohophysiology of Stress Urinary Inconitnence. World Journal of Urology 15, 268-274. 1997.

5. Sampselle CM, DeLancey JOL. Anatomy of Female Continence. Journal of Wound Ostomy Continence Nursing 25[2], 63-74. 1998.

6. Delancey JOL and Ashton-Miller J. Pathophysiology of adult urinary incontinence. Gastroenterology 126, s23-s32. 2004.

7. Ashton-Miller J, Howard D, and Delancey JOL. The Functional Anatomy of the Female Pelvic Floor and Stress Continence Control System. Scandinavian Journal of Urology and Nephrology 207[Supplement], 1-124. 2001.

8. Ashton-Miller J and Delancey JOL. Functional Anatomy of the Female Pelvic Floor. Annals of the New York Acadamey of Sciences 1101, 266-296. 2007.

9. Petros PE and Ulmsten UI. An Integral Theory of Female Urinary Incontinence. Acta Obstetricia et Gynecologica Scandinavica 153[Supplement], 7-31. 1990.

10. Petros PE and Ulmsten UI. Role of the Pelvic Floor in Bladder Neck Opening and Closure I: Muscle Forces. International Urogynecology Journal 8, 74-80. 1997.

11. Petros PE and Ulmsten UI. Role of the Pelvic Floor in Bladder Neck Opening and Closure II: Vagina. International Urogynecology Journal 8, 69-73. 1997.

12. Delancey JOL. Structural support of the urethra as it relates to stress urinary incontinence: The hammock hypothesis. American Journal of Obstetrics and Gynecology 170, 1713-1720. 1994.

13. Pemberton J, Swash M, and Henry MM: The Pelvic Floor: Its Function and Disorders. New York, NY: WB Saunders, 2002.

14. Drake RL, Vogl W, and Mitchell AWM: Gray's Anatomy for Students. New York, NY: Elsevier Churchill Livingstone, 2005.

15. Haderer JM, Pannu HK, Genadry R, and Hutchins GM. Controversies in Female Urethral Anatomy and their Significance for Understanding Urinary Continence: Observations and Literature Review. International Urogynecology Journal 13, 236-252. 2002.

16. Colleselli K, Stenzl A, Eder R, Strasser H, Poisel S, and Bartsch G. The Female Urethral Sphincter: A Morphological and Topographical Study. The Journal of Urology 160, 49-54. 1998.

17. Huisman AB. Aspects on the anatomy of the female urethra with special relation to urinary continence. Contributions to Gynecology and Obstetrics 10, 1. 1983.

18. Rud T, Asmusssen M, Andersson KE, Hunting A, and Ulmsten U. Factors maintianing the intra-urethral pressure in women. Investigative Urology 17, 343. 1980.

19. Becco J, Leonard D, and Leonard F. Study of the female urethra's submucous vascular plexus. World Journal of Urology 16, 224. 1998.

20. Siracusano S, Bertolotto M, Cucchi A, Lampropoulou N, Tiberio A, Gasparini C, Ciciliato S, and Belgrano E. Application of ultrasound contrast agents for the characterization of female urethral vascularization in healthy pre- and postmenopausal volunteers: Preliminary Report. European Urology 50, 1316. 2006.

21. Fritsch H, Pinggera GM, Lienemann A, Mitterberger M, Bartsch G, and Strasser H. What are the Supportive Structures of the Female Urethra. Neurourology and Urodynamics 25, 128-134. 2006.

22. Sebe P, Fritsch H, Oswald J, Schwentner C, Lunacek A, Bartsch G, and Radmayr C. Fetal development of the female external urinary sphincter comples: An anatomical and histological study. The Journal of Urology 173, 1738-1742. 2005.

23. Viktrup L and Bump RC. Simplified neurophysiology of the lower urinary tract. Primary Care Update Ob/Gyns 10, 261-264. 2003.

24. Yucel S and Baskin LS. An anatomical description of the male and female urethral sphincter complex. The Journal of Urology 171, 1890-1897. 2004.

25. Keane DP and O'Sullivan S. Urinary Incontinence: Anatomy, Physiology and Pathophysiology. Clinical Obstetrics and Gynaecology 14[2], 207-226. 2002.

26. Borirakchanyavat S, Aboseif SR, Carroll PR, Tanagho EA, and Lue TF. Continence mechanism of the isolated female urethra: An anatomical study of the intrapelvic somatic nerves. The Journal of Urology 158, 822-826. 1997.

27. Pit MJ, DeRuiter MC, Nijeholt ABLA, Marani E, and Zwartendijk J. Anatomy of the Arcus Tendineus Fasciae Pelvis in Females. Clinical Anatomy 16, 131-137. 2003.

28. Chen L, Ashton-Miller J, Hsu Y, and Delancey JOL. Interaction among apical support, levator ani impairment, and anterior vaginal wall prolapse. Obstetrics and Gynecology 108[2], 323-332. 2006.

29. Chou Q and Delancey JOL. A Structured System to Evaluate Urethral Support Anatomy in Magnetic Resonance Images. American Journal of Obstetrics and Gynecology 185, 44-50. 2001.

30. Antonakos CL, Miller JM, and Sampselle CM. Indices for studying urinary incontinence and levator ani function in primiparous women. Journal of Clinical Nursing 12, 554-561. 2003.

31. Barber MD. Contemporary views on female pelvic anatomy. Cleveland Clinic Journal of Medicine 72, S3-S11. 2005.

32. Vazzoler N, Soulie' M, Escourrou G, Seguin P, Pontonnier F, Becue J, and Plante P. Pubourethral Ligaments in Women: Anatomical and Clinical Aspects. Surgical and Radiologic Anatomy 24, 33-37. 2002.

33. El Sayed, Morsy MM, El Mashed SM, and Abdel-Azim MS. Anatomy of the urethral supporting ligaments defined by dissection, histology and mri of female cadavers adn mri of healthy nulliparous women. American Journal of Radiology 189, 1145-1157. 2007.

34. Massey A and Abrams P. Urodynamics of the Lower Urinary Tract. Clinics in Obstetrics and Gynaecology 12[2], 319. 1985.

35. Hilton P and Stanton S. Urethal Pressure Measurements by Microtransducer. The results in symptom-free women and in those with genuine stress incontinence. British Journal of Obstetrics and Gynaecology 90, 919-933. 1983.

36. Reigner CH, Kolsky H, Richardson PD, Ghoniem GM, and Susset JG. The elastic behavior of the urinary bladder for large deformations. Journal of Biomechanics 16, 915-922. 1983.

37. Torzen A. Assessment of fiber strength in a urinary bladder using experimental pressure volume curves. Jounal of Biomechanical Engineering 108, 301-305. 1986.

38. Damaser MS and Lehman SL. The Effect of Urinary Bladder Shape on its Mechanics During Filling. Journal of Biomechanics 28[6], 725-732. 1995.

39. Chi Y, Liang J, and Yan D. A material sensitivity study on the accuracy of deformable organ registration using linear biomechanical models. Medical Physics 33[2], 421-433. 2006.

40. Backman KA: Effective Urethral Diameter. In: Hydrodynamics of Micturition Springfield, IL: Charles C. Thomas, pp 250-256, 1971.

41. Ritter BC, Zinner NR, and Paquin AJ. Clinical Urodynamics II: Analysis of pressure-flow rleation in the normal female urethra. The Journal of Urology 91, 161-165. 1964.

42. Griffiths DJ. Urethral elastcitiy and micturition hydrodynamics in females. Medical and Biological Engineering 7, 201. 1969.

43. Griffiths DJ. Hydrodynamics of male micturition - 1. Medical and Biological Engineering 9, 581. 1971.

44. Griffiths DJ. Hydrodynamics of male micturition - 2. Medical and Biological Engineering 9, 589. 1971.

45. Spangberg A, Terio H, Engberg A, and Ask P. Quantification of urethral function based on Griffiths model of flow through elastic tubes. Neurourology and Urodynamics 8, 29-52. 1989.

46. Horak M and Kren J. Mathematical model of the male urinary tract. Mathematics and Computers in Simulation 61, 573. 2003.

47. Kim KJ. Biomechanical Analyses of Female Stress Urinary Incontinence. 1994. University of Michigan.

48. Zhang Y, Kim S, Erdman AG, Roberts KP, and Timm GW. Feasibility of using a computer modeling approach to study sui induced by landing a jump. Annals of Biomedical Engineering 37, 1425-1433. 2009.

49. Haridas B, Hong H, Minoguchi R, Owens S, and Osborn T. PelvicSim - A Computational Experimental System for Biomechanical Evaluation of Female Pelvic Floor Organ Disorders and Associated Minimally Invasive Interventions. Studies in Health Technology and Informatics 119, 182-187. 2006.

50. Logan DL: A First Course in the Finite Element Method Using Algor. Pacific Grove, CA: Brooks/Cole, 2001.

51. Huebner KH, Dewhirst DL, Smith DE, and Byrom TG: The Finite Element Method for Engineers. New York, NY: John Wiley and Sons, 2001.

52. Rao SS: The Finite Element Method in Engineering. Boston, MA: Elsevier, 2005.

53. Encyclopedia of Computational Mechanics. John Wiley & Sons Ltd, 2004.

54. Cor A, Barbic M, and Kralj B. Differences in the Quantity of Elastic Fibres and Collagen Type I and Type III in Endopelvic Fascia Between Women with Stress Urinary Incontinence and Controls. Urological Research 31, 61-65. 2002.

55. Zienkiewicz OC, Taylor RL, and Zhu JZ: The Finite Element Method: Its Basics and Fundamentals. New York: Elsevier Butterworth Hienemann, 2005.

56. Cook RD, Malkus DS, Plesha ME, and Witt RJ: Concepts and Applications of Finite Element Analysis. New York: John Wiley and Sons Inc., 2002.

57. Sun JS, Lee KH, and Lee HP. Comparison of implicit and explicit finite lement methods for dynamic problems. Journal of Materials Procssing Technology 105, 110. 2000.

58. Kim J, Kang Y, Choi H, Hwang S, and Kang B. Comparison of Implicit and Explicit Finite-Element Methods for the Hydroforming Process of an Automobile Lower Arm. The International Journal of Advanced Manufacturing Technology 20, 407. 2002.

59. Hopkins AR. Total Shoulder Arthroplasty Simulation using Finite Element Analysis. 2004. Imperial College London.

60. Harewood FJ and McHugh PE. Comparison of the implicit and explicit finite element methods using crystal plasticity. Computational Materials Science 39, 481. 2007.

61. Carmody CJ, Burriesci G, Howard IC, and Patterson EA. An approach to the simulation of fluid-structure interaction in the aortic valve. Journal of Biomechanics 39, 158. 2006.

62. Nicosia MA, Cochran RP, Einstein DR, Rutland CJ, and Kunzelman KS. A Coupled Fluid Structure Finite Element Model of the Aortic Valve and Root. The Journal of Heart Valve Disease 12, 781. 2003.

63. Weinberg EJ and Mofrad MRK. Transient, Three-Dimensional, Multiscalesimulations of the Human Aortic Valve. Cardiovascular Engineering 7. 2007.

64. Weinberg EJ and Mofrad MRK. A multiscale computational comparison of the bicuspid and tricuspid aortic valves in relation to alcific aortic stenosis. Journal of Biomechanics 41, 3482. 2008.

65. Zhang A and Suzuki K. A Comparative Study of Numerical Simulations for Fluid-Structure Interaction of Liquid-Filled Tank During Ship Collision. Ocean Engineering 34, 645-652. 2007.

66. Anghileri M, Castelletti LML, and Tirelli M. Fluid-Structure Interaction of Water Filled Tanks During Impact with the Ground. International Journal of Impact Engineering 31, 235-254. 2005.

67. Liu GR: Mesh Free Methods: Moving Beyond the Finite Element Method. Boca Raton, FL: CRC Press, 2003.

68. Donea J, Huerta A, Ponthot J-Ph, and Rodriquez-Ferran A: Arbitrary Lagrangian-Eulerian Methods. In: Encyclopedia of Computational Mechanics. Edited by Stein E, de Borst R, and Hughes TJR: New York, NY: John Wiley & Sons, vol. 1, chapt. 14, 2004.

69. Souli M, Ouahsine A, and Lewin L. ALE Formulation for Fluid-Structure Interaction Problems. Computer Methods in Applied Mechanics and Engineering 190, 659-675. 2000.

70. Benson DJ. Computational Methods in Lagrangian and Eulerian Hydrocodes. Computer Methods in Applied Mechanics and Engineering 99, 235. 1992.

71. Kuhl E, Hulshoff S, and de Borst R. An Arbitrary Lagrangian Eulerian Finite-Element Approach for Fluid-Structure Interaction Phenomena. International Journal For Numerical Methods in Engineering 57, 117-142. 2003.

72. Le Tallec P and Mouro J. Fluid Structure Interaction with Large Structural Displacements. Computer Methods in Applied Mechanics and Engineering 190, 3039-3067. 2001.

73. Wang J and Gadala MS. Formulation and Survey of ALE Method in Nonlinear Solic Mechanics. Finite Elements in Analysis and Design 24, 253-269. 1997.

74. Mendes PA and Branco FA. Analysis of Fluid Structure Interaction by an Arbitrary Lagrangian-Eulerian Finite Element Formulation. International Journal For Numerical Methods in Fluids 30, 897-919. 1999.

75. Cho JR and Lee SY. Dynamic analysis of baffled fuel-storage tanks using the ALE finite element method. International Journal For Numerical Methods in Fluids 41, 185-208. 2003.

76. Aquelet N, Souli M, and Olovsson L. Euler-Lagrange coupling with damping effects: Application to slamming problems. Computer Methods in Applied Mechanics and Engineering 195, 110. 2006.

77. Sarthou A, Vincent S, Clatagirone P, and Angot Ph. Eulerian-Lagrangian grid coupling and penalty methods for the simulation of multiphase flows interacting with complex objects. International Journal For Numerical Methods in Fluids 56, 1093. 2008.

78. Pericevic IO and Moatamedi M. Application of the penalty coupling method for the analysis of blood vessels. European Journal of Computational Mechanics 16, 537. 2010.

79. Yamada H: Strength of Biological Materials. Baltimore, MD: Williams and Wilkins, 1970.

80. Taber L: Nonlinear Theory of Elasticity: Applications in Biomechanics. River Edge, NJ: World Scientific Publishing Co., 2004.

81. Hallquist JO: LS Dyna Keyword Manual. Livermore Software Technology Co., 2008.

82. Hallquist JO: LS Dyna Theory Manual. Livermore Software Technology Co, 2008.

83. Van Mastrigt R and Griffiths DJ. An evaluation of contractility parameters determined from isometric contractions and micturition studies. Urological Research 14, 45-52. 1986.

84. Bastiaanssen EHC, van Leeuwen JL, Vanderschoot J, and Redert PA. A myocybernetic model of the lower urinary tract. Journal of Theoretical Biology 178, 113-133. 1996.

85. Bastiaanssen EHC, Vanderschoot J, and van Leeuwen JL. State-space analysis of a myocybernetic model of the lower urinary tract. Journal of Theoretical Biology 180, 215-227. 1996.

86. Hosein RA and Griffiths DJ. Computer simulation of the neural control of the bladder and urethral. Neurourology and Urodynamics 9, 601. 1990.

87. Chan L, The S, Titus J, and Tse V. The value of bladder wall thickness measurement in the assessment of overactive bladder syndrome. Ultrasound in Obstetrics and Gynecology 26, 460. 2005.

88. Umek WH, Obermair A, Stutterecker D, Hausler G, Leodolter S, and Hanzal E. Three-dimensional ultrasound of the female urethra: comparing transvaginal and transrectal scanning. Ultrasound in Obstetrics and Gynecology 17, 425-430. 2001.

89. Umek WH, Laml T, Stutterecker D, Obermair A, Leodolter S, and Hanzal E. The urethra during pelvic floor contraction observations on three-dimensional ultrasound. Obstetrics and Gynecology 100[4], 796-800. 2002.

90. Netter FH: Atlas of Human Anatomy. Philadelphia: Saunders Elsevier, 2006.

91. Janda S, van der Helm FCT, and de Blok SB. Measuring Morphological Parameters of the Pelvic Floor for Finite Element Modelling Purposes. Journal of Biomechanics 36, 749-757. 2003.

92. D'Aulignac D, Martins JAC, Pires EB, Mascarenhas T, and Natal Jorge RM. A shell finite element model of the pelvic floor muscles. Computer Methods in Biomechanics and Biomedical Engineering 8[5], 339-347. 2005.

93. Yingchun Z, Seoggwan K, Erdman AG, Roberts KP, and Timm GW. Feasibility of using a computer modeling approach to study SUI induced by landing a jump. Annals of Biomedical Engineering 37[7], 1425. 2009.

94. Strohbehn K, Ellis JH, Strohbehn JA, and Delancey JOL. Magnetic resonance imaging of the levator ani with anatomic correlation. Obstetrics and Gynecology 87[2], 277-285. 1996.

95. Bush MB, Petros PE, and Barrett-Lennard BR. On the flow through the human female urethra. Journal of Biomechanics 30[9], 967-969. 1997.

96. Petros PE. The Pubourethral Ligaments - An Anatomical and Histological Study in the LIve Patient. International Urogynecology Journal 9, 154-157. 1998.

97. Petros PE and Skilling PM. Pelvic Floor Rehabilitation in the Female According to the Integral Theory of Female Urinary Incontinence. European Journal of Obstetrics and Gynecology 94, 264-269. 2001.

98. Petros PE. Vault Prolapse I: Dynamic Supports of the Vagina. International Urogynecology Journal 12, 292-295. 2001.

99. Fielding JR, Griffiths DJ, Versi E, Mulkern RV, Lee MLT, and Jolesz FA. MR imaging of pelvic floor and continence mechanisms in the supine and sitting positions. American Journal of Radiology 171, 1607-1610. 1998.

100. Kearney R, Sawhney R, and Delancey JOL. Levator Ani Muscle Anatomy Evaluated by Origin-Insertion Pairs. Obstetrics and Gynecology 104[1], 168-173. 2004.

101. Fung YC: Biomechanics Mechanical Properties of Living Tissues. New York: Springer-Verlag, 1993.

102. Lotz HT, Remeijer P, van herk M, Lebesque JV, deBois JA, Zijp LJ, and Moonen LM. A Model to Predict Bladder Shapes from Changes in Bladder and Rectal Filling. Medical Physics 31[6], 1415-1423. 2004.

103. Benson DJ. Volume of fluid interface reconstruction methods for multi-material problems. Appl Mech Rev 55, 151. 2002.

104. Chung WJ, Cho JW, and Belytschko T. On the dynamic effects of explicit FEM in sheet metal forming analysis. Engineering Computation 15, 750. 1998.

105. Mattiasson K, Bernspang L, and Samuelsson L. Solution of quasi-static, force-driven problems by means of a dynamic-explicit approach and an adaptive loading procedure. Engineering Computation 13, 172. 1996.

106. Mattiasson K, Bernspang L, and Samuelsson A. Solution of quasi-static, force-driven problems by means of a dynamic-explicit approach and an adaptive loading procedure. Engineering Computation 13, 172. 1996.

107. Pullan BR, Phillips JI, and Hickey DS. Urethral lumen cross-sectional shape: It's radiological determination and relationship to function. British Journal of Urology 54, 399. 1982.

108. Gleason DM, Bottaccini MR, and Reilly RJ. The shape and cross-sectional area of the distal urethra critically affects urinary flow. Investigative Urology 8, 585. 1971.

109. Anderson AE, Ellis BJ, and Weiss JA. Verification, validationa and sensitivity studies in computational biomechanics. Computer Methods in Biomechanics and Biomedical Engineering 00, 110. 2006.

110. DeLancey, J. O., Trowbridge, E. R., Miller, J. M., Morgan, D. M., Guire, K., Fenner, D. E. et al.: Stress urinary incontinence: relative importance of urethral support and urethral closure pressure. Journal of Urology, 179**:** 2286, 2290.

APPENDIX A:

ABRIDGED LS DYNA KEYWORD FILE:

FIRST OBJECTIVE NON-LINEAR MODEL

First Objective Non-Linear Model

Units	
Length	Meter
Time	Second
Mass	Kilogram
Force	Newton

```
*KEYWORD
*TITLE
$# title
LS-DYNA keyword deck by LS-Prepost
*CONTROL_TERMINATION
$#  endtim    endcyc     dtmin    endeng    endmas
  1.800000         0     0.000     0.000     0.000
*DATABASE_BINARY_D3PLOT
$#      dt      lcdt      beam     npltc    psetid
   0.050000         0         0         0         0
*CONTACT_SURFACE_TO_SURFACE_ID
$ SLIDING INTERFACE DEFINITIONS
$ TrueGrid Sliding Interface #    1
$#     cid                                                          title
         1TrueGridSlidingInterface#1
$#    ssid      msid     sstyp     mstyp    sboxid    mboxid       spr       mpr
         3         1         3         3         0         0         0         0
$#      fs        fd        dc        vc       vdc    penchk        bt        dt
     0.000     0.000     0.000     0.000     0.000         0     0.000     0.000
$#     sfs       sfm       sst       mst      sfst      sfmt      fsf       vsf
     0.000     0.000     0.000     0.000     0.000     0.000     0.000     0.000
*CONTACT_SURFACE_TO_SURFACE_ID
$#     cid                                                          title
         2TrueGridSlidingInterface#2
$#    ssid      msid     sstyp     mstyp    sboxid    mboxid       spr       mpr
         3         4         3         3         0         0         0         0
$#      fs        fd        dc        vc       vdc    penchk        bt        dt
     0.000     0.000     0.000     0.000     0.000         0     0.000     0.000
$#     sfs       sfm       sst       mst      sfst      sfmt      fsf       vsf
     0.000     0.000     0.000     0.000     0.000     0.000     0.000     0.000
*CONTACT_SURFACE_TO_SURFACE_ID
$#     cid                                                          title
         3TrueGridSlidingInterface#3
$#    ssid      msid     sstyp     mstyp    sboxid    mboxid       spr       mpr
         2         3         3         3         0         0         0         0
$#      fs        fd        dc        vc       vdc    penchk        bt        dt
     0.000     0.000     0.000     0.000     0.000         0     0.000     0.000
$#     sfs       sfm       sst       mst      sfst      sfmt      fsf       vsf
     0.000     0.000     0.000     0.000     0.000     0.000     0.000     0.000
*PART
$# title
bladder wall mooney rivlin hyperelastic
$#     pid     secid       mid     eosid      hgid      grav    adpopt      tmid
         1         1         1         0         1         0         0         0
*SECTION_SOLID
$#   secid    elform       aet
         1         2         0
*MAT_MOONEY-RIVLIN_RUBBER
$#     mid        ro        pr         a         b       ref
         1 1030.0000  0.450000 7500.0000 2500.0000     0.000
$#     sgl        sw        st      lcid
     0.000     0.000     0.000         0
*HOURGLASS
$#    hgid       ihq        qm       ibq        q1        q2    qb/vdc        qw
         1         1  1.000000         0     0.000     0.000     0.000     0.000
*PART
$# title
liquid treated as quasi solid
```

```
$#     pid     secid       mid     eosid      hgid      grav    adpopt      tmid
         2         2         2         0         2         0         0         0
*SECTION_SOLID
$#   secid    elform       aet
         2         2         0
*MAT_ELASTIC_FLUID
$ DEFINITION OF MATERIAL     2
$#     mid        ro         e        pr        da        db         k
         2 1000.0000 2.2000E+9  0.000000     0.000     0.000 2.2000E+9
$#      vc        cp
  0.100000     0.000
*HOURGLASS
$#    hgid       ihq        qm       ibq        q1        q2    qb/vdc        qw
         2         1  1.000000         0     0.000     0.000     0.000     0.000
*PART
$# title
linearly elastic contracted muscle support structure
$#     pid     secid       mid     eosid      hgid      grav    adpopt      tmid
         3         3         3         0         3         0         0         0
*SECTION_SOLID
$#   secid    elform       aet
         3         2         0
*MAT_ELASTIC
$ DEFINITION OF MATERIAL     3
$#     mid        ro         e        pr        da        db  not used
         3 1040.0000 5.0000E+6  0.450000     0.000     0.000         0
*HOURGLASS
$#    hgid       ihq        qm       ibq        q1        q2    qb/vdc        qw
         3         1  1.000000         0     0.000     0.000     0.000     0.000
*PART
$# title
blatz ko rubber urethra
$#     pid     secid       mid     eosid      hgid      grav    adpopt      tmid
         4         4         4         0         4         0         0         0
*SECTION_SOLID
$#   secid    elform       aet
         4         2         0
*MAT_BLATZ-KO_RUBBER
$ DEFINITION OF MATERIAL     4
$#     mid        ro         g       ref
         4 1030.0000 1.0000E+5     0.000
*HOURGLASS
$#    hgid       ihq        qm       ibq        q1        q2    qb/vdc        qw
         4         1  1.000000         0     0.000     0.000     0.000     0.000
*DEFINE_CURVE
$ LOAD CURVES
$#    lcid      sidr       sfa       sfo      offa      offo    dattyp
         1         0     0.000     0.000     0.000     0.000         0
$#               a1                  o1
             0.000               0.000
          0.2000000         372.7000122
          0.4000000         245.1999969
          0.6000000        1981.0000000
          0.8000000        8218.0000000
          1.0000000        11033.000000
          1.2000000        2746.0000000
          1.4000000        6011.7001953
          1.6000000         921.7999878
          1.8000000               0.000
```

```
*DEFINE_CURVE
$#     lcid      sidr       sfa       sfo      offa      offo    dattyp
         2         0     0.000     0.000     0.000     0.000         0
$#               a1                  o1
                0.000               0.000
            0.2000000        -372.7000122
            0.4000000        -245.1999969
            0.6000000       -1981.0000000
            0.8000000       -8218.0000000
            1.0000000       -11033.000000
            1.2000000       -2746.0000000
            1.4000000       -6011.7001953
            1.6000000        -921.7999878
            1.8000000               0.000
```

APPENDIX B:

ABRIDGED LS DYNA KEYWORD FILE:

FIRST OBJECTIVE LINEAR MODEL

First Objective Linear Model

Units

Length	Meter
Time	Second
Mass	Kilogram
Force	Newton

```
*KEYWORD
*TITLE
$# title
LS-DYNA keyword deck by LS-Prepost
*CONTROL_TERMINATION
$#  endtim    endcyc     dtmin    endeng    endmas
  1.800000         0     0.000     0.000     0.000
*DATABASE_BINARY_D3PLOT
$#      dt      lcdt      beam     npltc    psetid
   0.050000         0         0         0         0
*CONTACT_SURFACE_TO_SURFACE_ID
$ SLIDING INTERFACE DEFINITIONS
$ TrueGrid Sliding Interface #    1
$#     cid                                                         title
         1TrueGridSlidingInterface#1
$#    ssid      msid     sstyp     mstyp    sboxid    mboxid       spr       mpr
         3         1         3         3         0         0         0         0
$#      fs        fd        dc        vc       vdc    penchk        bt        dt
     0.000     0.000     0.000     0.000     0.000         0     0.000     0.000
$#     sfs       sfm       sst       mst      sfst      sfmt       fsf       vsf
     0.000     0.000     0.000     0.000     0.000     0.000     0.000     0.000
*CONTACT_SURFACE_TO_SURFACE_ID
$#     cid                                                         title
         2TrueGridSlidingInterface#2
$#    ssid      msid     sstyp     mstyp    sboxid    mboxid       spr       mpr
         3         4         3         3         0         0         0         0
$#      fs        fd        dc        vc       vdc    penchk        bt        dt
     0.000     0.000     0.000     0.000     0.000         0     0.000     0.000
$#     sfs       sfm       sst       mst      sfst      sfmt       fsf       vsf
     0.000     0.000     0.000     0.000     0.000     0.000     0.000     0.000
*CONTACT_SURFACE_TO_SURFACE_ID
$#     cid                                                         title
         3TrueGridSlidingInterface#3
$#    ssid      msid     sstyp     mstyp    sboxid    mboxid       spr       mpr
         2         4         3         3         0         0         0         0
$#      fs        fd        dc        vc       vdc    penchk        bt        dt
     0.000     0.000     0.000     0.000     0.000         0     0.000     0.000
$#     sfs       sfm       sst       mst      sfst      sfmt       fsf       vsf
     0.000     0.000     0.000     0.000     0.000     0.000     0.000     0.000
*PART
$# title
linearly elastic bladder wall
$#     pid     secid       mid     eosid      hgid      grav    adpopt      tmid
         1         1         1         0         1         0         0         0
*SECTION_SOLID
$#   secid    elform       aet
         1         2         0
*MAT_ELASTIC
$#     mid        ro         e        pr        da        db  not used
         1 1030.0000 50000.000  0.450000     0.000     0.000         0
*HOURGLASS
$#    hgid       ihq        qm       ibq        q1        q2    qb/vdc        qw
         1         1  1.000000         0     0.000     0.000     0.000     0.000
*PART
$# title
liquid treated as quasi solid
$#     pid     secid       mid     eosid      hgid      grav    adpopt      tmid
         2         2         2         0         2         0         0         0
```

```
*SECTION_SOLID
$#   secid    elform       aet
         2         2         0
*MAT_ELASTIC_FLUID
$ DEFINITION OF MATERIAL     2
$#     mid        ro         e        pr        da        db         k
         2 1000.0000 2.2000E+9  0.000000     0.000     0.000 2.2000E+9
$#      vc        cp
  0.100000     0.000
*HOURGLASS
$#    hgid       ihq        qm       ibq        q1        q2    qb/vdc        qw
         2         1  1.000000         0     0.000     0.000     0.000     0.000
*PART
$# title
linearly elastic contracted muscle support structure
$#     pid     secid       mid     eosid      hgid      grav    adpopt      tmid
         3         3         3         0         3         0         0         0
*SECTION_SOLID
$#   secid    elform       aet
         3         2         0
*MAT_ELASTIC
$ DEFINITION OF MATERIAL     3
$#     mid        ro         e        pr        da        db  not used
         3 1040.0000 5.0000E+6  0.450000     0.000     0.000         0
*HOURGLASS
$#    hgid       ihq        qm       ibq        q1        q2    qb/vdc        qw
         3         1  1.000000         0     0.000     0.000     0.000     0.000
*PART
$# title
linearly elastic Urethra
$#     pid     secid       mid     eosid      hgid      grav    adpopt      tmid
         4         4         4         0         4         0         0         0
*SECTION_SOLID
$#   secid    elform       aet
         4         2         0
*MAT_ELASTIC
$ DEFINITION OF MATERIAL     4
$#     mid        ro         e        pr        da        db  not used
         4 1040.0000 5.0000E+6  0.450000     0.000     0.000         0
*HOURGLASS
$#    hgid       ihq        qm       ibq        q1        q2    qb/vdc        qw
         4         1  1.000000         0     0.000     0.000     0.000     0.000
*DEFINE_CURVE
$ LOAD CURVES
$#    lcid      sidr       sfa       sfo      offa      offo    dattyp
         1         0     0.000     0.000     0.000     0.000         0
$#               a1                  o1
             0.000               0.000
          0.2000000         372.7000122
          0.4000000         245.1999969
          0.6000000        1981.0000000
          0.8000000        8218.0000000
          1.0000000        11033.000000
          1.2000000        2746.0000000
          1.4000000        6011.7001953
          1.6000000         921.7999878
          1.8000000               0.000
*DEFINE_CURVE
$#    lcid      sidr       sfa       sfo      offa      offo    dattyp
         2         0     0.000     0.000     0.000     0.000         0
$#               a1                  o1
             0.000               0.000
          0.2000000        -372.7000122
          0.4000000        -245.1999969
          0.6000000       -1981.0000000
          0.8000000       -8218.0000000
          1.0000000       -11033.000000
          1.2000000       -2746.0000000
          1.4000000       -6011.7001953
          1.6000000        -921.7999878
          1.8000000               0.000
```

APPENDIX C:

ABRIDGED LS DYNA KEYWORD FILE

SECOND OBJECTIVE NON-LEAKING MODEL

Second Objective Non-Leaking Model

Units

Length	Millimeter
Time	Second
Mass	Tonne
Force	Newton

```
*KEYWORD
*TITLE
$# title
LS-DYNA keyword deck by LS-Prepost
*CONTROL_ALE
$#     dct      nadv      meth      afac      bfac      cfac      dfac      efac
         1         1         1 -1.000000     0.000     0.000     0.000     0.000
$#   start       end     aafac     vfact      prit       ebc      pref   nsidebc
     0.0001.0000E+20  1.000000 1.0000E-6         0         0     0.000         0
*CONTROL_CONTACT
$#  slsfac    rwpnal    islchk    shlthk    penopt    thkchg     orien    enmass
  0.100000     0.000         1         0         0         0         1         0
$#  usrstr    usrfrc     nsbcs    interm     xpene     ssthk     ecdt   tiedprj
         0         0         0         0  4.000000         0         0         0
$#   sfric     dfric       edc       vfc        th     th_sf    pen_sf
     0.000     0.000     0.000     0.000     0.000     0.000     0.000
$#  ignore    frceng   skiprwg    outseg   spotstp   spotdel   spothin
         0         0         0         0         0         0     0.000
$#    isym    nserod    rwgaps    rwgdth     rwksf      icov    swradf    ithoff
         0         0         0     0.000  1.000000         0     0.000         0

*CONTROL_ENERGY
$#    hgen      rwen    slnten     rylen
         2         2         1         1
*CONTROL_SHELL
$#  wrpang     esort     irnxx    istupd    theory       bwc     miter      proj
 20.000000         0        -1         0         2         2         1         0
$# rotascl    intgrd    lamsht    cstyp6    tshell    nfail1    nfail4   psnfail
  1.000000         0         0         1         0         0         0         0
$# psstupd    irquad
         0         0
*CONTROL_TERMINATION
$#  endtim    endcyc     dtmin    endeng    endmas
  0.300000         0     0.000     0.000     0.000
*CONTROL_TIMESTEP
$#  dtinit    tssfac      isdo    tslimt     dt2ms      lctm     erode     ms1st
     0.000  0.900000         0     0.000     0.000         0         0         0
$#  dt2msf   dt2mslc     imscl
     0.000         0         0
*DATABASE_BINARY_D3PLOT
$#      dt      lcdt      beam     npltc    psetid
  0.005000         0         0         0         0
$ MATERIAL CARDS
$ DEFINITION OF MATERIAL     1
$#   ioopt
         0
*DATABASE_BINARY_RUNRSF
$#      dt      lcdt      beam     npltc    psetid
 1.0000E+5         0         0         0         0
```

```
*CONTACT_SINGLE_SURFACE_ID
$ SLIDING INTERFACE DEFINITIONS
$ TrueGrid Sliding Interface #    1
$#     cid                                                              title
         1TrueGridSlidingInterface#1
$#    ssid      msid     sstyp     mstyp    sboxid    mboxid       spr       mpr
         5         0         3         0         0         0         0         0
$#      fs        fd        dc        vc       vdc    penchk        bt        dt
     0.000     0.000     0.000     0.000     0.000         0     0.000     0.000
$#     sfs       sfm       sst       mst      sfst      sfmt      fsf       vsf
     0.000     0.000     0.000     0.000     0.000     0.000     0.000     0.000
*PART
$# title
bladder wall mooney rivlin hyperelastic
$#     pid     secid       mid     eosid      hgid      grav    adpopt      tmid
         1         1         1         0         1         0         0         0
*SECTION_SHELL
$#   secid    elform      shrf       nip     propt   qr/irid     icomp     setyp
         1         1  0.830000         0         1         0         0         1
$#      t1        t2        t3        t4      nloc     marea      idof    edgset
  2.000000  2.000000  2.000000  2.000000 -1.000000     0.000     0.000         0
*MAT_MOONEY-RIVLIN_RUBBER
$#     mid        ro        pr         a         b       ref
         1 1.0300E-9  0.450000  0.007500  0.002500     0.000
$#     sgl        sw        st      lcid
     0.000     0.000     0.000         0
*HOURGLASS
$#    hgid       ihq        qm       ibq        q1        q2    qb/vdc        qw
         1         1  0.100000         0     0.000     0.000     0.000     0.000
*PART
$# title
urethra and bladder neck modeled as blatz ko hyperelastic materials
$#     pid     secid       mid     eosid      hgid      grav    adpopt      tmid
         4         4         4         0         4         0         0         0
*SECTION_SHELL
$#   secid    elform      shrf       nip     propt   qr/irid     icomp     setyp
         4         1  0.830000         0         1         0         0         1
$#      t1        t2        t3        t4      nloc     marea      idof    edgset
  2.000000  2.000000  2.000000  2.000000 -1.000000     0.000     0.000         0
*MAT_BLATZ-KO_RUBBER
$ DEFINITION OF MATERIAL     4
$#     mid        ro         g       ref
         4 1.0400E-9  0.100000     0.000
*HOURGLASS
$#    hgid       ihq        qm       ibq        q1        q2    qb/vdc        qw
         4         1  0.100000         0     0.000     0.000     0.000     0.000
*PART
$# title
urethra and bladder neck modeled as blatz ko hyperelastic materials
$#     pid     secid       mid     eosid      hgid      grav    adpopt      tmid
         5         5         5         0         5         0         0         0
*SECTION_SHELL
$#   secid    elform      shrf       nip     propt   qr/irid     icomp     setyp
         5         1  0.830000         0         1         0         0         1
$#      t1        t2        t3        t4      nloc     marea      idof    edgset
  4.000000  4.000000  4.000000  4.000000 -1.000000     0.000     0.000         0
*MAT_BLATZ-KO_RUBBER
$ DEFINITION OF MATERIAL     5
$#     mid        ro         g       ref
         5 1.0400E-9  0.100000     0.000
*HOURGLASS
$#    hgid       ihq        qm       ibq        q1        q2    qb/vdc        qw
         5         1  0.100000         0     0.000     0.000     0.000     0.000
*PART
$# title
material type # 9  (Fluid)
$#     pid     secid       mid     eosid      hgid      grav    adpopt      tmid
         7         7        24         0         7         0         0         0
```

```
*SECTION_SOLID_ALE
$#   secid    elform       aet
         7        11         0
$#    afac      bfac      cfac      dfac     start       end     aafac
     0.000     0.000     0.000     0.000     0.000     0.000     0.000
*MAT_ELASTIC_FLUID
$#     mid        ro         e        pr        da        db         k
        24 1.0000E-9     0.000     0.000     0.000     0.000 2250.0000
$#      vc        cp
  0.1000001.0000E+20
*HOURGLASS
$#    hgid       ihq        qm       ibq        q1        q2    qb/vdc        qw
         7         1 1.0000E-5         0     0.000     0.000     0.000     0.000
*PART
$# title
material type # 9  (Fluid)
$#     pid     secid       mid     eosid      hgid      grav    adpopt      tmid
         8         8        21         0         8         0         0         0
*SECTION_SOLID_ALE
$#   secid    elform       aet
         8        11         3
$#    afac      bfac      cfac      dfac     start       end     aafac
     0.000     0.000     0.000     0.000     0.000     0.000     0.000
*MAT_ALE_VACUUM
$#     mid       rho
        21 1.0000E-9
*HOURGLASS
$#    hgid       ihq        qm       ibq        q1        q2    qb/vdc        qw
         8         1 1.0000E-5         0     0.000     0.000     0.000     0.000
*PART
$# title
material type # 9  (Fluid)
$#     pid     secid       mid     eosid      hgid      grav    adpopt      tmid
         9         9        22         0         9         0         0         0
*SECTION_SOLID_ALE
$#   secid    elform       aet
         9        11         1
$#    afac      bfac      cfac      dfac     start       end     aafac
     0.000     0.000     0.000     0.000     0.000     0.000     0.000
*MAT_ALE_VACUUM
$#     mid       rho
        22 1.0000E-9
*HOURGLASS
$#    hgid       ihq        qm       ibq        q1        q2    qb/vdc        qw
         9         1 1.0000E-5         0     0.000     0.000     0.000     0.000
*PART
$# title
material type # 9  (Fluid)
$#     pid     secid       mid     eosid      hgid      grav    adpopt      tmid
        10        10        23         0        10         0         0         0
*SECTION_SOLID_ALE
$#   secid    elform       aet
        10        11         0
$#    afac      bfac      cfac      dfac     start       end     aafac
     0.000     0.000     0.000     0.000     0.000     0.000     0.000
*MAT_ALE_VACUUM
$#     mid       rho
        23 1.0000E-9
*HOURGLASS
$#    hgid       ihq        qm       ibq        q1        q2    qb/vdc        qw
        10         1 1.0000E-5         0     0.000     0.000     0.000     0.000
*MAT_NULL
$ DEFINITION OF MATERIAL     7
$#     mid        ro        pc        mu     terod     cerod        ym        pr
         7 1.0000E-9     0.000 1.0000E-9     0.000     0.000     0.000     0.000
```

```
*DEFINE_CURVE
$ LOAD CURVES
$#    lcid      sidr       sfa       sfo      offa      offo    dattyp
         1         0     0.000     0.000     0.000     0.000         0
$#                a1                  o1
                0.000               0.000
            0.0100000               0.000
            0.0200000      7.8455999e-004
            0.0400000           0.0015691
            0.0600000           0.0023537
            0.0800000           0.0031382
            0.1000000           0.0038443
            0.1200000           0.0042170
            0.1400000           0.0040895
            0.1600000           0.0058254
            0.1800000           0.0120626
            0.2000000           0.0148772
            0.2200000           0.0065903
            0.2400000           0.0098560
            0.2600000           0.0047662
            0.2800000           0.0032363
            0.3000000           0.0038443
*DEFINE_CURVE
$#    lcid      sidr       sfa       sfo      offa      offo    dattyp
         2         0     0.000     0.000     0.000     0.000         0
$#                a1                  o1
                0.000               0.000
            0.0100000               0.000
            0.0200000     -7.8455999e-004
            0.0400000          -0.0015691
            0.0600000          -0.0023537
            0.0800000          -0.0031382
            0.1000000          -0.0038443
            0.1200000          -0.0042170
            0.1400000          -0.0040895
            0.1600000          -0.0058254
            0.1800000          -0.0120626
            0.2000000          -0.0148772
            0.2200000          -0.0065903
            0.2400000          -0.0098560
            0.2600000          -0.0047662
            0.2800000          -0.0032363
            0.3000000          -0.0038443
*DEFINE_CURVE
$#    lcid      sidr       sfa       sfo      offa      offo    dattyp
         3         0     0.000     0.000     0.000     0.000         0
$#                a1                  o1
                0.000               0.000
            0.0100000               0.000
            0.0200000      7.8455999e-004
            0.0400000               0.000
            0.0600000               0.000
            0.0800000               0.000
            0.1000000               0.000
            0.1200000               0.000
            0.1400000               0.000
            0.1600000               0.000
            0.1800000               0.000
            0.2000000               0.000
            0.2200000               0.000
            0.2400000               0.000
            0.2600000               0.000
            0.2800000               0.000
            0.3000000               0.000
```

```
*DEFINE_CURVE
$#     lcid      sidr       sfa       sfo      offa      offo    dattyp
         4         0     0.000     0.000     0.000     0.000         0
$#               a1                  o1
             0.000               0.000
           0.0100000               0.000
           0.0200000    -7.8455999e-004
           0.0400000               0.000
           0.0600000               0.000
           0.0800000               0.000
           0.1000000               0.000
           0.1200000               0.000
           0.1400000               0.000
           0.1600000               0.000
           0.1800000               0.000
           0.2000000               0.000
           0.2200000               0.000
           0.2400000               0.000
           0.2600000               0.000
           0.2800000               0.000
           0.3000000               0.000
*DEFINE_CURVE
$#     lcid      sidr       sfa       sfo      offa      offo    dattyp
         5         0     0.000     0.000     0.000     0.000         0
$#               a1                  o1
             0.000               0.000
           0.0100000           0.0014110
           0.0200000           0.0014110
           0.0400000           0.0028220
           0.0600000           0.0042330
           0.0800000           0.0056439
           0.1000000           0.0069533
           0.1200000           0.0066373
           0.1400000           0.0070041
           0.1600000           0.0081837
           0.1800000           0.0109718
           0.2000000           0.0124336
           0.2200000           0.0083812
           0.2400000           0.0091093
           0.2600000           0.0083135
           0.2800000           0.0067219
           0.3000000           0.0069533
*DEFINE_CURVE
$#     lcid      sidr       sfa       sfo      offa      offo    dattyp
         6         0     0.000     0.000     0.000     0.000         0
$#               a1                  o1
             0.000               0.000
           0.0100000          -0.0014110
           0.0200000          -0.0014110
           0.0400000          -0.0028220
           0.0600000          -0.0042330
           0.0800000          -0.0056439
           0.1000000          -0.0069533
           0.1200000          -0.0066373
           0.1400000          -0.0070041
           0.1600000          -0.0081837
           0.1800000          -0.0109718
           0.2000000          -0.0124336
           0.2200000          -0.0083812
           0.2400000          -0.0091093
           0.2600000          -0.0083135
           0.2800000          -0.0067219
           0.3000000          -0.0069533
```

```
*DEFINE_CURVE
$#     lcid      sidr       sfa       sfo      offa      offo    dattyp
         7         0     0.000     0.000     0.000     0.000         0
$#               a1                  o1
             0.000               0.000
         0.0100000           0.0018379
         0.0200000           0.0018379
         0.0400000           0.0036759
         0.0600000           0.0055138
         0.0800000           0.0073517
         0.1000000           0.0090573
         0.1200000           0.0086456
         0.1400000           0.0091235
         0.1600000           0.0106600
         0.1800000           0.0142918
         0.2000000           0.0161959
         0.2200000           0.0109173
         0.2400000           0.0118657
         0.2600000           0.0108291
         0.2800000           0.0087559
         0.3000000           0.0090573
*DEFINE_CURVE
$#     lcid      sidr       sfa       sfo      offa      offo    dattyp
         8         0     0.000     0.000     0.000     0.000         0
$#               a1                  o1
             0.000               0.000
         0.0100000          -0.0018379
         0.0200000          -0.0018379
         0.0400000          -0.0036759
         0.0600000          -0.0055138
         0.0800000          -0.0073517
         0.1000000          -0.0090573
         0.1200000          -0.0086456
         0.1400000          -0.0091235
         0.1600000          -0.0106600
         0.1800000          -0.0142918
         0.2000000          -0.0161959
         0.2200000          -0.0109173
         0.2400000          -0.0118657
         0.2600000          -0.0108291
         0.2800000          -0.0087559
         0.3000000          -0.0090573
*DEFINE_CURVE
$#     lcid      sidr       sfa       sfo      offa      offo    dattyp
         9         0     0.000     0.000     0.000     0.000         0
$#               a1                  o1
             0.000               0.000
         0.0100000           0.0021106
         0.0200000           0.0021106
         0.0400000           0.0042212
         0.0600000           0.0063318
         0.0800000           0.0084424
         0.1000000           0.0104010
         0.1200000           0.0099282
         0.1400000           0.0104770
         0.1600000           0.0122414
         0.1800000           0.0164120
         0.2000000           0.0185986
         0.2200000           0.0125369
         0.2400000           0.0136260
         0.2600000           0.0124356
         0.2800000           0.0100549
         0.3000000           0.0104010
```

```
*DEFINE_CURVE
$#     lcid      sidr       sfa       sfo      offa      offo    dattyp
        10         0     0.000     0.000     0.000     0.000         0
$#               a1                  o1
             0.000               0.000
         0.0100000          -0.0021106
         0.0200000          -0.0021106
         0.0400000          -0.0042212
         0.0600000          -0.0063318
         0.0800000          -0.0084424
         0.1000000          -0.0104010
         0.1200000          -0.0099282
         0.1400000          -0.0104770
         0.1600000          -0.0122414
         0.1800000          -0.0164120
         0.2000000          -0.0185986
         0.2200000          -0.0125369
         0.2400000          -0.0136260
         0.2600000          -0.0124356
         0.2800000          -0.0100549
         0.3000000          -0.0104010
*DEFINE_CURVE
$#     lcid      sidr       sfa       sfo      offa      offo    dattyp
        11         0     0.000     0.000     0.000     0.000         0
$#               a1                  o1
             0.000               0.000
         0.0100000           0.0021873
         0.0200000           0.0021873
         0.0400000           0.0043745
         0.0600000           0.0065618
         0.0800000           0.0087491
         0.1000000           0.0107788
         0.1200000           0.0102889
         0.1400000           0.0108576
         0.1600000           0.0126861
         0.1800000           0.0170082
         0.2000000           0.0192742
         0.2200000           0.0129924
         0.2400000           0.0141210
         0.2600000           0.0128874
         0.2800000           0.0104201
         0.3000000           0.0107788
*DEFINE_CURVE
$#     lcid      sidr       sfa       sfo      offa      offo    dattyp
        12         0     0.000     0.000     0.000     0.000         0
$#               a1                  o1
             0.000               0.000
         0.0100000          -0.0021873
         0.0200000          -0.0021873
         0.0400000          -0.0043745
         0.0600000          -0.0065618
         0.0800000          -0.0087491
         0.1000000          -0.0107788
         0.1200000          -0.0102889
         0.1400000          -0.0108576
         0.1600000          -0.0126861
         0.1800000          -0.0170082
         0.2000000          -0.0192742
         0.2200000          -0.0129924
         0.2400000          -0.0141210
         0.2600000          -0.0128874
         0.2800000          -0.0104201
         0.3000000          -0.0107788
```

```
*DEFINE_CURVE
$#     lcid      sidr       sfa       sfo      offa      offo    dattyp
        13         0     0.000     0.000     0.000     0.000         0
$#               a1                  o1
             0.000               0.000
         0.0100000           0.0022622
         0.0200000           0.0022622
         0.0400000           0.0045243
         0.0600000           0.0067865
         0.0800000           0.0090486
         0.1000000           0.0111479
         0.1200000           0.0106412
         0.1400000           0.0112293
         0.1600000           0.0131205
         0.1800000           0.0175905
         0.2000000           0.0199341
         0.2200000           0.0134372
         0.2400000           0.0146045
         0.2600000           0.0133286
         0.2800000           0.0107769
         0.3000000           0.0111479
*DEFINE_CURVE
$#     lcid      sidr       sfa       sfo      offa      offo    dattyp
        14         0     0.000     0.000     0.000     0.000         0
$#               a1                  o1
             0.000               0.000
         0.0100000          -0.0022622
         0.0200000          -0.0022622
         0.0400000          -0.0045243
         0.0600000          -0.0067865
         0.0800000          -0.0090486
         0.1000000          -0.0111479
         0.1200000          -0.0106412
         0.1400000          -0.0112293
         0.1600000          -0.0131205
         0.1800000          -0.0175905
         0.2000000          -0.0199341
         0.2200000          -0.0134372
         0.2400000          -0.0146045
         0.2600000          -0.0133286
         0.2800000          -0.0107769
         0.3000000          -0.0111479
*DEFINE_CURVE
$#     lcid      sidr       sfa       sfo      offa      offo    dattyp
        15         0     0.000     0.000     0.000     0.000         0
$#               a1                  o1
             0.000               0.000
         0.0100000           0.0024221
         0.0200000           0.0024221
         0.0400000           0.0048442
         0.0600000           0.0072663
         0.0800000           0.0096885
         0.1000000           0.0119362
         0.1200000           0.0113936
         0.1400000           0.0120234
         0.1600000           0.0140483
         0.1800000           0.0188344
         0.2000000           0.0213437
         0.2200000           0.0143874
         0.2400000           0.0156372
         0.2600000           0.0142711
         0.2800000           0.0115390
         0.3000000           0.0119362
```

```
*DEFINE_CURVE
$#     lcid      sidr       sfa       sfo      offa      offo    dattyp
        16         0     0.000     0.000     0.000     0.000         0
$#               a1                  o1
             0.000               0.000
         0.0100000          -0.0024221
         0.0200000          -0.0024221
         0.0400000          -0.0048442
         0.0600000          -0.0072663
         0.0800000          -0.0096885
         0.1000000          -0.0119362
         0.1200000          -0.0113936
         0.1400000          -0.0120234
         0.1600000          -0.0140483
         0.1800000          -0.0188344
         0.2000000          -0.0213437
         0.2200000          -0.0143874
         0.2400000          -0.0156372
         0.2600000          -0.0142711
         0.2800000          -0.0115390
         0.3000000          -0.0119362
*DEFINE_CURVE
$#     lcid      sidr       sfa       sfo      offa      offo    dattyp
        17         0     0.000     0.000     0.000     0.000         0
$#               a1                  o1
             0.000               0.000
         0.0100000           0.0021450
         0.0200000           0.0021450
         0.0400000           0.0042901
         0.0600000           0.0064351
         0.0800000           0.0085802
         0.1000000           0.0105708
         0.1200000           0.0100903
         0.1400000           0.0106480
         0.1600000           0.0124413
         0.1800000           0.0166799
         0.2000000           0.0189021
         0.2200000           0.0127416
         0.2400000           0.0138484
         0.2600000           0.0126386
         0.2800000           0.0102190
         0.3000000           0.0105708
*DEFINE_CURVE
$#     lcid      sidr       sfa       sfo      offa      offo    dattyp
        18         0     0.000     0.000     0.000     0.000         0
$#               a1                  o1
             0.000               0.000
         0.0100000          -0.0021450
         0.0200000          -0.0021450
         0.0400000          -0.0042901
         0.0600000          -0.0064351
         0.0800000          -0.0085802
         0.1000000          -0.0105708
         0.1200000          -0.0100903
         0.1400000          -0.0106480
         0.1600000          -0.0124413
         0.1800000          -0.0166799
         0.2000000          -0.0189021
         0.2200000          -0.0127416
         0.2400000          -0.0138484
         0.2600000          -0.0126386
         0.2800000          -0.0102190
         0.3000000          -0.0105708
```

```
*DEFINE_CURVE
$#     lcid      sidr       sfa       sfo      offa      offo    dattyp
        19         0     0.000     0.000     0.000     0.000         0
$#               a1                  o1
             0.000               0.000
         0.0100000           0.0014717
         0.0200000           0.0014717
         0.0400000           0.0029434
         0.0600000           0.0044151
         0.0800000           0.0058868
         0.1000000           0.0072525
         0.1200000           0.0069228
         0.1400000           0.0073055
         0.1600000           0.0085358
         0.1800000           0.0114439
         0.2000000           0.0129685
         0.2200000           0.0087418
         0.2400000           0.0095012
         0.2600000           0.0086712
         0.2800000           0.0070111
         0.3000000           0.0072525
*DEFINE_CURVE
$#     lcid      sidr       sfa       sfo      offa      offo    dattyp
        20         0     0.000     0.000     0.000     0.000         0
$#               a1                  o1
             0.000               0.000
         0.0100000          -0.0014717
         0.0200000          -0.0014717
         0.0400000          -0.0029434
         0.0600000          -0.0044151
         0.0800000          -0.0058868
         0.1000000          -0.0072525
         0.1200000          -0.0069228
         0.1400000          -0.0073055
         0.1600000          -0.0085358
         0.1800000          -0.0114439
         0.2000000          -0.0129685
         0.2200000          -0.0087418
         0.2400000          -0.0095012
         0.2600000          -0.0086712
         0.2800000          -0.0070111
         0.3000000          -0.0072525
*DEFINE_CURVE
$#     lcid      sidr       sfa       sfo      offa      offo    dattyp
        21         0     0.000     0.000     0.000     0.000         0
$#               a1                  o1
             0.000               0.000
         0.0100000      9.2868198e-004
         0.0200000      9.2868198e-004
         0.0400000           0.0018574
         0.0600000           0.0027860
         0.0800000           0.0037147
         0.1000000           0.0045765
         0.1200000           0.0043685
         0.1400000           0.0046100
         0.1600000           0.0053864
         0.1800000           0.0072214
         0.2000000           0.0081835
         0.2200000           0.0055164
         0.2400000           0.0059956
         0.2600000           0.0054718
         0.2800000           0.0044242
         0.3000000           0.0045765
```

```
*DEFINE_CURVE
$#     lcid      sidr       sfa       sfo      offa      offo    dattyp
        22         0     0.000     0.000     0.000     0.000         0
$#               a1                  o1
             0.000               0.000
         0.0100000     -9.2868198e-004
         0.0200000     -9.2868198e-004
         0.0400000          -0.0018574
         0.0600000          -0.0027860
         0.0800000          -0.0037147
         0.1000000          -0.0045765
         0.1200000          -0.0043685
         0.1400000          -0.0046100
         0.1600000          -0.0053864
         0.1800000          -0.0072214
         0.2000000          -0.0081835
         0.2200000          -0.0055164
         0.2400000          -0.0059956
         0.2600000          -0.0054718
         0.2800000          -0.0044242
         0.3000000          -0.0045765
*DEFINE_CURVE
$#     lcid      sidr       sfa       sfo      offa      offo    dattyp
        23         0     0.000     0.000     0.000     0.000         0
$#               a1                  o1
             0.000               0.000
         0.0100000      6.1999698e-004
         0.0200000      6.1999698e-004
         0.0400000           0.0012400
         0.0600000           0.0018600
         0.0800000           0.0024800
         0.1000000           0.0030553
         0.1200000           0.0029165
         0.1400000           0.0030777
         0.1600000           0.0035960
         0.1800000           0.0048211
         0.2000000           0.0054634
         0.2200000           0.0036828
         0.2400000           0.0040027
         0.2600000           0.0036530
         0.2800000           0.0029537
         0.3000000           0.0030553
*DEFINE_CURVE
$#     lcid      sidr       sfa       sfo      offa      offo    dattyp
        24         0     0.000     0.000     0.000     0.000         0
$#               a1                  o1
             0.000               0.000
         0.0100000     -6.1999698e-004
         0.0200000     -6.1999698e-004
         0.0400000          -0.0012400
         0.0600000          -0.0018600
         0.0800000          -0.0024800
         0.1000000          -0.0030553
         0.1200000          -0.0029165
         0.1400000          -0.0030777
         0.1600000          -0.0035960
         0.1800000          -0.0048211
         0.2000000          -0.0054634
         0.2200000          -0.0036828
         0.2400000          -0.0040027
         0.2600000          -0.0036530
         0.2800000          -0.0029537
         0.3000000          -0.0030553
```

```
*SET_PART_LIST
$#     sid       da1       da2       da3       da4
         1     0.000     0.000     0.000     0.000
$#    pid1      pid2      pid3      pid4      pid5      pid6      pid7      pid8
         1         4         5         7         8         9        10         0
*SET_PART_LIST
$#     sid       da1       da2       da3       da4
         2     0.000     0.000     0.000     0.000
$#    pid1      pid2      pid3      pid4      pid5      pid6      pid7      pid8
         1         4         5         0         0         0         0         0
*SET_PART_LIST
$#     sid       da1       da2       da3       da4
         3     0.000     0.000     0.000     0.000
$#    pid1      pid2      pid3      pid4      pid5      pid6      pid7      pid8
         7         8         9        10         0         0         0         0
*SET_PART_LIST
$#     sid       da1       da2       da3       da4
         4     0.000     0.000     0.000     0.000
$#    pid1      pid2      pid3      pid4      pid5      pid6      pid7      pid8
         7         0         0         0         0         0         0         0
*SET_PART_LIST
$#     sid       da1       da2       da3       da4
         5     0.000     0.000     0.000     0.000
$#    pid1      pid2      pid3      pid4      pid5      pid6      pid7      pid8
         8         9         0         0         0         0         0         0
*SET_PART_LIST
$#     sid       da1       da2       da3       da4
         6     0.000     0.000     0.000     0.000
$#    pid1      pid2      pid3      pid4      pid5      pid6      pid7      pid8
        10         0         0         0         0         0         0         0
*ALE_MULTI-MATERIAL_GROUP
$#     sid    idtype
         4         0
*ALE_MULTI-MATERIAL_GROUP
$#     sid    idtype
         5         0
*ALE_MULTI-MATERIAL_GROUP
$#     sid    idtype
         6         0
*CONSTRAINED_LAGRANGE_IN_SOLID
$#   slave    master     sstyp     mstyp     nquad     ctype     direc     mcoup
         2         3         0         0         0         4         1         0
$#   start       end      pfac      fric    frcmin      norm   normtyp      damp
     0.0001.0000E+10  0.100000     0.000  0.100000         0         0         0
$#      cq      hmin      hmax     ileak     pleak   lcidpor     nvent  blockage
     0.000     0.000     0.000         2  0.010000         0         0         0
$#  iboxid   ipenchk   intforc   ialesof    lagmul    pfacmm      thkf
         0         0         0         0     0.000         0     0.000
```

APPENDIX D:

ABRIDGED LS DYNA KEYWORD FILE

SECOND OBJECTIVE LEAKING MODEL

Second Objective Leaking Model

Units	
Length	Millimeter
Time	Second
Mass	Tonne
Force	Newton

```
*KEYWORD
*TITLE
$# title
LS-DYNA keyword deck by LS-Prepost
*CONTROL_ALE
$#     dct      nadv      meth      afac      bfac      cfac      dfac      efac
         1         1         1 -1.000000     0.000     0.000     0.000     0.000
$#   start       end     aafac     vfact      prit       ebc      pref   nsidebc
     0.0001.0000E+20  1.000000 1.0000E-6         0         0     0.000         0
*CONTROL_CONTACT
$#  slsfac    rwpnal    islchk    shlthk    penopt    thkchg     orien    enmass
  0.100000     0.000         1         0         0         0         1         0
$#  usrstr    usrfrc     nsbcs    interm     xpene     ssthk      ecdt   tiedprj
         0         0         0         0  4.000000         0         0         0
$#   sfric     dfric       edc       vfc        th     th_sf    pen_sf
     0.000     0.000     0.000     0.000     0.000     0.000     0.000
$#  ignore    frceng   skiprwg    outseg   spotstp   spotdel   spothin
         0         0         0         0         0         0     0.000
$#    isym    nserod    rwgaps    rwgdth     rwksf      icov    swradf    ithoff
         0         0         0     0.000  1.000000         0     0.000         0

*CONTROL_ENERGY
$#    hgen      rwen    slnten     rylen
         2         2         1         1
*CONTROL_SHELL
$#  wrpang     esort     irnxx    istupd    theory       bwc     miter      proj
 20.000000         0        -1         0         2         2         1         0
$# rotascl    intgrd    lamsht    cstyp6    tshell    nfail1    nfail4   psnfail
  1.000000         0         0         1         0         0         0         0
$# psstupd    irquad
         0         0
*CONTROL_TERMINATION
$#  endtim    endcyc     dtmin    endeng    endmas
  0.300000         0     0.000     0.000     0.000
*CONTROL_TIMESTEP
$#  dtinit    tssfac      isdo    tslimt     dt2ms      lctm     erode     ms1st
     0.000  0.900000         0     0.000     0.000         0         0         0
$#  dt2msf   dt2mslc     imscl
     0.000         0         0
*DATABASE_BINARY_D3PLOT
$#      dt      lcdt      beam     npltc    psetid
  0.005000         0         0         0         0
$ MATERIAL CARDS
$ DEFINITION OF MATERIAL     1
$#   ioopt
         0
*DATABASE_BINARY_RUNRSF
$#      dt      lcdt      beam     npltc    psetid
 1.0000E+5         0         0         0         0
```

```
*CONTACT_SINGLE_SURFACE_ID
$ SLIDING INTERFACE DEFINITIONS
$ TrueGrid Sliding Interface #    1
$#     cid                                                                title
         1TrueGridSlidingInterface#1
$#    ssid      msid     sstyp     mstyp    sboxid    mboxid       spr       mpr
         5         0         3         0         0         0         0         0
$#      fs        fd        dc        vc       vdc    penchk        bt        dt
     0.000     0.000     0.000     0.000     0.000         0     0.000     0.000
$#     sfs       sfm       sst       mst      sfst      sfmt       fsf       vsf
     0.000     0.000     0.000     0.000     0.000     0.000     0.000     0.000
*PART
$# title
bladder wall mooney rivlin hyperelastic
$#     pid     secid       mid     eosid      hgid      grav    adpopt      tmid
         1         1         1         0         1         0         0         0
*SECTION_SHELL
$#   secid    elform      shrf       nip     propt   qr/irid     icomp     setyp
         1         1  0.830000         0         1         0         0         1
$#      t1        t2        t3        t4      nloc     marea      idof    edgset
  2.000000  2.000000  2.000000  2.000000 -1.000000     0.000     0.000         0
*MAT_MOONEY-RIVLIN_RUBBER
$#     mid        ro        pr         a         b       ref
         1 1.0300E-9  0.450000  0.007500  0.002500     0.000
$#     sgl        sw        st      lcid
     0.000     0.000     0.000         0
*HOURGLASS
$#    hgid       ihq        qm       ibq        q1        q2    qb/vdc        qw
         1         1  0.100000         0     0.000     0.000     0.000     0.000
*PART
$# title
urethra and bladder neck modeled as blatz ko hyperelastic materials
$#     pid     secid       mid     eosid      hgid      grav    adpopt      tmid
         4         4         4         0         4         0         0         0
*SECTION_SHELL
$#   secid    elform      shrf       nip     propt   qr/irid     icomp     setyp
         4         1  0.830000         0         1         0         0         1
$#      t1        t2        t3        t4      nloc     marea      idof    edgset
  2.000000  2.000000  2.000000  2.000000 -1.000000     0.000     0.000         0
*MAT_BLATZ-KO_RUBBER
$ DEFINITION OF MATERIAL     4
$#     mid        ro         g       ref
         4 1.0400E-9  0.100000     0.000
*HOURGLASS
$#    hgid       ihq        qm       ibq        q1        q2    qb/vdc        qw
         4         1  0.100000         0     0.000     0.000     0.000     0.000
*PART
$# title
urethra and bladder neck modeled as blatz ko hyperelastic materials
$#     pid     secid       mid     eosid      hgid      grav    adpopt      tmid
         5         5         5         0         5         0         0         0
*SECTION_SHELL
$#   secid    elform      shrf       nip     propt   qr/irid     icomp     setyp
         5         1  0.830000         0         1         0         0         1
$#      t1        t2        t3        t4      nloc     marea      idof    edgset
  4.000000  4.000000  4.000000  4.000000 -1.000000     0.000     0.000         0
*MAT_BLATZ-KO_RUBBER
$ DEFINITION OF MATERIAL     5
$#     mid        ro         g       ref
         5 1.0400E-9  0.100000     0.000
*HOURGLASS
$#    hgid       ihq        qm       ibq        q1        q2    qb/vdc        qw
         5         1  0.100000         0     0.000     0.000     0.000     0.000
*PART
$# title
material type # 9  (Fluid)
$#     pid     secid       mid     eosid      hgid      grav    adpopt      tmid
         7         7        24         0         7         0         0         0
```

```
*SECTION_SOLID_ALE
$#   secid    elform       aet
         7        11         0
$#    afac      bfac      cfac      dfac     start       end     aafac
     0.000     0.000     0.000     0.000     0.000     0.000     0.000
*MAT_ELASTIC_FLUID
$#     mid        ro         e        pr        da        db         k
        24 1.0000E-9     0.000     0.000     0.000     0.000 2250.0000
$#      vc        cp
  0.1000001.0000E+20
*HOURGLASS
$#    hgid       ihq        qm       ibq        q1        q2    qb/vdc        qw
         7         1 1.0000E-5         0     0.000     0.000     0.000     0.000
*PART
$# title
material type # 9  (Fluid)
$#     pid     secid       mid     eosid      hgid      grav    adpopt      tmid
         8         8        21         0         8         0         0         0
*SECTION_SOLID_ALE
$#   secid    elform       aet
         8        11         3
$#    afac      bfac      cfac      dfac     start       end     aafac
     0.000     0.000     0.000     0.000     0.000     0.000     0.000
*MAT_ALE_VACUUM
$#     mid       rho
        21 1.0000E-9
*HOURGLASS
$#    hgid       ihq        qm       ibq        q1        q2    qb/vdc        qw
         8         1 1.0000E-5         0     0.000     0.000     0.000     0.000
*PART
$# title
material type # 9  (Fluid)
$#     pid     secid       mid     eosid      hgid      grav    adpopt      tmid
         9         9        22         0         9         0         0         0
*SECTION_SOLID_ALE
$#   secid    elform       aet
         9        11         1
$#    afac      bfac      cfac      dfac     start       end     aafac
     0.000     0.000     0.000     0.000     0.000     0.000     0.000
*MAT_ALE_VACUUM
$#     mid       rho
        22 1.0000E-9
*HOURGLASS
$#    hgid       ihq        qm       ibq        q1        q2    qb/vdc        qw
         9         1 1.0000E-5         0     0.000     0.000     0.000     0.000
*PART
$# title
material type # 9  (Fluid)
$#     pid     secid       mid     eosid      hgid      grav    adpopt      tmid
        10        10        23         0        10         0         0         0
*SECTION_SOLID_ALE
$#   secid    elform       aet
        10        11         0
$#    afac      bfac      cfac      dfac     start       end     aafac
     0.000     0.000     0.000     0.000     0.000     0.000     0.000
*MAT_ALE_VACUUM
$#     mid       rho
        23 1.0000E-9
*HOURGLASS
$#    hgid       ihq        qm       ibq        q1        q2    qb/vdc        qw
        10         1 1.0000E-5         0     0.000     0.000     0.000     0.000
*MAT_NULL
$ DEFINITION OF MATERIAL     7
$#     mid        ro        pc        mu     terod     cerod        ym        pr
         7 1.0000E-9     0.000 1.0000E-9     0.000     0.000     0.000     0.000
```

```
*DEFINE_CURVE
$ LOAD CURVES
$#    lcid      sidr       sfa       sfo      offa      offo    dattyp
         1         0     0.000     0.000     0.000     0.000         0
$#                a1                  o1
                0.000               0.000
            0.0100000               0.000
            0.0200000      7.8455999e-004
            0.0400000           0.0015691
            0.0600000           0.0023537
            0.0800000           0.0031382
            0.1000000           0.0038443
            0.1200000           0.0042170
            0.1400000           0.0040895
            0.1600000           0.0058254
            0.1800000           0.0120626
            0.2000000           0.0148772
            0.2200000           0.0065903
            0.2400000           0.0098560
            0.2600000           0.0047662
            0.2800000           0.0032363
            0.3000000           0.0038443
*DEFINE_CURVE
$#    lcid      sidr       sfa       sfo      offa      offo    dattyp
         2         0     0.000     0.000     0.000     0.000         0
$#                a1                  o1
                0.000               0.000
            0.0100000               0.000
            0.0200000     -7.8455999e-004
            0.0400000          -0.0015691
            0.0600000          -0.0023537
            0.0800000          -0.0031382
            0.1000000          -0.0038443
            0.1200000          -0.0042170
            0.1400000          -0.0040895
            0.1600000          -0.0058254
            0.1800000          -0.0120626
            0.2000000          -0.0148772
            0.2200000          -0.0065903
            0.2400000          -0.0098560
            0.2600000          -0.0047662
            0.2800000          -0.0032363
            0.3000000          -0.0038443
*DEFINE_CURVE
$#    lcid      sidr       sfa       sfo      offa      offo    dattyp
         3         0     0.000     0.000     0.000     0.000         0
$#                a1                  o1
                0.000               0.000
            0.0100000               0.000
            0.0200000      7.8455999e-004
            0.0400000               0.000
            0.0600000               0.000
            0.0800000               0.000
            0.1000000               0.000
            0.1200000               0.000
            0.1400000               0.000
            0.1600000               0.000
            0.1800000               0.000
            0.2000000               0.000
            0.2200000               0.000
            0.2400000               0.000
            0.2600000               0.000
            0.2800000               0.000
            0.3000000               0.000
```

```
*DEFINE_CURVE
$#     lcid      sidr       sfa       sfo      offa      offo    dattyp
         4         0     0.000     0.000     0.000     0.000         0
$#               a1                  o1
             0.000               0.000
           0.0100000               0.000
           0.0200000    -7.8455999e-004
           0.0400000               0.000
           0.0600000               0.000
           0.0800000               0.000
           0.1000000               0.000
           0.1200000               0.000
           0.1400000               0.000
           0.1600000               0.000
           0.1800000               0.000
           0.2000000               0.000
           0.2200000               0.000
           0.2400000               0.000
           0.2600000               0.000
           0.2800000               0.000
           0.3000000               0.000
*DEFINE_CURVE
$#     lcid      sidr       sfa       sfo      offa      offo    dattyp
         5         0     0.000     0.000     0.000     0.000         0
$#               a1                  o1
             0.000               0.000
           0.0100000     7.0549198e-004
           0.0200000     7.0549198e-004
           0.0400000          0.0014110
           0.0600000          0.0021165
           0.0800000          0.0028220
           0.1000000          0.0034767
           0.1200000          0.0033186
           0.1400000          0.0035021
           0.1600000          0.0040919
           0.1800000          0.0054859
           0.2000000          0.0062168
           0.2200000          0.0041906
           0.2400000          0.0045547
           0.2600000          0.0041568
           0.2800000          0.0033610
           0.3000000          0.0034767
*DEFINE_CURVE
$#     lcid      sidr       sfa       sfo      offa      offo    dattyp
         6         0     0.000     0.000     0.000     0.000         0
$#               a1                  o1
             0.000               0.000
           0.0100000    -7.0549198e-004
           0.0200000    -7.0549198e-004
           0.0400000         -0.0014110
           0.0600000         -0.0021165
           0.0800000         -0.0028220
           0.1000000         -0.0034767
           0.1200000         -0.0033186
           0.1400000         -0.0035021
           0.1600000         -0.0040919
           0.1800000         -0.0054859
           0.2000000         -0.0062168
           0.2200000         -0.0041906
           0.2400000         -0.0045547
           0.2600000         -0.0041568
           0.2800000         -0.0033610
           0.3000000         -0.0034767
```

```
*DEFINE_CURVE
$#     lcid      sidr       sfa       sfo      offa      offo    dattyp
         7         0     0.000     0.000     0.000     0.000         0
$#               a1                  o1
              0.000               0.000
          0.0100000      9.1896701e-004
          0.0200000      9.1896701e-004
          0.0400000           0.0018379
          0.0600000           0.0027569
          0.0800000           0.0036759
          0.1000000           0.0045287
          0.1200000           0.0043228
          0.1400000           0.0045618
          0.1600000           0.0053300
          0.1800000           0.0071459
          0.2000000           0.0080979
          0.2200000           0.0054587
          0.2400000           0.0059328
          0.2600000           0.0054146
          0.2800000           0.0043780
          0.3000000           0.0045287
*DEFINE_CURVE
$#     lcid      sidr       sfa       sfo      offa      offo    dattyp
         8         0     0.000     0.000     0.000     0.000         0
$#               a1                  o1
              0.000               0.000
          0.0100000     -9.1896701e-004
          0.0200000     -9.1896701e-004
          0.0400000          -0.0018379
          0.0600000          -0.0027569
          0.0800000          -0.0036759
          0.1000000          -0.0045287
          0.1200000          -0.0043228
          0.1400000          -0.0045618
          0.1600000          -0.0053300
          0.1800000          -0.0071459
          0.2000000          -0.0080979
          0.2200000          -0.0054587
          0.2400000          -0.0059328
          0.2600000          -0.0054146
          0.2800000          -0.0043780
          0.3000000          -0.0045287
*DEFINE_CURVE
$#     lcid      sidr       sfa       sfo      offa      offo    dattyp
         9         0     0.000     0.000     0.000     0.000         0
$#               a1                  o1
              0.000               0.000
          0.0100000           0.0010553
          0.0200000           0.0010553
          0.0400000           0.0021106
          0.0600000           0.0031659
          0.0800000           0.0042212
          0.1000000           0.0052005
          0.1200000           0.0049641
          0.1400000           0.0052385
          0.1600000           0.0061207
          0.1800000           0.0082060
          0.2000000           0.0092993
          0.2200000           0.0062685
          0.2400000           0.0068130
          0.2600000           0.0062178
          0.2800000           0.0050274
          0.3000000           0.0052005
```

```
*DEFINE_CURVE
$#     lcid      sidr       sfa       sfo      offa      offo    dattyp
        10         0     0.000     0.000     0.000     0.000         0
$#               a1                  o1
             0.000               0.000
         0.0100000          -0.0010553
         0.0200000          -0.0010553
         0.0400000          -0.0021106
         0.0600000          -0.0031659
         0.0800000          -0.0042212
         0.1000000          -0.0052005
         0.1200000          -0.0049641
         0.1400000          -0.0052385
         0.1600000          -0.0061207
         0.1800000          -0.0082060
         0.2000000          -0.0092993
         0.2200000          -0.0062685
         0.2400000          -0.0068130
         0.2600000          -0.0062178
         0.2800000          -0.0050274
         0.3000000          -0.0052005
*DEFINE_CURVE
$#     lcid      sidr       sfa       sfo      offa      offo    dattyp
        11         0     0.000     0.000     0.000     0.000         0
$#               a1                  o1
             0.000               0.000
         0.0100000           0.0010936
         0.0200000           0.0010936
         0.0400000           0.0021873
         0.0600000           0.0032809
         0.0800000           0.0043745
         0.1000000           0.0053894
         0.1200000           0.0051444
         0.1400000           0.0054288
         0.1600000           0.0063431
         0.1800000           0.0085041
         0.2000000           0.0096371
         0.2200000           0.0064962
         0.2400000           0.0070605
         0.2600000           0.0064437
         0.2800000           0.0052101
         0.3000000           0.0053894
*DEFINE_CURVE
$#     lcid      sidr       sfa       sfo      offa      offo    dattyp
        12         0     0.000     0.000     0.000     0.000         0
$#               a1                  o1
             0.000               0.000
         0.0100000          -0.0010936
         0.0200000          -0.0010936
         0.0400000          -0.0021873
         0.0600000          -0.0032809
         0.0800000          -0.0043745
         0.1000000          -0.0053894
         0.1200000          -0.0051444
         0.1400000          -0.0054288
         0.1600000          -0.0063431
         0.1800000          -0.0085041
         0.2000000          -0.0096371
         0.2200000          -0.0064962
         0.2400000          -0.0070605
         0.2600000          -0.0064437
         0.2800000          -0.0052101
         0.3000000          -0.0053894
```

```
*DEFINE_CURVE
$#     lcid      sidr       sfa       sfo      offa      offo    dattyp
        13         0     0.000     0.000     0.000     0.000         0
$#               a1                  o1
             0.000               0.000
         0.0100000           0.0011311
         0.0200000           0.0011311
         0.0400000           0.0022622
         0.0600000           0.0033932
         0.0800000           0.0045243
         0.1000000           0.0055739
         0.1200000           0.0053206
         0.1400000           0.0056147
         0.1600000           0.0065602
         0.1800000           0.0087953
         0.2000000           0.0099670
         0.2200000           0.0067186
         0.2400000           0.0073022
         0.2600000           0.0066643
         0.2800000           0.0053884
         0.3000000           0.0055739
*DEFINE_CURVE
$#     lcid      sidr       sfa       sfo      offa      offo    dattyp
        14         0     0.000     0.000     0.000     0.000         0
$#               a1                  o1
             0.000               0.000
         0.0100000          -0.0011311
         0.0200000          -0.0011311
         0.0400000          -0.0022622
         0.0600000          -0.0033932
         0.0800000          -0.0045243
         0.1000000          -0.0055739
         0.1200000          -0.0053206
         0.1400000          -0.0056147
         0.1600000          -0.0065602
         0.1800000          -0.0087953
         0.2000000          -0.0099670
         0.2200000          -0.0067186
         0.2400000          -0.0073022
         0.2600000          -0.0066643
         0.2800000          -0.0053884
         0.3000000          -0.0055739
*DEFINE_CURVE
$#     lcid      sidr       sfa       sfo      offa      offo    dattyp
        15         0     0.000     0.000     0.000     0.000         0
$#               a1                  o1
             0.000               0.000
         0.0100000           0.0012111
         0.0200000           0.0012111
         0.0400000           0.0024221
         0.0600000           0.0036332
         0.0800000           0.0048442
         0.1000000           0.0059681
         0.1200000           0.0056968
         0.1400000           0.0060117
         0.1600000           0.0070241
         0.1800000           0.0094172
         0.2000000           0.0106718
         0.2200000           0.0071937
         0.2400000           0.0078186
         0.2600000           0.0071356
         0.2800000           0.0057695
         0.3000000           0.0059681
```

```
*DEFINE_CURVE
$#     lcid      sidr       sfa       sfo      offa      offo    dattyp
        16         0     0.000     0.000     0.000     0.000         0
$#               a1                  o1
             0.000               0.000
         0.0100000          -0.0012111
         0.0200000          -0.0012111
         0.0400000          -0.0024221
         0.0600000          -0.0036332
         0.0800000          -0.0048442
         0.1000000          -0.0059681
         0.1200000          -0.0056968
         0.1400000          -0.0060117
         0.1600000          -0.0070241
         0.1800000          -0.0094172
         0.2000000          -0.0106718
         0.2200000          -0.0071937
         0.2400000          -0.0078186
         0.2600000          -0.0071356
         0.2800000          -0.0057695
         0.3000000          -0.0059681
*DEFINE_CURVE
$#     lcid      sidr       sfa       sfo      offa      offo    dattyp
        17         0     0.000     0.000     0.000     0.000         0
$#               a1                  o1
             0.000               0.000
         0.0100000           0.0010725
         0.0200000           0.0010725
         0.0400000           0.0021450
         0.0600000           0.0032176
         0.0800000           0.0042901
         0.1000000           0.0052854
         0.1200000           0.0050451
         0.1400000           0.0053240
         0.1600000           0.0062206
         0.1800000           0.0083399
         0.2000000           0.0094511
         0.2200000           0.0063708
         0.2400000           0.0069242
         0.2600000           0.0063193
         0.2800000           0.0051095
         0.3000000           0.0052854
*DEFINE_CURVE
$#     lcid      sidr       sfa       sfo      offa      offo    dattyp
        18         0     0.000     0.000     0.000     0.000         0
$#               a1                  o1
             0.000               0.000
         0.0100000          -0.0010725
         0.0200000          -0.0010725
         0.0400000          -0.0021450
         0.0600000          -0.0032176
         0.0800000          -0.0042901
         0.1000000          -0.0052854
         0.1200000          -0.0050451
         0.1400000          -0.0053240
         0.1600000          -0.0062206
         0.1800000          -0.0083399
         0.2000000          -0.0094511
         0.2200000          -0.0063708
         0.2400000          -0.0069242
         0.2600000          -0.0063193
         0.2800000          -0.0051095
         0.3000000          -0.0052854
```

```
*DEFINE_CURVE
$#     lcid      sidr       sfa       sfo      offa      offo    dattyp
        19         0     0.000     0.000     0.000     0.000         0
$#                a1                  o1
                0.000               0.000
            0.0100000      7.3584600e-004
            0.0200000      7.3584600e-004
            0.0400000           0.0014717
            0.0600000           0.0022075
            0.0800000           0.0029434
            0.1000000           0.0036262
            0.1200000           0.0034614
            0.1400000           0.0036527
            0.1600000           0.0042679
            0.1800000           0.0057219
            0.2000000           0.0064843
            0.2200000           0.0043709
            0.2400000           0.0047506
            0.2600000           0.0043356
            0.2800000           0.0035056
            0.3000000           0.0036262
*DEFINE_CURVE
$#     lcid      sidr       sfa       sfo      offa      offo    dattyp
        20         0     0.000     0.000     0.000     0.000         0
$#                a1                  o1
                0.000               0.000
            0.0100000     -7.3584600e-004
            0.0200000     -7.3584600e-004
            0.0400000          -0.0014717
            0.0600000          -0.0022075
            0.0800000          -0.0029434
            0.1000000          -0.0036262
            0.1200000          -0.0034614
            0.1400000          -0.0036527
            0.1600000          -0.0042679
            0.1800000          -0.0057219
            0.2000000          -0.0064843
            0.2200000          -0.0043709
            0.2400000          -0.0047506
            0.2600000          -0.0043356
            0.2800000          -0.0035056
            0.3000000          -0.0036262
*DEFINE_CURVE
$#     lcid      sidr       sfa       sfo      offa      offo    dattyp
        21         0     0.000     0.000     0.000     0.000         0
$#                a1                  o1
                0.000               0.000
            0.0100000      4.6434099e-004
            0.0200000      4.6434099e-004
            0.0400000      9.2868198e-004
            0.0600000           0.0013930
            0.0800000           0.0018574
            0.1000000           0.0022883
            0.1200000           0.0021843
            0.1400000           0.0023050
            0.1600000           0.0026932
            0.1800000           0.0036107
            0.2000000           0.0040918
            0.2200000           0.0027582
            0.2400000           0.0029978
            0.2600000           0.0027359
            0.2800000           0.0022121
            0.3000000           0.0022883
```

```
*DEFINE_CURVE
$#     lcid      sidr       sfa       sfo      offa      offo    dattyp
        22         0     0.000     0.000     0.000     0.000         0
$#               a1                  o1
             0.000               0.000
         0.0100000     -4.6434099e-004
         0.0200000     -4.6434099e-004
         0.0400000     -9.2868198e-004
         0.0600000          -0.0013930
         0.0800000          -0.0018574
         0.1000000          -0.0022883
         0.1200000          -0.0021843
         0.1400000          -0.0023050
         0.1600000          -0.0026932
         0.1800000          -0.0036107
         0.2000000          -0.0040918
         0.2200000          -0.0027582
         0.2400000          -0.0029978
         0.2600000          -0.0027359
         0.2800000          -0.0022121
         0.3000000          -0.0022883
*DEFINE_CURVE
$#     lcid      sidr       sfa       sfo      offa      offo    dattyp
        23         0     0.000     0.000     0.000     0.000         0
$#               a1                  o1
             0.000               0.000
         0.0100000      3.0999799e-004
         0.0200000      3.0999799e-004
         0.0400000      6.1999698e-004
         0.0600000      9.2999497e-004
         0.0800000           0.0012400
         0.1000000           0.0015277
         0.1200000           0.0014582
         0.1400000           0.0015388
         0.1600000           0.0017980
         0.1800000           0.0024105
         0.2000000           0.0027317
         0.2200000           0.0018414
         0.2400000           0.0020013
         0.2600000           0.0018265
         0.2800000           0.0014768
         0.3000000           0.0015277
*DEFINE_CURVE
$#     lcid      sidr       sfa       sfo      offa      offo    dattyp
        24         0     0.000     0.000     0.000     0.000         0
$#               a1                  o1
             0.000               0.000
         0.0100000     -3.0999799e-004
         0.0200000     -3.0999799e-004
         0.0400000     -6.1999698e-004
         0.0600000     -9.2999497e-004
         0.0800000          -0.0012400
         0.1000000          -0.0015277
         0.1200000          -0.0014582
         0.1400000          -0.0015388
         0.1600000          -0.0017980
         0.1800000          -0.0024105
         0.2000000          -0.0027317
         0.2200000          -0.0018414
         0.2400000          -0.0020013
         0.2600000          -0.0018265
         0.2800000          -0.0014768
         0.3000000          -0.0015277
*SET_PART_LIST
$#      sid       da1       da2       da3       da4
         1     0.000     0.000     0.000     0.000
$#     pid1      pid2      pid3      pid4      pid5      pid6      pid7      pid8
         1         4         5         7         8         9        10         0
```

```
*SET_PART_LIST
$#     sid       da1       da2       da3       da4
         2     0.000     0.000     0.000     0.000
$#    pid1      pid2      pid3      pid4      pid5      pid6      pid7      pid8
         1         4         5         0         0         0         0         0
*SET_PART_LIST
$#     sid       da1       da2       da3       da4
         3     0.000     0.000     0.000     0.000
$#    pid1      pid2      pid3      pid4      pid5      pid6      pid7      pid8
         7         8         9        10         0         0         0         0
*SET_PART_LIST
$#     sid       da1       da2       da3       da4
         4     0.000     0.000     0.000     0.000
$#    pid1      pid2      pid3      pid4      pid5      pid6      pid7      pid8
         7         0         0         0         0         0         0         0
*SET_PART_LIST
$#     sid       da1       da2       da3       da4
         5     0.000     0.000     0.000     0.000
$#    pid1      pid2      pid3      pid4      pid5      pid6      pid7      pid8
         8         9         0         0         0         0         0         0
*SET_PART_LIST
$#     sid       da1       da2       da3       da4
         6     0.000     0.000     0.000     0.000
$#    pid1      pid2      pid3      pid4      pid5      pid6      pid7      pid8
        10         0         0         0         0         0         0         0
*ALE_MULTI-MATERIAL_GROUP
$#     sid    idtype
         4         0
*ALE_MULTI-MATERIAL_GROUP
$#     sid    idtype
         5         0
*ALE_MULTI-MATERIAL_GROUP
$#     sid    idtype
         6         0
*CONSTRAINED_LAGRANGE_IN_SOLID
$#   slave    master     sstyp     mstyp     nquad     ctype     direc     mcoup
         2         3         0         0         0         4         1         0
$#   start       end      pfac      fric    frcmin      norm   normtyp      damp
     0.0001.0000E+10  0.100000     0.000  0.100000         0         0         0
$#      cq      hmin      hmax     ileak     pleak   lcidpor     nvent  blockage
     0.000     0.000     0.000         2  0.010000         0         0         0
$#  iboxid   ipenchk   intforc   ialesof    lagmul    pfacmm      thkf
         0         0         0         0     0.000         0     0.000
```

APPENDIX E:

COPYRIGHT PERMISSION DOCUMENTATION

For Figure 2:

ELSEVIER LICENSE
TERMS AND CONDITIONS

Jun 09, 2010

This is a License Agreement between Thomas Spirka ("You") and Elsevier ("Elsevier") provided by Copyright Clearance Center ("CCC"). The license consists of your order details, the terms and conditions provided by Elsevier, and the payment terms and conditions.

All payments must be made in full to CCC. For payment instructions, please see information listed at the bottom of this form.

Supplier	Elsevier Limited The Boulevard,Langford Lane Kidlington,Oxford,OX5 1GB,UK
Registered Company Number	1982084
Customer name	Thomas Spirka
Customer address	9500 Euclid Ave Cleveland, OH 44195
License Number	1926090811306
License date	Apr 11, 2008
Licensed content publisher	Elsevier Limited
Licensed content publication	Gastroenterology
Licensed content title	Pathophysiology of adult urinary incontinence
Licensed content author	Delancey John O. L. and Ashton-miller James A.
Licensed content date	January 2004
Volume number	126
Issue number	ment 1
Pages	1
Type of Use	Thesis / Dissertation
Portion	Figures/table/illustration/abstracts
Format	Print
You are an author of the Elsevier article	No
Are you translating?	No
Order Reference Number	
Expected publication date	May 2008
Elsevier VAT number	GB 494 6272 12
Permissions price	0.00 USD
Value added tax 0.0%	0.00 USD
Total	0.00 USD
Terms and Conditions	

INTRODUCTION

The publisher for this copyrighted material is Elsevier. By clicking "accept" in connection

with completing this licensing transaction, you agree that the following terms and conditions apply to this transaction (along with the Billing and Payment terms and conditions established by Copyright Clearance Center, Inc. ("CCC"), at the time that you opened your Rightslink account and that are available at any time at http://myaccount.copyright.com).

GENERAL TERMS

Elsevier hereby grants you permission to reproduce the aforementioned material subject to the terms and conditions indicated.

Acknowledgement: If any part of the material to be used (for example, figures) has appeared in our publication with credit or acknowledgement to another source, permission must also be sought from that source. If such permission is not obtained then that material may not be included in your publication/copies. Suitable acknowledgement to the source must be made, either as a footnote or in a reference list at the end of your publication, as follows:

"Reprinted from Publication title, Vol number, Author(s), Title of article, Pages No., Copyright (Year), with permission from Elsevier [OR APPLICABLE SOCIETY COPYRIGHT OWNER]." Also Lancet special credit - "Reprinted from The Lancet, Vol. number, Author(s), Title of article, Pages No., Copyright (Year), with permission from Elsevier."

Reproduction of this material is confined to the purpose and/or media for which permission is hereby given.

Altering/Modifying Material: Not Permitted. However figures and illustrations may be altered/adapted minimally to serve your work. Any other abbreviations, additions, deletions and/or any other alterations shall be made only with prior written authorization of Elsevier Ltd. (Please contact Elsevier at permissions@elsevier.com)

If the permission fee for the requested use of our material is waived in this instance, please be advised that your future requests for Elsevier materials may attract a fee.

Reservation of Rights: Publisher reserves all rights not specifically granted in the combination of (i) the license details provided by you and accepted in the course of this licensing transaction, (ii) these terms and conditions and (iii) CCC's Billing and Payment terms and conditions.

License Contingent Upon Payment: While you may exercise the rights licensed immediately upon issuance of the license at the end of the licensing process for the transaction, provided that you have disclosed complete and accurate details of your proposed use, no license is finally effective unless and until full payment is received from you (either by publisher or by CCC) as provided in CCC's Billing and Payment terms and conditions. If full payment is not received on a timely basis, then any license preliminarily

granted shall be deemed automatically revoked and shall be void as if never granted. Further, in the event that you breach any of these terms and conditions or any of CCC's Billing and Payment terms and conditions, the license is automatically revoked and shall be void as if never granted. Use of materials as described in a revoked license, as well as any use of the materials beyond the scope of an unrevoked license, may constitute copyright infringement and publisher reserves the right to take any and all action to protect its copyright in the materials.

Warranties: Publisher makes no representations or warranties with respect to the licensed material.

Indemnity: You hereby indemnify and agree to hold harmless publisher and CCC, and their respective officers, directors, employees and agents, from and against any and all claims arising out of your use of the licensed material other than as specifically authorized pursuant to this license.

No Transfer of License: This license is personal to you and may not be sublicensed, assigned, or transferred by you to any other person without publisher's written permission.

No Amendment Except in Writing: This license may not be amended except in a writing signed by both parties (or, in the case of publisher, by CCC on publisher's behalf).

Objection to Contrary Terms: Publisher hereby objects to any terms contained in any purchase order, acknowledgment, check endorsement or other writing prepared by you, which terms are inconsistent with these terms and conditions or CCC's Billing and Payment terms and conditions. These terms and conditions, together with CCC's Billing and Payment terms and conditions (which are incorporated herein), comprise the entire agreement between you and publisher (and CCC) concerning this licensing transaction. In the event of any conflict between your obligations established by these terms and conditions and those established by CCC's Billing and Payment terms and conditions, these terms and conditions shall control.

Revocation: Elsevier or Copyright Clearance Center may deny the permissions described in this License at their sole discretion, for any reason or no reason, with a full refund payable to you. Notice of such denial will be made using the contact information provided by you. Failure to receive such notice will not alter or invalidate the denial. In no event will Elsevier or Copyright Clearance Center be responsible or liable for any costs, expenses or damage incurred by you as a result of a denial of your permission request, other than a refund of the amount(s) paid by you to Elsevier and/or Copyright Clearance Center for denied permissions.

LIMITED LICENSE

The following terms and conditions apply to specific license types:

Translation: This permission is granted for non-exclusive world **English** rights only unless

your license was granted for translation rights. If you licensed translation rights you may only translate this content into the languages you requested. A professional translator must perform all translations and reproduce the content word for word preserving the integrity of the article. If this license is to re-use 1 or 2 figures then permission is granted for non-exclusive world rights in all languages.

Website: The following terms and conditions apply to electronic reserve and author websites:
Electronic reserve: If licensed material is to be posted to website, the web site is to be password-protected and made available only to bona fide students registered on a relevant course if:
This license was made in connection with a course,
This permission is granted for 1 year only. You may obtain a license for future website posting,
All content posted to the web site must maintain the copyright information line on the bottom of each image,
A hyper-text must be included to the Homepage of the journal from which you are licensing at http://www.sciencedirect.com/science/journal/xxxxx , and
Central Storage: This license does not include permission for a scanned version of the material to be stored in a central repository such as that provided by Heron/XanEdu.

Author website with the following additional clauses: This permission is granted for 1 year only. You may obtain a license for future website posting,
All content posted to the web site must maintain the copyright information line on the bottom of each image, and
The permission granted is limited to the personal version of your paper. You are not allowed to download and post the published electronic version of your article (whether PDF or HTML, proof or final version), nor may you scan the printed edition to create an electronic version,
A hyper-text must be included to the Homepage of the journal from which you are licensing at http://www.sciencedirect.com/science/journal/xxxxx , and
Central Storage: This license does not include permission for a scanned version of the material to be stored in a central repository such as that provided by Heron/XanEdu.

Website (regular and for author): "A hyper-text must be included to the Homepage of the journal from which you are licensing at
http://www.sciencedirect.com/science/journal/xxxxx."

Thesis/Dissertation: If your license is for use in a thesis/dissertation your thesis may be submitted to your institution in either print or electronic form. Should your thesis be published commercially, please reapply for permission. These requirements include permission for the Library and Archives of Canada to supply single copies, on demand, of the complete thesis and include permission for UMI to supply single copies, on demand, of the complete thesis. Should your thesis be published commercially, please reapply for permission.

Other Terms and Conditions:

Gratis licenses (referencing $0 in the Total field) are free. Please retain this printable license for your reference. No payment is required.

If you would like to pay for this license now, please remit this license along with your payment made payable to "COPYRIGHT CLEARANCE CENTER" otherwise you will be invoiced within 48 hours of the license date. Payment should be in the form of a check or money order referencing your account number and this invoice number RLNK10508141.
Once you receive your invoice for this order, you may pay your invoice by credit card. Please follow instructions provided at that time.

Make Payment To:
Copyright Clearance Center
Dept 001
P.O. Box 843006
Boston, MA 02284-3006

If you find copyrighted material related to this license will not be used and wish to cancel, please contact us referencing this license number 1926090811306 and noting the reason for cancellation.

Questions? customercare@copyright.com or +1-877-622-5543 (toll free in the US) or +1-978-646-2777.

For Figure 3:

Dear Sir,

With reference to your request (copy herewith) to reprint material on which Springer Science and Business Media controls the copyright, our permission is granted, free of charge, for the use indicated in your enquiry.

This permission

- allows you non-exclusive reproduction rights throughout the World.

- permission includes use in an electronic form, provided that
content is

  * password protected;

  * at intranet;

- excludes use in any other electronic form. Should you have a
specific project in mind, please reapply for permission.

- requires a full credit (Springer/Kluwer Academic Publishers book/journal title, volume, year of publication, page, chapter/article title, name(s) of author(s), figure number(s), original copyright notice) to the publication in which the material was originally published, by adding: with kind permission of Springer Science and Business Media.

The material can only be used for the purpose of defending your dissertation, and with a maximum of 100 extra copies in paper.

Permission free of charge on this occasion does not prejudice any rights
we might have to charge for reproduction of our copyrighted material in the future.

Best wishes,

Nel van der Werf (Ms)
Rights and Permissions/Springer

Van Godewijckstraat 30 | P.O. Box 17
3300 AA Dordrecht | The Netherlands
tel +31 (0) 78 6576 298

fax +31 (0)78 65 76-300
Nel.vanderwerf @springer.com
www.springeronline.com

-----Original Message-----
From: Spirka, Thomas [mailto:spirkat@ccf.org]
Sent: maandag 14 april 2008 22:44
To: Permissions Europe/NL
Subject: RE: Rightslink/ Springer Redirected Order Request

I would like to request permission to use figures 4a, 4b,and 4c.

The figures will be used in a written research proposal which will be presented to the members of my doctoral thesis committee to illustrate the mechanics of the Integral Theory.

Publication will be limited to no more than 7 copies. One copy will be presented to each of the five members of the dissertation committee for review, one copy will be presented to the College of Graduate Studies at
Cleveland State University for review and the final copy will be retained by myself for my own personal records

Thank you for your attention in this matter and let me know if you need any additional information

Thomas Spirka

-----Original Message-----
From: Japajoe, Estella, Springer SBM NL
[mailto:Estella.Japajoe@springer.com] On Behalf Of Permissions Europe/NL
Sent: Monday, April 14, 2008 8:54 AM
To: Spirka, Thomas
Subject: FW: Rightslink/ Springer Redirected Order Request
Importance: High

Dear Thomas Spirka,

Thank you for your email. Please send us the following information so that we can further handle your request:

Concerning our publication:

* Please mention the figure number(s) you would like to use.

Concerning your publication:

* The exact intended use of the material.

* Publishing house, editor (of book), tentative title, expected amount of pages in new publication, price, print run, expected date to publish,
to whom the publication would appeal to.

Kind regards,

Estella Jap A Joe
Springer
Rights & Permissions
-
Van Godewijckstraat 30 | 3311 GX
P.O. Box 990 | 3300 AZ
Dordrecht | The Netherlands
fax +31 (0) 78 657 6300
estella.japajoe@springer.com
www.springeronline.com

2008 Bookfairs we attend:

* 14-16 April - London
  1-4 September - Peking (Tianjin)
  15-19 October - Frankfurt

For appointments please contact permissions.bookfairs@springer.com

-----Original Message-----
From: customercare@copyright.com [mailto:customercare@copyright.com]
Sent: vrijdag 11 april 2008 21:25
To: Permissions Europe/NL
Subject: Rightslink/ Springer Redirected Order Request
Importance: High

Attention: Springer Customer Service

Please note below information pertaining to a customer request for reuse
of Springer content. This request is being forwarded to you by Copyright
Clearance Center's Rightslink Service as established by Springer. Please
contact the customer below regarding this request and to provide a
corresponding price quote.

Customer information:
Name: Thomas Spirka
Address: 9500 Euclid Ave Mail Location ND 20 Cleveland, OH 44195 United States
Telephone: (216) 445-2443
Email: mailto:spirkat@ccf.org

Article information:

Publication: International Urogynecology Journal
Pages: 69 - 73
Volume number: 8
Issue number: 2
Publication date: December 03, 2007
Title: Role of the pelvic floor in Bladder neck opening and closure II: Vagina
Author: P. E. Papa Petros